$IDH1^{R132H}$ Mutations Actively Contribute to the Epigenetic State of Glioma Cells

by

Casey Moure

Department of Pathology
Duke University

Date: _____

Approved:

_____
Hai Yan, Supervisor

_____
Jen-Tsan Ashley Chi

_____
Yiping He

_____
Jiaoti Huang

_____
Kris Wood

Dissertation submitted in partial fulfillment of the requirements for the degree of
Doctor of Philosophy in the Department of Pathology
in the Graduate School of Duke University
2019

Abstract

$IDH1^{R132H}$ Mutations Actively Contribute to the Epigenetic State of Glioma Cells

by

Casey Moure

Department of Pathology
Duke University

Date: _____

Approved:

_____
Hai Yan, Supervisor

_____
Jen-Tsan Ashley Chi

_____
Yiping He

_____
Jiaoti Huang

_____
Kris Wood

An abstract of a dissertation submitted in partial fulfillment of the requirements for the degree of Doctor of Philosophy in the Department of Pathology in the Graduate School of Duke University
2019

Abstract

Point mutations in the active site of isocitrate dehydrogenases 1 and 2 (*IDH*) occur in the majority of WHO grade II and III gliomas, resulting in a unique milieu of signaling and metabolism. IDH1/2 active site mutations confer a gain-of-function activity to the enzyme, which results in the production of the oncometabolite D-2-hydroxyglutarate (D-2HG). D-2HG accumulation in turn promotes tumor formation through competitive inhibition of α-ketoglutarate dependent (α-KG) enzymes. Inhibition of α-KG-dependent enzymes, such as histone demethylases and DNA demethylases, is sufficient to induce tumor-promoting epigenetic changes, but can also impose situational constraints on cell proliferation. To develop better therapies for mutant IDH1-bearing gliomas, it is essential to determine whether the epigenetic changes induced by the mutant IDH proteins actively require the mutation after tumor formation. Furthermore, it is imperative to decode the molecular mechanisms that promote tumor cells' fitness under IDH mutation-dependent constraints in representative models. Here, we describe and characterize CRISPR-Cas9 based isogenic cell line models using patient-derived IDH1$^{R132H/WT}$ glioma cell lines. We uncover that these models show persistent DNA hypermethylation in CpG loci of the glioma CpG island methylator phenotype even after D-2HG production has been abolished. We also report a genome wide pattern of DNA demethylation in CpG sites outside of CpG islands, which reflect the acquisition of a G-CIMP-low like state after loss of D-2HG production. Then, using these cell line tools, we performed an unbiased

sub-genomic CRISPR-library screening to identify genes whose functions supported the growth of glioma cells bearing endogenous IDH1 mutations. This work thus provides new patient derived models for exploring novel therapeutic opportunities for IDH1 mutant tumors, and uncovers the extent to which IDH mutation linked hypermethylation profiles in glioma depend upon D-2HG production from the IDH mutation.

Contents

List of Tables

List of Figures

Acknowledgements

With deep gratitude, I thank H. Yan and Y. He for providing mentoring during my time at Duke, and H. Yan for support of the work presented here. I would also like to thank J. Huang, J. Chi, K. Wood, Y. He, and H. Yan for guidance on my thesis committee. I thank our collaborators I. Spasojevic, P. Fan and the DUCC Clinical Pharmacology Lab for quantitative analysis of D-2-HG. D. Thiele for providing access to a Lonza Nucleofector 4-D machine. K. Abramson and the Duke CHG Molecular Genetics Core for assistance with Illumina methylation array processing; and the Duke Microarray Core Facility for their assistance with microarrays. I thank Michael Cook and the Duke DCI flow cytometry core for cell sorting. I thank Hudson Alpha for providing NGS services for the CRISPR screen. I would like to thank K. Poss, N. Bursac, and D. Kiehart for allowing me to rotate through their laboratories and learn fundamentals of research in biology. I thank the Duke DSCB program for support and collegiality. I thank D.D. Bigner and R. McClendon and their respective laboratories for their support of our work, and the rest of the Preston Robert Tisch Brain Tumor Center tissue bank staff for their tireless work providing the center with biobanking of primary glioma tissue samples.

I would like to thank B.H. Diplas for the establishment of single-allele polymerase chain reaction methods used to initially screen potential CRISPR-edited clones, and for consistent and superlative collegiality throughout my time in the Yan lab. I thank M.S. Waitkus for providing me with scientific mentoring and constructive discussions.

I thank L.H. Chen for programming mentoring and helpful critique of my code and analysis plans. I thank R. Yang and G. Jin for the initial establishment of original parental cell lines used in this work. I thank C.J. Pirozzi for mentoring on scientific writing and for helping to convince me to attend Duke at the original interview. I thank P. Killela and Z. Wang for helpful guidance during my early years in the Yan lab. I thank L. Hansen for collaboration on other applications of CRIPSR editing in glioma research outside the scope of this thesis. I would like to thank P. Greer for tireless work managing the Yan lab and providing much needed support over the years. I thank M. Atchison and S.N. Abraham as well as the rest of the Pathology department at Duke for support during the Ph.D. program.

I would like to thank my parents B. Lear and J. Moure for their wonderful and empathetic support over the years. I would like to thank my sister S. Moure for providing inspiration and encouraging my own creativity. I thank J. Todd and M. Matalenas for their friendship over the years. I thank my grandmothers M. Moure and M. Hauser for encouragement over the years as well as the rest of my family for their support. Finally, I would like to give a special thanks to Maria Moure for immigrating to America and undertaking much hardship to provide the opportunities my father and I have enjoyed during our lives; your life has always been an inspiration to me.

Copyrighted and/or published content: Parts of this dissertation including parts of the abstract, introduction, chapter 2, and conclusion were reproduced according to the journal/publisher policies of the American Association for Cancer Research journals as described in Appendix A. The results shown here are in whole or part based upon data generated by the TCGA Research Network: http://cancergenome.nih.gov/.

Support: These studies were supported by NIH grant R01CA140316 to Hai Yan M.D., Ph.D. Casey Moure was supported by an NRSA Fellowship F31CA203399. Bill Diplas was supported by NRSA Fellowship F30CA206423

1

Introduction

1.1 Permissions

Work in this dissertation includes both unpublished figures and text created by the author as well as figures and excerpts of text from published articles. Explicit permissions for reproduction of figures and excerpts from published work are described in Appendix A.1 where required. For publishers that do not require explicit permissions for reproduction of figures and excerpts, work was reproduced in accordance with the policy of the publisher as described in Appendix A.1. The work in this dissertation was performed primarily by the candidate, and in those cases where work was aided by collaborators, as in analysis or sample acquisition, individual contributions are described in the Acknowledgements section.

1.2 Overview of Introduction

This thesis begins with a description of the historical context in which recurrent genetic mutations within NADP-dependent isocitrate dehydrogenases (*IDH*) were first discovered in human cancer. The purpose is twofold; to introduce the historical terms primary glioblastoma and secondary glioblastoma and to illustrate to the reader the

progressive course of disease often found in *IDH* mutant gliomas. Evidence from the literature is provided that *IDH* mutant gliomas are a different pathological entity from *IDH* wildtype gliomas with *IDH* mutations present early on in the evolution of *IDH* mutant glioma. Then the introduction will focus on the known biochemical consequences of mutant IDH proteins in human cancer including the causal role of IDH mutations in the glioma CpG island methylator phenotype, and unknowns about the continuing role for IDH proteins in the malignant phenotype of IDH mutant cancer will be highlighted.

1.3 Broad context: overview of progressive gliomas

Among humans, the most common primary malignant brain tumor is the glioblastoma (Ostrom et al., 2018), making up approximately 15 percent of total primary brain and central nervous system tumors in the United States (Ostrom et al., 2014, 2018). Glioblastomas have historically been subdivided into *de novo* glioblastomas, which are called primary glioblastomas, and secondary glioblastomas which evolve from a progressing lower grade glioma (Ohgaki and Kleihues, 2007). This historical distinction, made first by German neuropathologist Hans-Joachim Scherer in 1940 (Ohgaki and Kleihues, 2007), had been made despite these subgroups of glioblastoma being histologically identical and typically lumped together for incidence reporting (Ohgaki and Kleihues, 2007). Then in 2008 and 2009, gene sequencing of human glioblastoma patient cohorts as well as lower grade glioma patients uncovered a hitherto unappreciated distinction between primary and secondary glioblastomas in the rates of recurrent genetic lesions in the NADP-dependent isocitrate dehydrogenases (Parsons et al., 2008; Yan et al., 2009). The finding of high rates of *IDH* lesions in secondary glioblastomas led to a paradigm shift in the classification and understanding of glioma (Parsons et al., 2008; Yan et al., 2009), and was arguably one of the major triumphs of the cancer genome sequencing project (Brat et al., 2015).

Although IDH mutations were relatively rare in primary glioblastomas, 6/123 cases in (Yan et al., 2009), the mutations were present in a majority of secondary glioblastomas, 11/13 cases, as well as a majority of several additional types of lower grade progressive glioma (Yan et al., 2009).

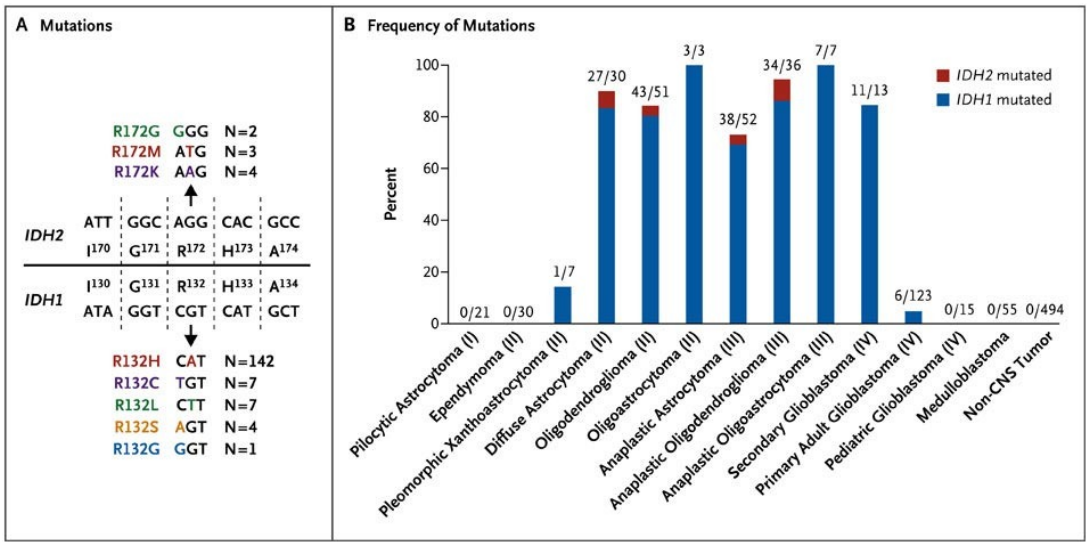

FIGURE 1.1: A: mutations in *IDH1/2* that were identified in human gliomas, along with the number of patients who carried each mutation. B: number and frequency of *IDH1* and *IDH2* mutations in gliomas and other types of tumors. Reproduced with permission from (Yan et al., 2009), Copyright Massachusetts Medical Society.

Furthermore, the presence of an active site IDH mutation was found to carry important prognostic implications for several types of lower grade malignant glioma, due to IDH mutant gliomas tending to have better prognosis than their grade matched IDH wildtype counterparts 1.2 (Yan et al., 2009). These observations led to the historical classification schemes of human glioma being supplanted by molecular classification of gliomas based on common genetic alterations (Kim et al., 2010). This change was codified in the newly updated 2016 World Health Organization (WHO) classifications of tumours of the central nervous system (Louis et al., 2016). Under the 2016 WHO guidelines, glioblastomas are now subdivided into three primary

subgroups including isocitrate dehydrogenase wildtype (IDH-WT) , isocitrate dehydrogenase mutant (IDH-mutant), and glioblastoma not otherwise specified (Louis et al., 2016). Likewise, lower grade oligodendroglial and astrocytomas also have subdivisions on the basis of IDH mutation status, and mixed histology tumors can now be grouped with other astrocytomas or oligodendroglial tumors based on the presence of specific genetic lesions (Louis et al., 2016; Kim et al., 2010; Jiao et al., 2012).

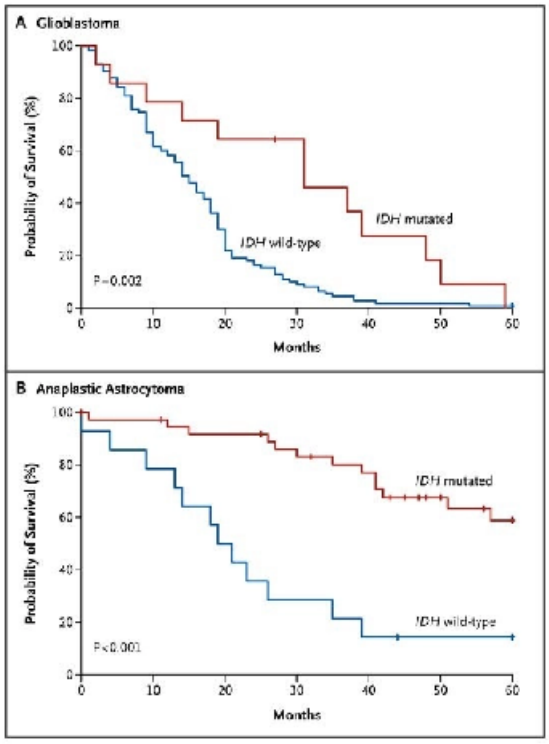

FIGURE 1.2: A: Survival curves of glioblastomas both secondary and primary either with or without the IDH mutation. Secondary glioblastoma survival is counted starting at diagnosis of secondary glioblastoma and not from previous lower grade tumor. B: Survival curves for anaplastic astrocytomas with or without IDH mutations. Reproduced with permission from (Yan et al., 2009), Copyright Massachusetts Medical Society.

Although more than 10 years have elapsed since the first publication observing *IDH* mutations in glioma and extensive investigation has been made into the mu-

tation's roles in oncogenesis, there remain unresolved questions as to the degree of necessity for the IDH mutations' presence in malignant gliomas on recurrence. There is also debate about how to utilize information about the biochemical action of mutant IDH for therapy, and whether direct or indirect targeting of the mutant enzyme will be most efficacious in ending glioma progression. Answering these questions is critical not only from a perspective of maximizing therapeutic efficacy, but also because the causal contributions to IDH mutant gliomas having a better prognosis than their matched IDH wildtype counterparts are still unclear (Bleeker et al., 2010; Houillier et al., 2010; Juratli et al., 2012).

1.4 Biochemical actions of the mutant IDH proteins

When mutations in *IDH* genes were first reported to be widely prevalent in secondary glioblastomas (Yan et al., 2009) it was also reported that the majority of these mutations occurred within the arginine 132 coding codon of isocitrate dehydrogenase 1, and that the mutations occurred in a heterozygous state with one *IDH1* allele retaining its wildtype coding sequence (Yan et al., 2009). IDH gene family member IDH2 was also found to contain recurrent mutations in an analogous codon, arginine 172, whose numbering is shifted further towards the C-terminal of the protein relative to IDH1 due to the presence of a cleaved 40 amino acid mitochondrial targeting sequence in IDH2 (Yan et al., 2009). Therefore, when fully processed both IDH1 and IDH2 have recurrent mutations within the same codon of the highly similar proteins suggesting to early researchers that there had been evolutionary selection for a similar mutant enzyme function (Yan et al., 2009; Ward et al., 2010). Later in 2009 it was discovered that these recurrent heterozygous mutations in IDH1 and IDH2 shared a gain of similar enzyme function, the catalysis of D-2-hydroxyglutarate (D-2HG) production from α-KG and reduced nicotinamide adenine dinucleotide phosphate (NADPH) (Dang et al., 2009).

However, despite observing the interesting biochemical action of mutant IDH it was unknown exactly which mechanisms the mutant IDH or D-2HG could use to promote tumor initiation or progression. Research by several groups quickly showed that D-2HG could potentially inhibit enzymes which utilized α-KG as co-substrates such as the 2-oxoglutarate-dependent dioxygenase family of proteins (Xu et al., 2011). Other groups were observing changes in redox stress as the result of reduced NADPH conversion to NADP or interference of D-2HG with the electron transport chain of cells (Dang et al., 2010). And yet another group showed that IDH mutations could promote cytokine independence through agonism instead of antagonism of 2-oxoglutarate dependent dioxygenase enzymes which utilized α-KG as a co-substrate (Losman et al., 2013). In this alternative model it is histone methylation which is key and this is supported by additional studies showing that the transformation ability of the IDH1 mutation occurs much faster than the on-set of DNA methylation (Johannessen et al., 2016). However, the myriad effects of IDH1 mutations on different aspects of cell biology make determination of the most critical function or functions of mutant IDH1 for transformation a still unresolved question and likely cell context dependent. Furthermore, whether some of the pro-tumorigenic effects observed by various research groups have tumor progression promoting effects vs. tumor initiating effects is unclear.

1.5 The Glioma CpG-Island Methylator Phenotype and mutant IDH proteins

D-2HG modulates the activity of alpha-ketoglutarate (α-KG) dependent enzymes due to structural similarity to α-KG, and by this mechanism causes pro-tumorigenic changes in chromatin structure and gene expression (Flavahan et al., 2016; Koivunen et al., 2012; Waitkus et al., 2016). One of these IDH1 mutation-linked epigenetic changes is the glioma CpG island methylator phenotype (G-CIMP), which is a pat-

tern of predominantly gene-promoter based CpG island hypermethylation found in WHO grade II, III, and IV glioma wherein IDH mutations commonly occur (Noushmehr et al., 2010). In previous reports, CpG promoter methylation in 7 different genes, most tightly linked to the proneural G-CIMP-positive status, were utilized to classify glioblastoma tumors as G-CIMP positive (Noushmehr et al., 2010). Utilizing immortalized astroctyes (Turcan et al., 2012) showed that the presence of the IDH1 mutation was sufficient to establish a genome-wide hypermethylation pattern similar to patient G-CIMP and with concomitant gene expression changes (Turcan et al., 2012). Similarly, (Duncan et al., 2012) found using adeno-associated viral vector mediated knock-in Hct116 cells that the IDH1 mutation was associated with genome-wide elevation of DNA methylation levels with some predisposition for originally moderately methylated loci becoming hypermethylated after knock-in of the IDH1 mutation. Therefore, there exists interesting correlational and experiment-based evidence that the IDH mutations in glioma are responsible for creating a genome-wide pattern of hypermethylation which may impinge on gene expression to promote tumorigenesis. The presence of a molecular mechanism, namely D-2HG mediated inhibition of the DNA demethylating enzyme family of TET proteins, supports an evidenced causal claim that the IDH mutations cause G-CIMP hypermethylation (Turcan et al., 2012).

1.6 Ways DNA methylation can impinge on gene expression

DNA methylation may be able to modulate gene expression and evidence exists that there are multiple modes by which this may occur. In the context of hypermethylation caused by IDH1 mutations in glioma, (Flavahan et al., 2016) present experimental evidence that IDH mutations may lead to methylation of CTCF binding sites within the genome causing loss of genomic insulator boundaries and increased expression of the gene *PDGFRA*. This study is an illustration of the paradigm whereby

a DNA binding protein factor, in this case CTCF, can bind at its target sequences when CpG sites at those sequences are unmethylated. However, when CpG dinucleotides are methylated at the cytosine nucleotide then binding by CTCF is reduced or completely abrogated impairing CTCF function at that particular site (Flavahan et al., 2016). The relative ability of DNA- binding proteins to have their binding affinity modulated by target site DNA methylation is thus one factor that determines whether a particular DNA-binding protein is likely to be affected by the presence of an IDH mutation and concomitant aberrant DNA methylation. Furthermore, DNA and histone methylation can be tightly linked and both contribute to chromatin structure, which ultimately influences the rate at which transcription factors and RNA synthesis machinery can interact with particular genes (Rose and Klose, 2014).

1.7 Tumor promoting functions vs. imposed liabilities of IDH mutations

Although multiple studies present evidence for a pro-tumorigenic role of IDH1 in the initiation of glioma several observations and lines of inquiry also suggest that these pro-tumorigenic functions can come with situational costs. Understanding these situational costs may allow rational development of therapies that would exploit the presence of the IDH1 mutation for precision molecular medicine in IDH1 mutant tumors. One previous example of an IDH1 mutation linked liability is in glutamine metabolism. In previous work by (Chen et al., 2014), it was observed that overexpression of mutant R132H but not wildtype *IDH1* alleles could suppress the growth of tumorigenic transformed murine neural progenitor cells. However, overexpression of the primate specific gene GLUD2 could resolve this liability by promoting flux of glutamine/glutamate into alpha-ketoglutarate (Chen et al., 2014). Similarly, knockdown of GLUD1/2 could suppress the *in vivo* growth of IDH1 mutant glioma lines (Chen et al., 2014; Waitkus et al., 2018), illustrating that with both gain-of-

function and loss-of-function approaches the IDH1 mutant gliomagenic cells likely require a threshold amount of glutamate dehydrogenase activity to compensate for depletion of alpha-ketoglutarate-maintaining metabolite production. This need for alpha-ketoglutarate-maintaining metabolite production was also observed in another study on the effect of D-2HG on transaminase inhibition, and is further supported by studies attempting to detect glutamate levels in IDH1 mutant vs. IDH1 wildtype human tumors with non-invasive imaging techniques (McBrayer et al., 2018; Fack et al., 2017).

In another similar vein of research one group showed that across multiple cell line models there was a difference in the growth suppression of various cell lines on over-expression of mutant IDH1 based on their levels of myc expression (Su et al., 2018). This effect was linked to the inhibition of the protein product of the gene FTO, which is an example of an 2-oxoglutarate dioxygenase that demethylates methylated adenine in RNA (Su et al., 2018). In this work cells with high enough amounts of myc mRNA, potentially from genetic amplifications, could escape from the growth inhibition induced by mRNA degradation downstream of increased m6A RNA methylation (Su et al., 2018). Whether and how this result interacts with the increased requirement for glutamate anaplerosis in IDH1 mutant cells remains to be elucidated.

Finally, there is an interesting genetic correlation between the frequency of specific neomorphic mutations in IDH1 and their prevalence in human cancers, with mutations with higher D-2HG production-potential being rarer than weaker D-2HG producing mutations suggesting a possible selection against high D-2HG production in early pre-cancerous cells (Pusch et al., 2014). An important limitation in all studies done to date stems from the fact that there are no systematic genetic searches for IDH1 mutation-linked genetic fitness dependencies due to the lack of well controlled and genetically relevant human glioma cell line models.

1.8 Evidence for losses of the IDH mutation in high grade astrocytomas

Although several studies looking at cohorts of secondary glioblastomas continued to identify prominent IDH1 mutations in all samples acquired, (Bai et al., 2015) there are examples in the literature of the loss of the IDH1 mutation, (Mazor et al., 2017), or the loss of the wildtype allele of IDH1 in recurrent tumors, (Zhang et al., 2014). It is important to note that loss of the wildtype allele of IDH1 has been shown both in cell line models and in patient tumors to lead to a severe reduction in the level of D-2HG (Jin et al., 2013). This level of reduction may be sufficient to free 2-oxoglutarate-dependent dioxygenases from D-2HG mediated competitive inhibition. Furthermore, it has previously been speculated that these losses may occur in treated tumors due to selection against IDH1 mutation carrying cells during treatment (Mazor et al., 2017). These studies have also shown that IDH1 mutant samples with prominent losses of the IDH1 mutant cells within their tumors have co-correlating distinct changes of methylation genomewide, but whether the loss of IDH1 mutations is causal for these changes is unknown.

1.9 G-CIMP-low a hypomethylated subgroup of G-CIMP positive astrocytomas

Within the glioma subset of astrocytomas the most prominently known change in DNA methylation is the acquisition of the G-CIMP-low state with its proposed correlation to worse outcome among the G-CIMP positive subset of tumors (Ceccarelli et al., 2016). This G-CIMP-low state was discovered by clustering analysis of cancer genome atlas (TCGA) data, and showed that some IDH1 mutant astrocytomas but not IDH1 mutant oligodendroglial tumors could exhibit a G-CIMP positive but relatively hypomethylated genome-wide methylation profile (Ceccarelli et al., 2016).

In more recent work, (Mazor et al., 2017), show that tumors with bona-fide loss of the mutant IDH1 allele tend to undergo genome-wide hypomethylation changes compared to their matched IDH1 mutant positive initial tumor leading to the possibility that loss of D-2HG production or the IDH1 mutation might be sufficient to induce a G-CIMP-low like state (Mazor et al., 2017). This correlations only well controlled experimental support, to date, is the observation in a single genetic immortalized astrocyte model that removing expression of doxycycline inducible mutant IDH1 could remodel the DNA methylome of the cells, and that many, but not all, of the IDH1 mutation linked hypermethylation events induced in the astrocytes could be reversed over twenty-population doublings (Turcan et al., 2018). Because only a single astrocyte cell line was chosen it remains unknown to what degree hypermethylation events that define G-CIMP can be reversed in human glioma samples with IDH1 mutations on the loss of the *IDH1* mutant allele.

1.10 Current questions in the field about losses of mutant IDH1 in advanced glioma and a possible correlation to acquisition of G-CIMP-low phenotype

The work presented in this thesis describes novel insights into the requirements for an active IDH1 mutation in the maintenance of epigenetic states causally linked to the IDH1 mutation in the context of malignant anaplastic astrocytoma cell lines as well as secondary glioblastoma cell lines. New isogenic cell line tools and proof of principle methods are developed for further work characterizing the epigenetic state induced by the loss of the IDH1 mutation in human glioma, and it is shown that these cell line tools can also be utilized for systematic screening of genes whose gene products promote the fitness of IDH1 mutant cells. Chapter 1 gives a brief overview of the known biochemical functions of mutant and wildtype IDH proteins with emphasis on available evidence in glial lineage cells for tumor promoting functions. Chapter 2 will

describe the initial testing for any requirements in our cell line models for an active IDH1 mutation for *in vitro* cell culture proliferation, and the methods developed for genetically altering low passage patient-derived primary glioma cell lines. This chapter will also report the observation of how DNA methylation states causally linked to the IDH1 mutation change after gene editing of the cell lines. Chapter 3 then reports on a proof-of-principle screen using a sub-genome sized CRISPR-Cas9 based screening library to show systematic characterization of genetic dependencies in isogenic IDH1 mutant cell lines is possible. Conclusions and possible future directions for the work will then be discussed in Chapter 4.

2

Chapter 2: Loss of IDH1 Results in Genome-wide CpG Demethylation

2.1 Introduction

Although the IDH1 mutation linked G-CIMP pattern of methylation is usually stable at tumor recurrence, there are specific decreases in DNA methylation within G-CIMP positive tumors with important prognostic implications (Ceccarelli et al., 2016). Specifically, among the G-CIMP positive astrocytic gliomas a pattern of hypomethylation termed G-CIMP-low has been identified in both low and high grade tumors (Ceccarelli et al., 2016; de Souza et al., 2018). This pattern shows enrichment for hypomethylation in CpG open seas (Ceccarelli et al., 2016), which are defined as regions more than 4 kilobases away from any annotated CpG island (Sandoval et al., 2011). For the G-CIMP-low phenotype, patient tumors were classified using 131 CpG probes which were hypomethylated in a subset of IDH mutant-non-codel tumors that had been previously classified as G-CIMP positive (Ceccarelli et al., 2016). Furthermore, G-CIMP-low status correlated with worse survival when compared to G-CIMP-high tumors (Ceccarelli et al., 2016; de Souza et al., 2018). Understanding

the genetic and environmental factors that contribute to the rise of the G-CIMP-low phenotype is therefore an important area of research for understanding glioma tumor progression and for prognostic purposes.

Recently, attempts to characterize progression of IDH1 mutant gliomas have identified copy number alterations in the *IDH1* gene in secondary glioblastomas (Mazor et al., 2017). These copy number changes include losses of the wildtype allele of *IDH1* (Zhang et al., 2014), deletions of the mutant allele of *IDH1* (Favero et al., 2015; Mazor et al., 2017), as well as amplifications of either allele (Mazor et al., 2017). Losses of the mutant *IDH1* allele have also co-occurred with acquisition of a G-CIMP-low like DNA methylation phenotype (Mazor et al., 2017), which has led to the hypothesis that loss of mutant IDH1-dependent D-2HG production is one path to a G-CIMP-low DNA methylation pattern (Mazor et al., 2017). Previous literature also suggests that oncogenic IDH1 mutations are not strictly required for continual proliferation of IDH1 mutant glioma cells *in vitro* (Johannessen et al., 2016; Luchman et al., 2013) and in *in vivo* orthotopic xenografts (Mazor et al., 2017; Tateishi et al., 2015). We took advantage of this finding to engineer isogenic cell line models from patient-derived glioma cell lines with endogenous heterozygous $IDH1^{R132H/WT}$, and generated knockouts of either the R132H or wildtype *IDH1* allele. We and others have previously shown that loss of either mutant or wildtype IDH1 is sufficient to suppress D-2HG production (Jin et al., 2013; Mazor et al., 2017). We utilized these genetically-engineered patient-derived models to ask whether the DNA methylation landscape in IDH1 mutant glioma relies on continual IDH1 mutation-dependent D-2HG production.

2.2 Methods

2.2.1 Cell Samples

Cell line IMA (also known as TB096 and TB09-0096-2), and cell line 08-0537 were isolated at the Preston Robert Tisch Brain Tumor Center at Duke University from a male Grade III anaplastic astrocytoma and secondary glioblastoma respectively and as previously described (Jin et al., 2013). Adherent line IMA was cultured in a media containing a 1:1 combination of [(Stem Cell Technologies human complete Neurocult^{TM} media supplemented with 20 ng/mL EGF, 10 ng/mL FGF, and 2 μg/mL heparin) : (DMEM (Invitrogen cat#11965-082)] + 10% Invitrogen FBS16000-044 lot 168075 as previously described (Jin et al., 2013). Cell line 08-0537 was grown in 1X human complete Neurocult^{TM} media with 20 ng/mL EGF, 10 ng/mL FGF, and 2 μg/mL heparin on laminin coated cell culture dishes for adherent culture. Cell media was refreshed every 4-6 days and cells were split approximately every 10 days or at 80% confluence. Cells were grown at 37°C and 5% CO2.

2.2.2 Cell Growth Assays

IMA cells were plated at 1000 cells per well in 6 well plates for long term growth assays or 2000 cells per well in 96 well plates for short term growth assays. For long term growth assays, plates were fixed in methanol and stained with 0.2% crystal violet solution before imaging plates on a Chemi-doc imager (Bio-Rad). Areas were determined in ImageJ using the Colony Area plugin. For short term growth assays cells were plated in 96-well black walled plates (Greiner), cultured for 6 days, and then processed following the manufacturer's recommended protocol for the Cyquant assay (Invitrogen).

2.2.3 Cell Line authentication and mycoplasma testing

Genomic DNA was extracted from IMA, 08-0537, and derivative subclones for cell line authentication by STR profiling assay against matched patient blood genomic DNA. Mycoplasma testing was performed by the Duke Cell Culture facility using the MycoAlert PLUS test (Lonza) and all cells tested negative. Patient derived cell line IMA was used between passages 10-20 and Cas9-edited derived clones were utilized between passages 10-20 post-cloning. Cell Line 08-0537 was utilized between passages 20-32 and clones were utilized between passages 10-20 post-cloning.

2.2.4 Transfection of Patient Derived Glioma Cell Lines

Patient derived glioma cell lines with endogenous IDH1 mutations were transiently transfected in one of two ways. IMA and 08-0537 clones from experiment 1 were created using the Lonza 4D-Nucleofector X Unit using 20 μL cuvette strips, program CA-137, and buffer P3 (Lonza). IMA clones from experiment 2 were produced using the Neon electroporator, 10uL R buffer, with program 1150V, 2 pulses, 30s pulse width (Invitrogen). All transfections were performed using 200,000 cells and 500ng of plasmid. Cells were allowed to recover following electroporation for 4 days by plating in full growth media in 24 well plates (1 electroporation per well and 500 μL of media) before selecting for the transfected clones through flow cytometry for GFP positive cells at the Duke Flow Cytometry core facility. After sorting, cells were allowed to recover for 1 week before plating single clones using limiting dilution cloning. For cell line 08-0537, to overcome low plating efficiency, cells were initially cloned through first plating clones at 1000 cells/dish on a 10 cm laminin coated plate wherein individual foci were eventually selected using Corning cloning cylinders, and promising polyclonal colonies were then passaged into limiting dilution plates to isolate true single clones.

2.2.5 Initial Screening and Allele Specific PCR of Single Clones

Initial screening of clones was performed using PCR primers that do not discriminate between mutant and wildtype *IDH1* alleles to identify clones carrying insertions or deletions in either allele (Supplementary Table 6). After selection of promising clones, allele-specific PCR of single clones was performed to amplify either the wildtype or mutant *IDH1* allele, and finally the resulting product was subjected to Sanger sequencing as reported previously (Diplas et al., 2018).

2.2.6 Plasmid Constructs

pSpCas9(BB)-2A-GFP (PX458) was a gift from Feng Zhang (Addgene plasmid # 48138) (Ran et al., 2013), and guides were cloned into the vectors using FastDigest BbsI (Fermentas) following Feng Zhang's Addgene supplementary cloning protocol and using synthesized oligonucleotides (IDT). The pCR-Blunt kit (Thermo-Scientific) was used according to the manufacturer's cloning protocol.

2.2.7 Whole Exome-Sequencing

Cell line DNA and normal DNA isolated from patient blood was provided to Personal Genome Diagnostics Inc. for next-generation sequencing of captured coding regions of the genome as previously described (Diplas et al., 2018).

2.2.8 Methylation Array Processing and Analysis

Genomic DNA was isolated from cells between passages 10 and 20 post-limiting dilution cloning using a Qiagen All Prep RNA/DNA kit following manufacturer's recommended instructions. gDNA was then processed through the Zymo genomic DNA Clean & Concentrator kit and eluted into diH2O. Samples were further processed by the Duke Molecular Genomics Shared Resource using Zymo EZ DNA methylation kit and Illumina's Infinium MethylationEPIC BeadChip following manufacturer's

recommended protocol. Arrays were captured using the Illumina iScan system and pre-processed in R version 3.5.2 using the ChAMP package (version 2.12.4) or minfi package (version 1.28.3) (Aryee et al., 2014; Morris et al., 2014; Zhou et al., 2017). Briefly, ChAMP processing removes probes with detection p-values >.01, or <3 beads in 5% of samples, as well as SNP-related probes, multi-hit probes, and non-CpG probes. After ChAMP processing, 720551 probes passed filtering and were used for downstream analysis. Beta-mixture quantile dilation normalization method was used to correct for probe-type design bias (Teschendorff et al., 2013). To assess stability of findings in the face of different choices of normalization method we also processed the data through minfi and GenomeStudio using Functional normalization and Illumina's proprietary normalization methods and results were consistent with ChAMP processed data. Differentially methylated probes were called using limma (Peters et al., 2015; Smyth, 2004; Wettenhall and Smyth, 2004). Copy number calls were performed by Conumee R package version 1.9.0 (Volker Hovestadt, 2017).

2.2.9 Western blotting

Total cell lysate in 1X RIPA buffer was quantitated by bicinchoninic acid assay and 20 μg of total protein was resolved using 4-12% Bis-Tris- buffered SDS-PAGE gels (Invitrogen). Gels were soaked in transfer buffer + 20% methanol and transferred to PVDF membranes using a mini Trans-Blot transfer cell (Bio-Rad) following manufacturer's protocol. After transfer, PVDF membranes were washed briefly in TBST and then blocked for 1 hour in TBST Protein-Free blocking buffer (Pierce catalog #37571). After blocking, primary antibodies were diluted either 1:500, for anti-IDH1^{R132H}, or otherwise 1:1000 in blocking buffer and incubated overnight at 4°C. Membranes were washed and incubated with horseradish peroxidase (HRP)-conjugated secondary antibody 1:2000 for one hour in TBST. Detection was performed via chemiluminescence on a Bio-Rad ChemiDoc MP system. Antibodies used included total IDH1 antibody

(D2H1, Cell Signaling #8137), COX IV antibody (3E11, Cell Signaling #4850), and $IDH1^{R132H}$ (DIA-H09, Dianova).

2.2.10 Analysis of D-2HG

Analysis of D-2HG in media and tissue was performed as previously described by the Duke Pharmacokinetics/Pharmacodynamics Laboratory (Waitkus et al., 2018). Normalization to total protein for cell pellets was performed using bicinchoninic acid assay (Thermo-Fischer).

2.2.11 Statistical Analysis

Comparisons between two groups were evaluated using two-tailed Student's t-test when only two groups were present. For categorical analysis of CpG genomic context a Chi square goodness of fit test was run against the frequency of CpG sites on the EPIC methylation chip to identify contexts enriched over CpG probe rate on the chip. Results are depicted as arithmetic mean $+/-$ SD unless otherwise indicated in the figure legend. Experimenters were not systematically blinded to group assignment or outcome assessment.

2.3 Results

2.3.1 Generating isogenic IDH1 R132H patient-derived cell lines

IDH1 mutations are thought to be an early initiating event in gliomagenesis (Lai et al., 2011), and mutant IDH1 activity has been shown to mediate transformation of normal human astrocytes (Johannessen et al., 2016). However, previous studies using inhibitors of mutant IDH1 have demonstrated that the mutation can become non-essential for viability and continual proliferation *in vitro* (Luchman et al., 2013) and *in vivo* (Johannessen et al., 2016; Tateishi et al., 2015). Using a mutant IDH1 astrocytoma cell line derived from a WHO Grade III anaplastic astrocytoma (IMA),

which also has astrocytoma pathognomonic mutations in TP53 and ATRX (Appendix A.1), we assessed the effects of mutant IDH1 inhibitor AGI-5198 on proliferation and D-2HG production. As in previous reports, D-2HG production was sup-

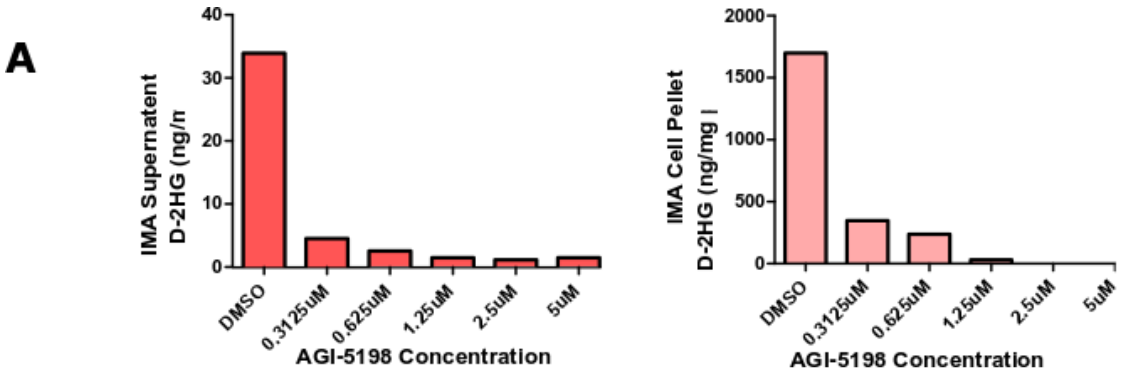

FIGURE 2.1: **Dose-response curves of AGI-5198 in IMA.** A, Dose-response curves of Agi-5198 show inhibition of D-2HG production from low grade astrocytoma cell line IMA as assessed by LC-MS in media (left) or cell pellet samples (right). Briefly, 2000 cells were plated in 100 μL of full growth media and left to attach overnight. Media was removed and media containing inhibitor or vehicle control was added and D-2HG was assessed 4 days post-media change.

pressed by 90-99% when cells were treated with 1.25 μM of the selective IDH1^{R132H} inhibitor AGI-5198 (Figure 2.1) (Rohle et al., 2013; Tateishi et al., 2015).

Despite this profound suppression of D-2HG, there was no difference in short term or long-term growth of this line, even upon treatment with 10 μM of AGI-5198 (Figure 2.2A and Figure 2.2B). In addition to the IMA cell line we have previously reported that the IDH1-mutant glioblastoma line 08-0537 does not show in vitro differences in proliferation upon treatment with AGI-5198, and has, similar to IMA, co-occurring mutations in TP53 and ATRX (Appendix A.2) (Waitkus et al., 2018). These results are in corroboration of previously published data wherein other groups have also observed a lack of IDH1 dependent proliferative potential *in vitro* (Kopinja et al., 2017). We next used CRISPR/Cas9-mediated gene editing to generate knock-

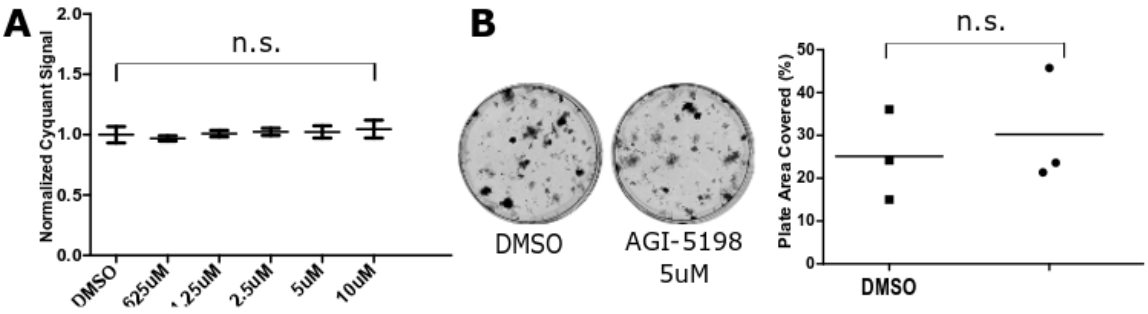

FIGURE 2.2: **IDH1^{R132H} is not required by some glioma lines in vitro for proliferation.** A, Cell line IMA showed no difference in 6 day proliferation by Cyquant assay when treated with 5 μM Agi-5198 compared to DMSO vehicle treated cells used as control. B, Longer time course treatment of IMA with Agi-5198 does not inhibit growth from single cells into colonies, plate area as assessed in ImageJ Colony Area Plugin p=.23; Student's two-tailed t-test

outs of the *IDH1* allele to create isogenic models of IDH1 loss. Because these lines are not amenable to chemical-based transfection methods, we utilized electroporation and transient expression of a plasmid encoding IDH1 targeting sgRNA and Cas9-2A-GFP (Figure 2.3). This experimental setup allowed us to transfect IDH1 mutant glioma line IMA at rates between 10-40%.

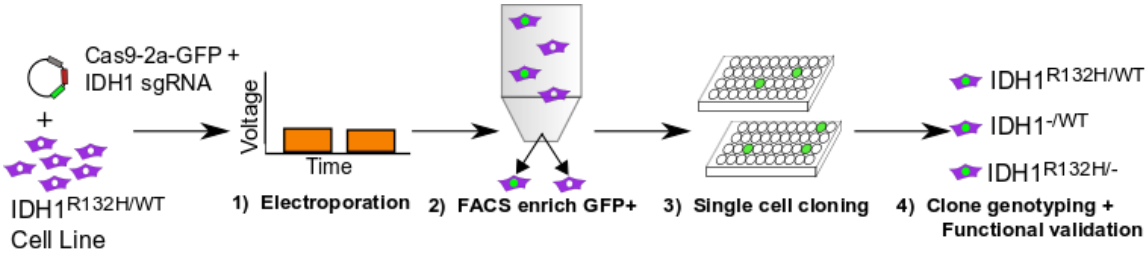

FIGURE 2.3: Diagram showing electroporation protocol for transient expression of plasmid based transgenes in patient-derived glioma lines with endogenous IDH1$^{R132H/WT}$ genotype.

Due to lower rates of clone formation in 08-0537 cells and other Neurocult-cultured cell lines, even before the electroporation step, we utilized a two step cloning procedure when attempting to isolate knockout clones in these cell lines (Figure 2.4).

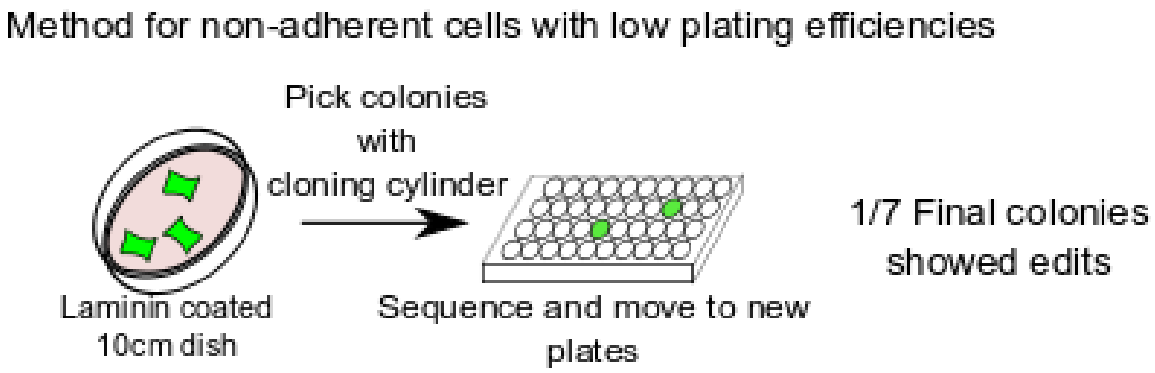

FIGURE 2.4: Diagram showing modifications to 08-0537 cloning proceedure.

To improve the likelihood of generating single cloned and edited cells we utilized flow cytometry to select for Cas9 activity using GFP expression as a surrogate marker, and strictly gated cells for GFP positivity before limiting dilution cloning (Figure 2.5). Utilization of this strategy allows for the systematic selection of clonal cells that have likely expressed Cas9 and an IDH1 targeting sgRNA due to the self-cleaving 2A peptide linking GFP protein expression and Cas9 protein expression (Pelletier and Sonenberg, 1988). Furthermore, selection of individual cell sub-clones after limiting clone dilution allows for picking "unedited" clones that could act as a control for DNA double strand break biological effects when attempting to identify effects linked to the active IDH1 mutation.

While attempting to grow clones we assessed ability to detect indels in the IDH1 locus in a qualitative fashion by amplifying in a non-biased PCR the IDH1 locus, without regard to IDH1 status, and then cloned amplicons into a plasmid for individual amplicon Sanger sequencing (Figure 2.6).

chch 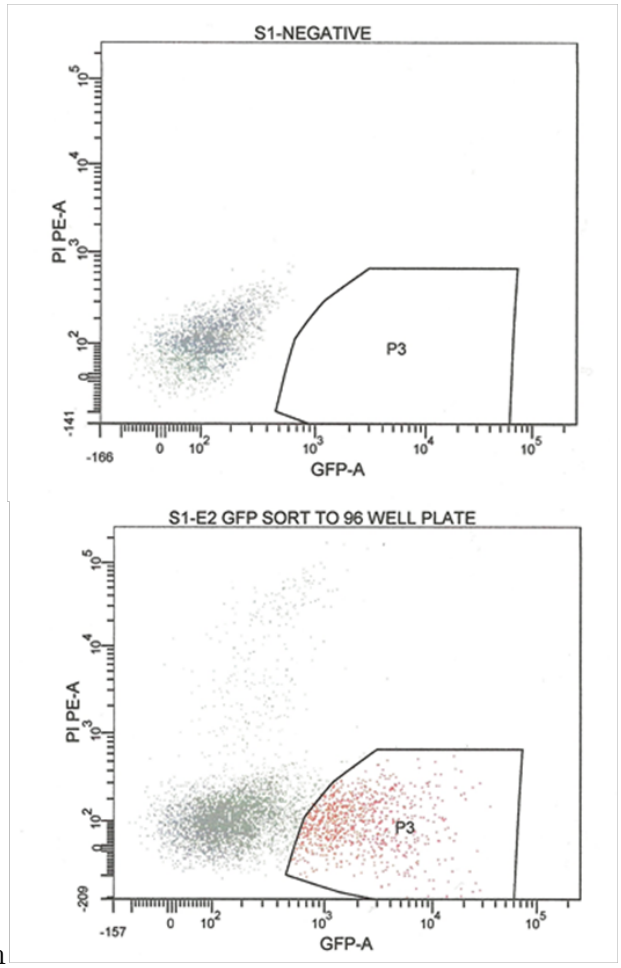

FIGURE 2.5: Example flow sorting results for IMA after electroporation. Cells mock-transfected with Cas9-2a-puro instead of Cas9-2a-GFP on top. Actual cells used for cloning gated for sorting on bottom. x-axis is GFP fluorescence and y-axis is counterstain with cell viability stain propidium iodide.

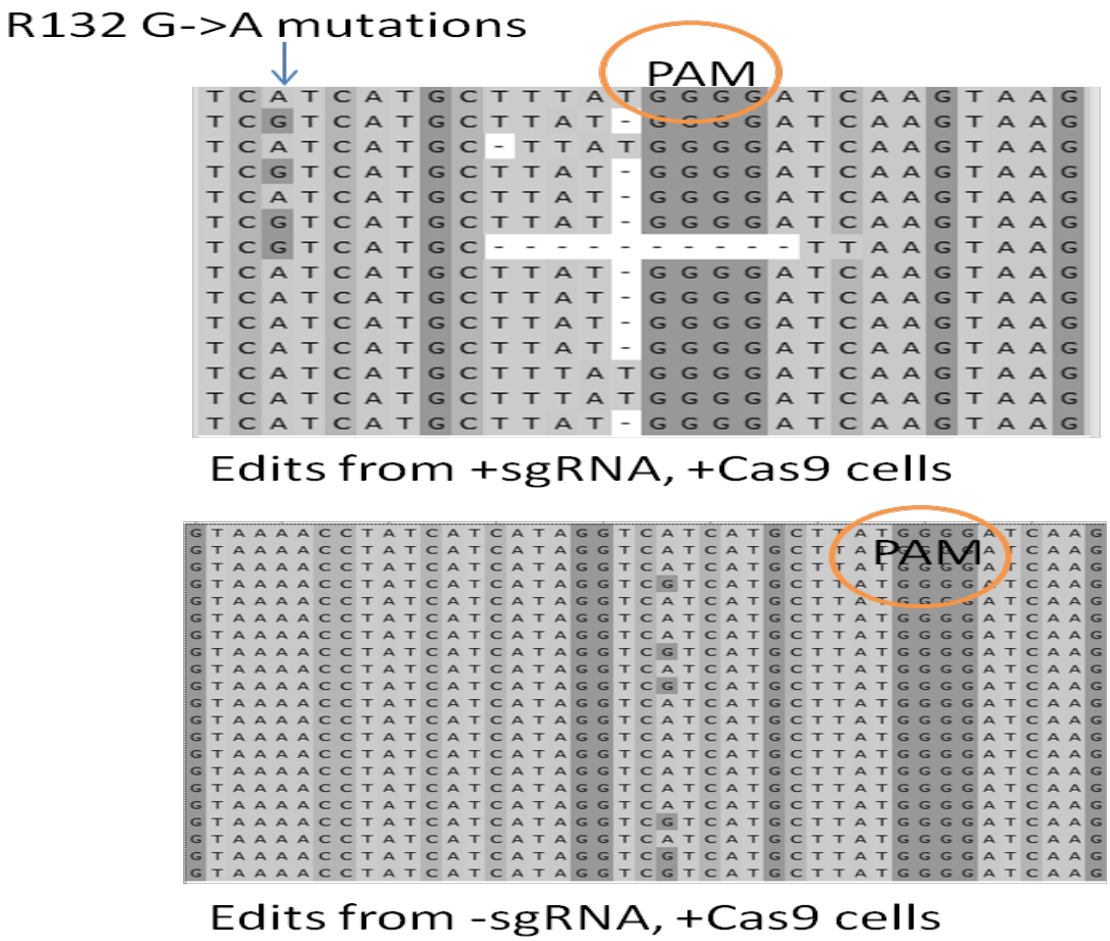

FIGURE 2.6: Cells were plated in 10cm dishes coated with laminin at low dilutions to allow identification of single attaching cells. After two months of culture one 10cm dish culture was sacrificed and PCR amplicons containing the targeting side were amplified, cloned into a plasmid vector, transformed and single colonies sequenced as previously reported (Cong et al., 2013).

Screening IMA cells across two experimental attempts using two sgRNAs against IDH1 produced approximately 200 clones for further characterization, which ultimately yielded three distinct clones with three distinct edits in the mutant allele (Figure 2.7). Although there were tens of clones containing IDH1 insertions/deletions (indels) in this experiment only three distinct edits were observable with two edits being from likely distinct clonal lineages because of mutually exclusive mutation pat-

terns. E.g. the presence of nucleotides in each clone that had been deleted in the other clone.

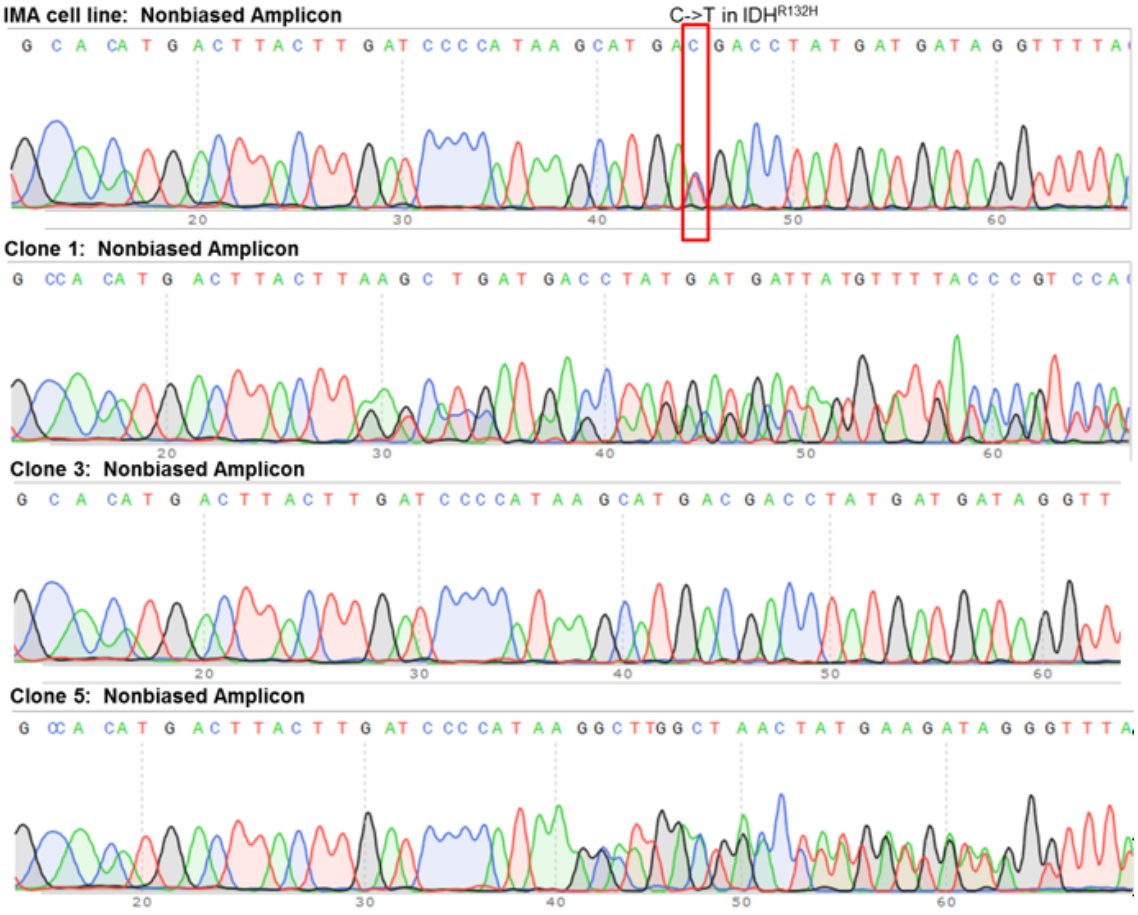

FIGURE 2.7: Amplicons containing the sgRNA binding site and IDH1c.395G¿A heterozygous mutation which gives rise to IDH1^{R132H} protein are shown for parental cells (top) and the three edited clones (bottom). Each clone contains a distinct pattern of edit with clone 3 showing a deletion larger than the amplicon, and hence only the wildtype *IDH1* allele.

To validate that indels in suspected knockout clones were truly knockouts we attempted Western Blot validation of IDH1 protein level. Western blotting cell protein lysates using a specific anti-human IDH1^{R132H} antibody or anti-total human IDH1 antibody showed IMA clones with nonsense mutations in the *IDH1*^{R132H} allele did not have detectable IDH1^{R132H} protein (Figure 2.9A and Figure 2.8).

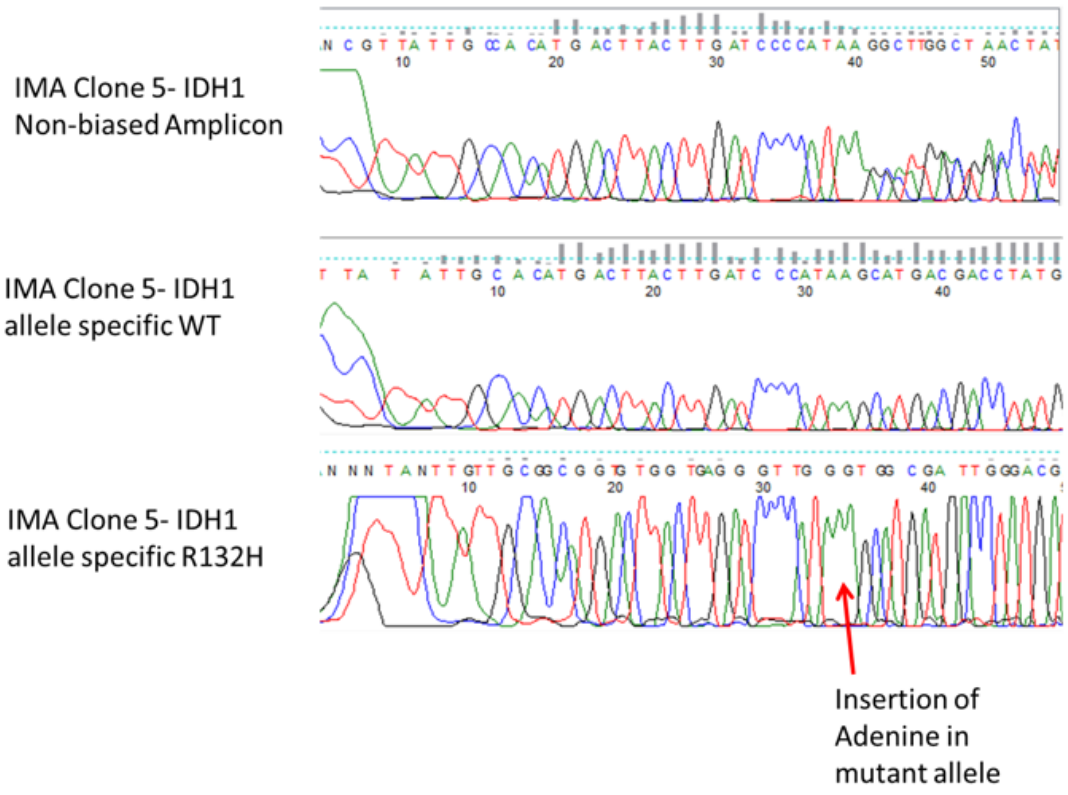

FIGURE 2.8: **Example Sanger sequence chromatograms for the IMA parental cells show evidence of CRISPR editing in several clones** A, Example edit in clone 5 showing a single base pair insertion overlapping the sgRNA binding site and causing a frameshift which is only present in the $IDH1^{\text{R132H}}$ allele specific PCR product. A single basepair insertion results in a frameshift and non-sense codon in the next exon

Furthermore, in IMA, D-2HG production levels were reduced by 100-1000 fold in clones with frameshift mutations in the $IDH1^{R132H}$ (2.10A and Figure 2.9B). Providing functional evidence that mutant IDH1 mediated D-2HG production had been eliminated due to the indels and loss of protein expression.

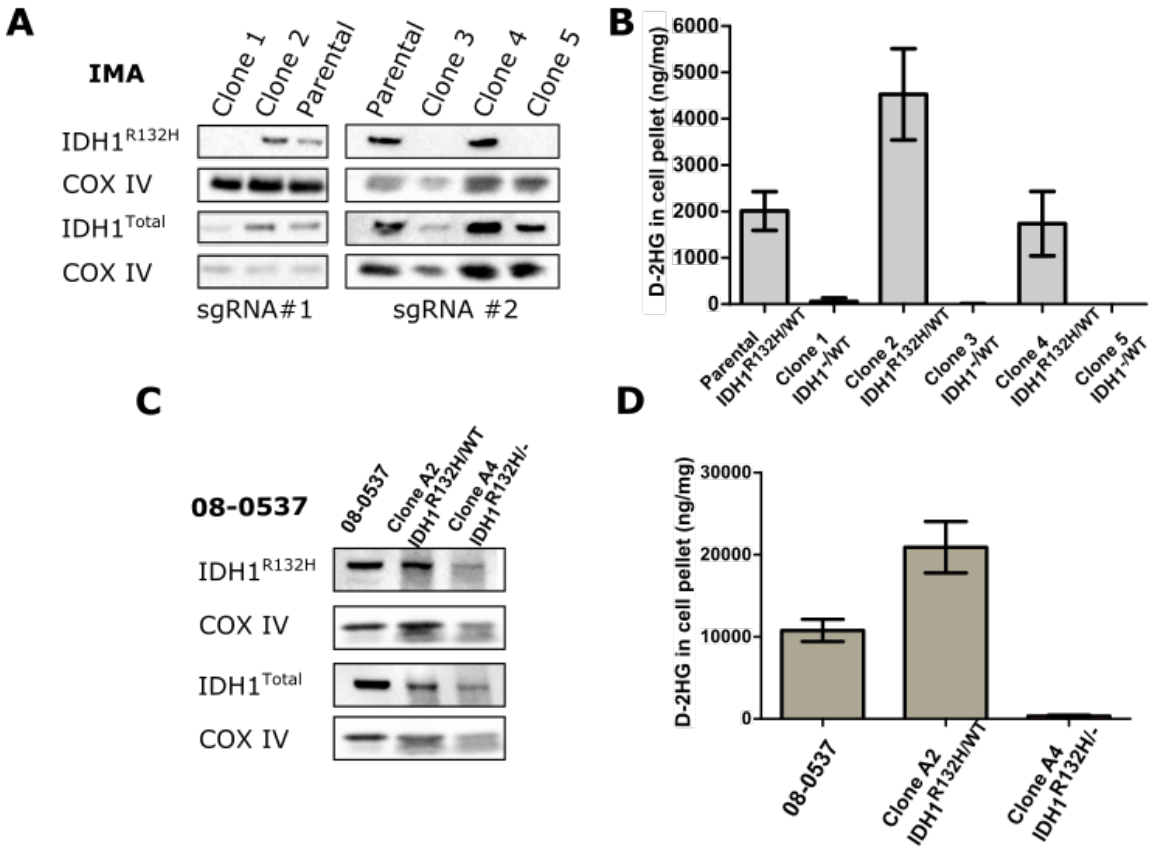

FIGURE 2.9: A, IMA single cell clones with edits in the IDH1R132H allele producing putative non-sense transcripts do not have IDH1R132H protein that is detectable by Western blot; however, they do retain a band in total IDH1 protein. COX IV as loading control. B, Functionally, cells without detectable expression of IDH1R132H protein and with putative heterozygous knockouts of the IDH1R132H allele by Sanger sequencing do not produce pathological amounts of D-2HG as assessed by LC-MS in the cell pellets. C, Western blotting of 08-0537 clones isolated in this study for total IDH1, IDH1R132H, or COXIV loading control. IDH1R132H protein is still detectable in edited clone A4 suggesting wildtype allele specific editing. D, D-2HG levels as assessed by LC-MS in 08-0537 parental cells in the cell culture pellet. Values for cell culture pellets are normalized to total protein content of the cell pellet sample using bicinchoninic acid assay. For all experiments, N=3. Images are representative results.

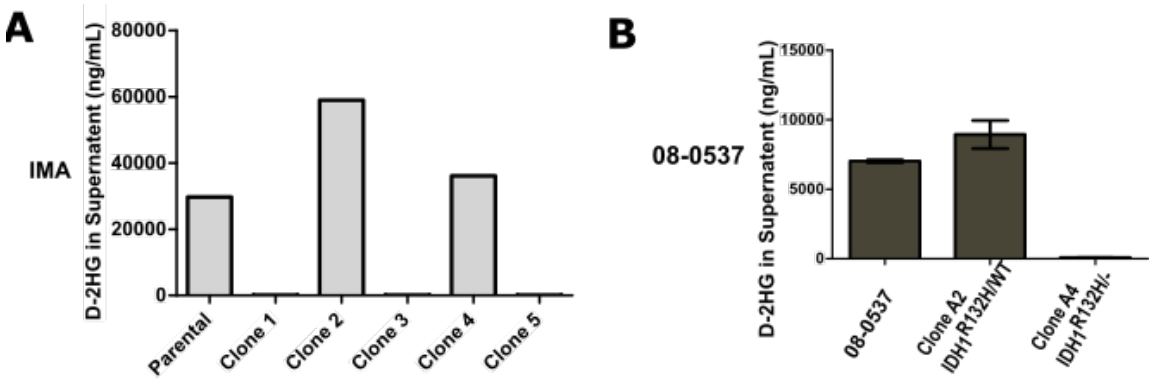

FIGURE 2.10: A, D-2HG level in the supernatant of IMA cells. 150,000 cells were plated in 6 well plates and D-2HG level was assessed 4 days post-plating. B, D-2HG level in the supernatant of 08-0537 parental cells or CRISPR treated clones. For 08-0537 cells were grown on laminin coated plates for these experiments.

Likewise, cloning of 08-0537 cells generated seven sub-clones which contained at least one clone with a nonsense mutation in the wildtype IDH1 allele (Figure 2.11).

08-0537 clones with nonsense mutations in the wildtype IDH1 allele retained a band at the expected weight for mutant IDH1 in a Western blot specific for $IDH1^{R132H}$ but no longer produced elevated amounts of D-2HG (Figure 2.9C and D and Figure 2.10B). This observation corroborates previous reports that heterozygosity for the IDH1 mutation is necessary for efficient production of D-2HG (Jin et al., 2013).

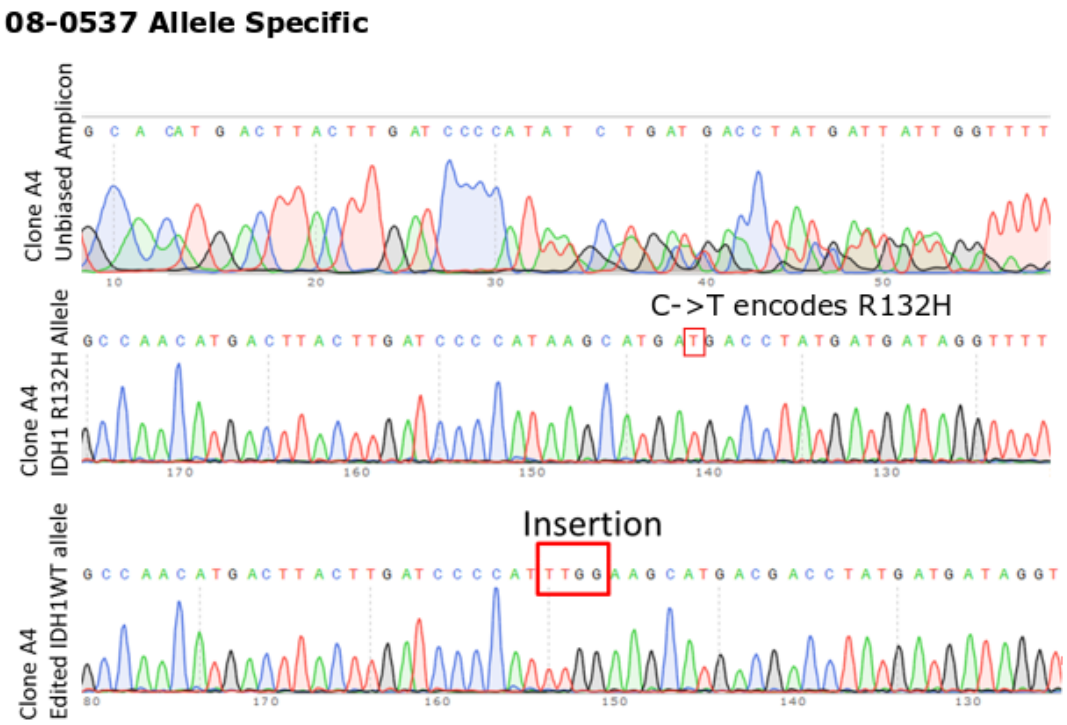

FIGURE 2.11: **Example Sanger sequence chromatograms for the 08-0537 parental cells show evidence of CRISPR editing in a clones** Confirmatory Sanger sequencing of allele specific products showing a four basepair insertion in the *IDH1-WT allele* of 08-0537 clone A4.

2.3.2 *Loss of D-2HG is not sufficient to completely reverse the G-CIMP phenotype in patient-derived glioma cell lines*

As D-2HG production is sufficient to induce a genome-wide pattern of CpG island hypermethylation and is necessary for the maintenance of a majority of this hypermethylation in previously described astrocyte models (Turcan et al., 2018), we investigated whether our genetic models of *IDH1* loss, of either WT or mutant allele, would show any widespread changes in CpG hypermethylation. We profiled CpG methylation using Illumina's EPIC array for parental, IDH1 knockout, or unedited IMA clones and performed unsupervised hierarchical clustering of samples. We observed that clones with loss of D-2HG production clustered together while parental and non-edited clones clustered together, suggesting that loss of $IDH1^{R132H}$ may be sufficient to induce genome-wide methylation changes, and is consistent with the previous report in human astrocytes (Turcan et al., 2018)(Figure 2.12A, and Figure 2.13).

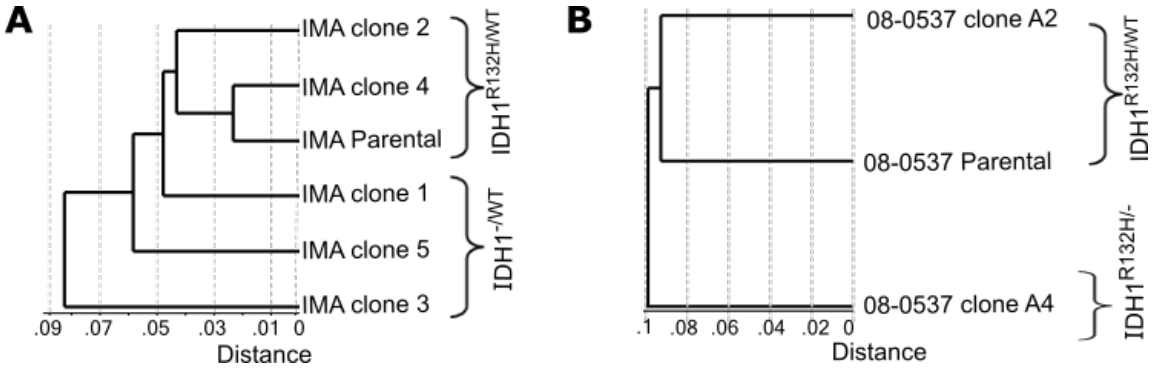

FIGURE 2.12: A, Unsupervised hierarchical clustering of IMA clones based on correlation of methylation beta values clusters IMA clones with $IDH1^{R132H/WT}$ genotype with parental $IDH1^{R132H/WT}$ IMA cells. Distance is given in 1-r (pearson correlation distance). B, Similarly, unsupervised hierarchical clustering of 08-0537 clones using the same methodology shows unedited clones cluster with parental cells.

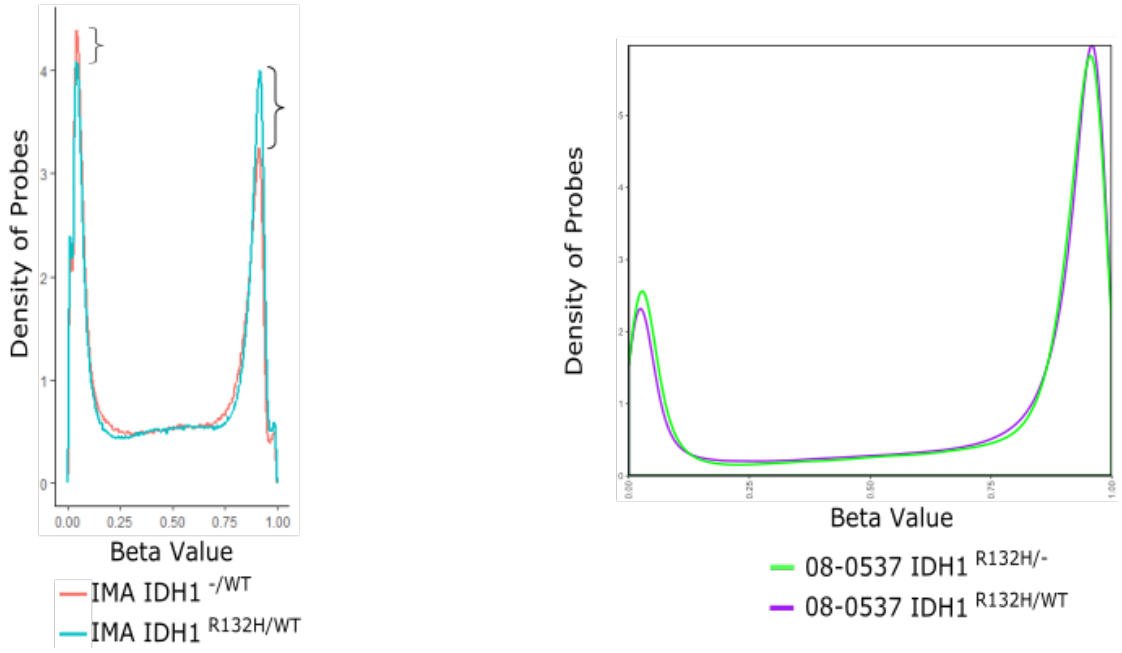

FIGURE 2.13: Averaged density plot of beta values of IMA IDH1$^{-/WT}$ clones compared to parental IMA cells. Shown in brackets is loss of hypermethylation peak in the parental cells and gain of hypomethylation peak in IMA$^{-/WT}$ clones.

Similarly, in cell line 08-0537 the parental cells and non-edited clones cluster together, while the wildtype loss clone shows greater distance (Figure 2.12B). Next, we grouped the clones into edited and unedited subsets, and assessed the difference in beta value between clones for each CpG site individually using the DMP algorithm in the ChAMP processing pipeline. In our control condition we detected 6417 CpG sites showing differential methylation between parental and unedited clones, but between parental and edited clones we detected many more significantly differentially methylated probes, 16777CpGs in total. We further refined this list by imposing a condition of delta Beta values $\leqslant$ -0.2 in all four D-2HG deficient clones across both IMA and 08-0537, and without recurrent delta Beta values $\leqslant$ -0.2 in any unedited clone. We identified a list of 971 probes most tightly associated with loss of mutant IDH1-mediated D-2HG production across both lines.

To determine what the observed DNA methylation differences mean in the context of known DNA methylation patterns conferred by the IDH1 mutation, we specifically focused on previously reported G-CIMP associated loci that are used for classification of G-CIMP status (Noushmehr et al., 2010). In cell line IMA we did not detect appreciable variation between clones in the methylation of the 7 CpG-loci previously identified as being most tightly linked to the G-CIMP phenotype (Figure 2.14) (Noushmehr et al., 2010). Specifically, in IMA cells 6/6 hypermethylated sites used to classify tumors as G-CIMP retained hypermethylation following $IDH1^{R132H}$ loss (β>0.7) and 1/1 sites hypomethylated in G-CIMP retained hypomethylation (β<0.2). (Figure 2.14) (Noushmehr et al., 2010). In comparison, the hypermutated line 08-0537 showed discrepancy in one probe used to classify G-CIMP hypermethylation and one probe for G-CIMP linked hypomethylation, yet knockout of wild-type IDH1, and consequent loss of D-2HG production, did not result in significant demethylation of those G-CIMP associated loci that were hypermethylated in the parental cells (Figure 2.14).

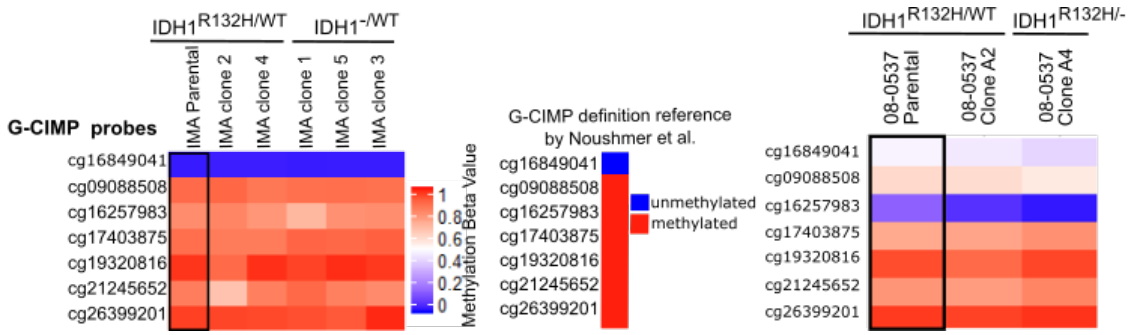

FIGURE 2.14: Observation that G-CIMP sites most indicative of G-CIMP retain G-CIMP linked alterations in methylation pattern in all clones irrespective of IDH1R132H allele status. Note that while 8 sites are typically used for G-CIMP identification on the 450K array only 7 of these sites are present in the methylation EPIC array used in this work. Therefore, conservatively 6/7 sites must display the G-CIMP pattern to enable a call of G-CIMP positive. Site cg16849041 is hypomethylated in G-CIMP and hypomethylated in all IMA samples analyzed. The other 6 sites are hypermethylated in G-CIMP and show hypermethylation ($\beta \geqslant .7$) in all IMA clones analyzed. The 08-0537 cells may not fit the definition of G-CIMP positivity based on the 7 site definition; however, sites that are hypermethylated retain hypermethylation in all clones.

When we attempted to cluster samples using Euclidean distance and complete linkage using only the 7 G-CIMP loci under consideration, there was no grouping of clones based on IDH1 editing status (Figure 2.15A). In looking at other CpG sites of potential clinical interest, such as MGMT-SPT27 (Capper et al., 2018), we observed methylation was retained, suggesting loss of $IDH1^{R132H}$ is not sufficient to completely remove the hypermethylation phenotype in human astrocytoma cell lines (Figure 2.15B).

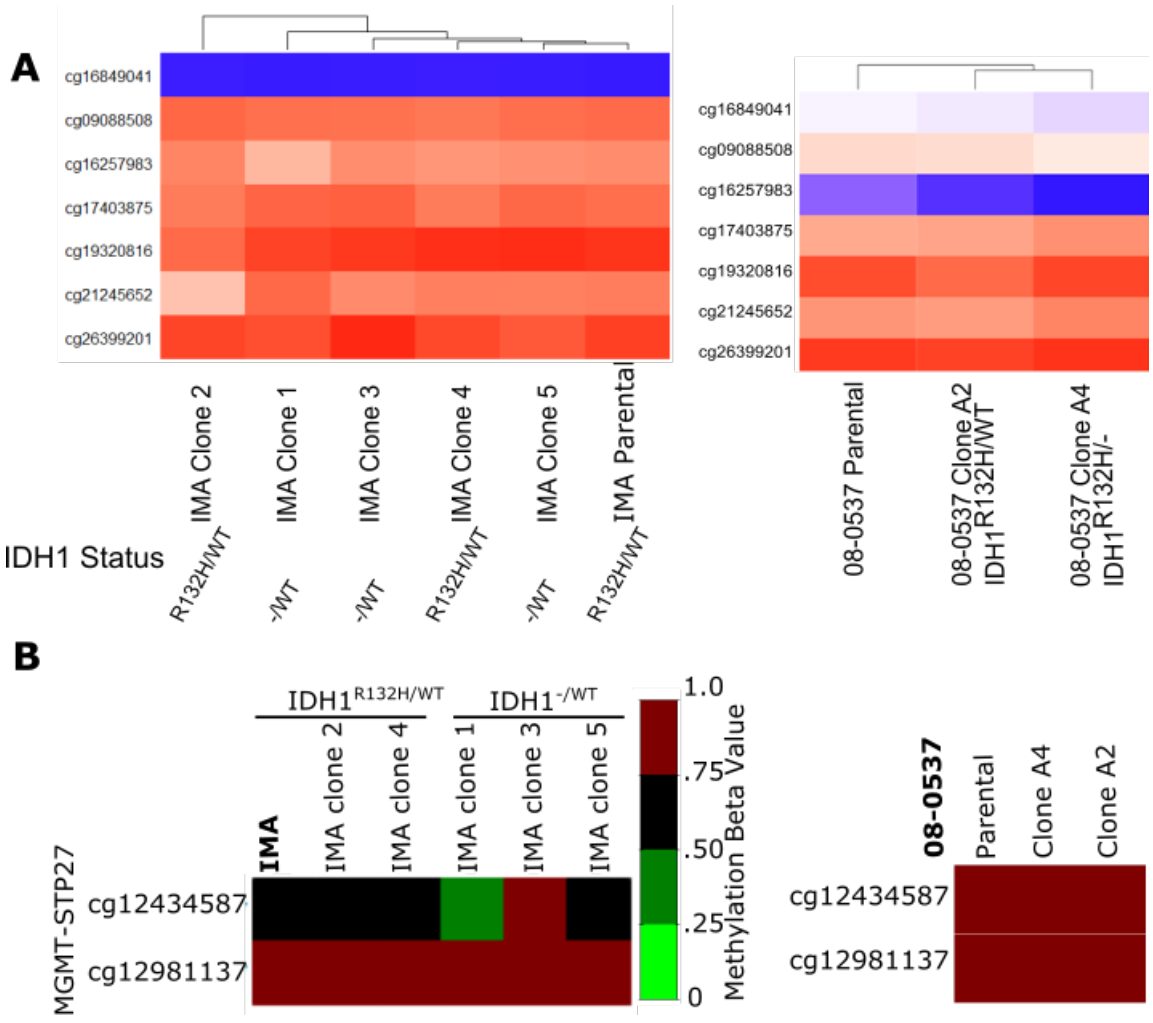

FIGURE 2.15: A, Hierarchical clustering of G-CIMP 7 loci using Euclidean distance and complete linkage; note no clustering by IDH1 editing status. B, MGMT promoter sites identified as being correlated with expression and used as the basis of the MGMT-STP27 classification tend to retain intermediate to high levels of methylation on IDH1-/WT knockout.

To observe differences in CpG methylation changes that might be driving the clustering of the edited clones, we binned extreme methylation changes (Beta value change of clone – parental <-0.4). We noted that in both IMA and 08-0537 cell lines the loss of the IDH1$^{R132H/WT}$ heterozygous state was associated with a greater number of probes showing dramatic demethylation (delta Beta <-0.4) than in unedited control cells (Figure 2.16A and 2.16B).

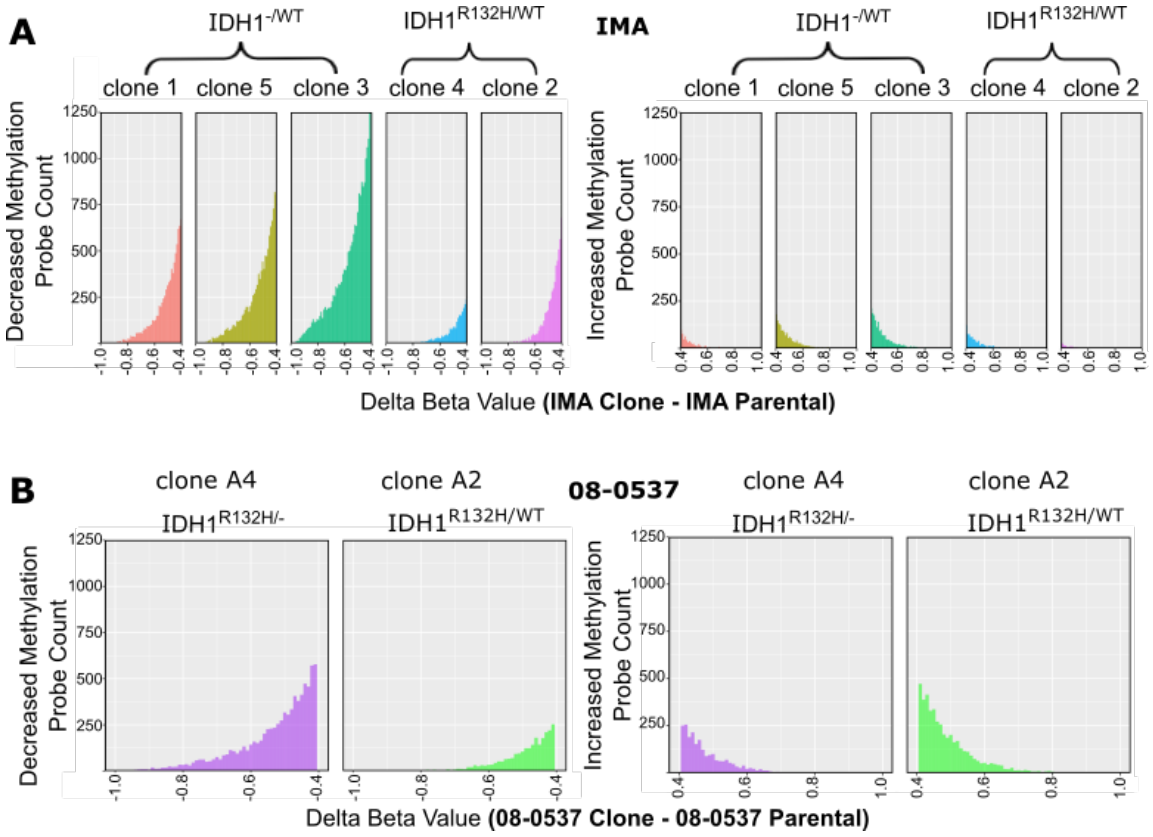

FIGURE 2.16: A, Histogram plots of genome-wide beta value differences (Parental IMA cells – averaged values from either IDH1$^{R132H/WT}$ clones or IDH1$^{-/WT}$ clones) shows that methylation loss is the predominant change in methylation identified in the genome-wide pattern of clones; and, the IDH1$^{-/WT}$ cells show greater loss of genome-wide methylation compared to IDH1$^{R132H/WT}$ clones. Each clone was passaged at least 10 population doublings post-single cell cloning. B, The 08-0537 clone with loss of heterozygosity at the IDH1 locus also shows more pronounced CpG demethylation patterns than its matched unedited clone.

2.3.3 Loss of D-2HG production is associated with reductions in DNA methylation at specific G-CIMP-low associated sites

Having seen differences in levels of demethylation between edited and unedited clones, we hypothesized that the demethylation could indicate the acquisition of a G-CIMP-low methylation state. We extracted the 131 probes identified as being hypomethylated in G-CIMP-low tumors as previously reported (Ceccarelli et al., 2016) and performed unsupervised hierarchical clustering using Euclidean distance of the samples (Figure 2.17).

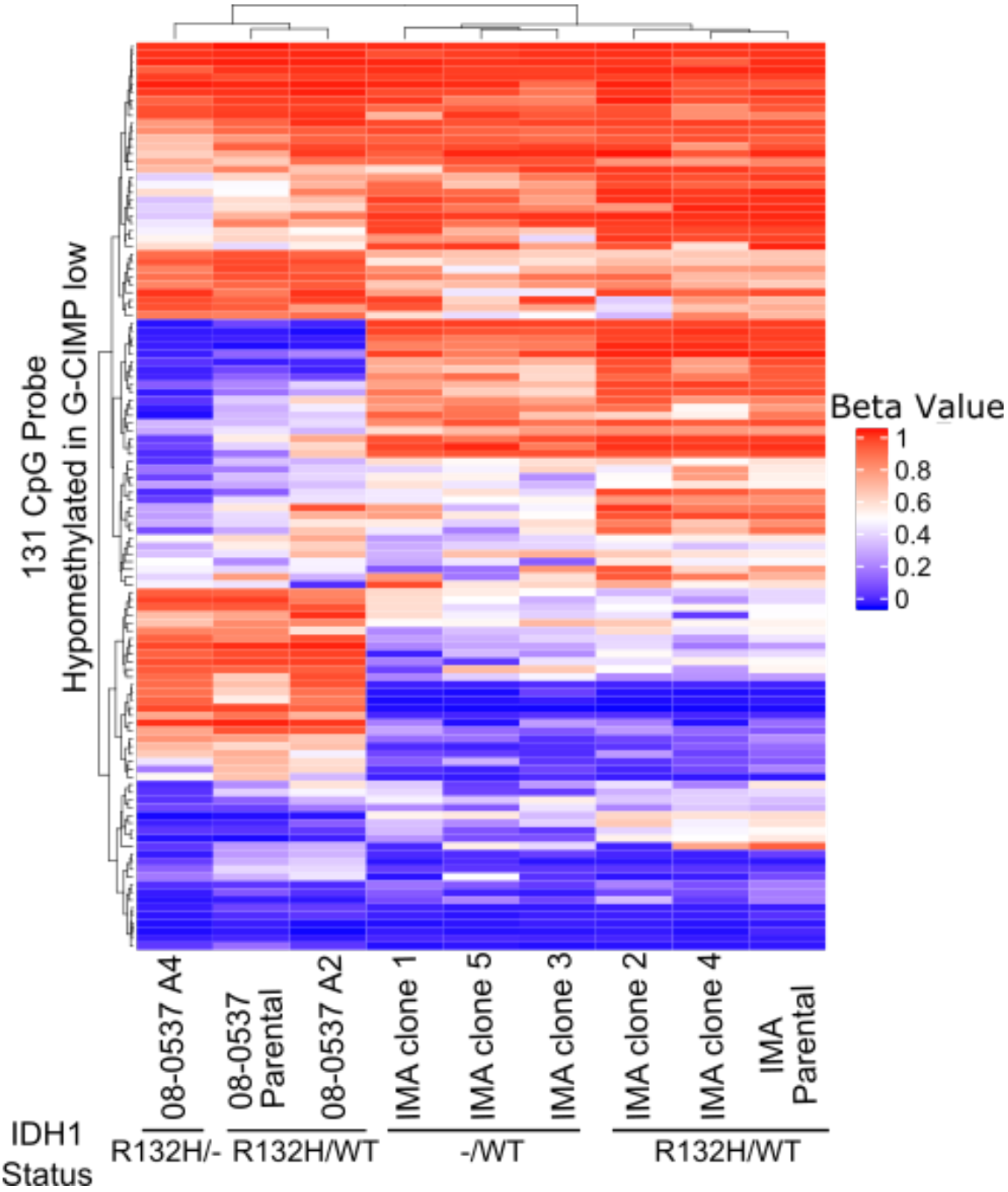

FIGURE 2.17: Unsupervised hierarchical clustering based on Euclidean distance of 131 probes hypomethylated in G-CIMP-low shows that, within cell lines, cells with intact heterozygous IDH1$^{R132H/WT}$ mutations tend to cluster together, and this clustering is likely driven by demethylation of a subset of probes in clones with altered IDH1.

We did not observe an exact recapitulation of the 131 site hypomethylation previously identified in patient tumors as defining the G-CIMP-low state, and many probes retained hypermethylation (Beta>0.7). However, we did observe that clones with CRISPR-mediated IDH1 alterations seemed to have overall lower levels of methylation in the 131 sites when we compared edited sub-clones to parental cells or to unedited sub-clones of the same cell line (Figure 2.18).

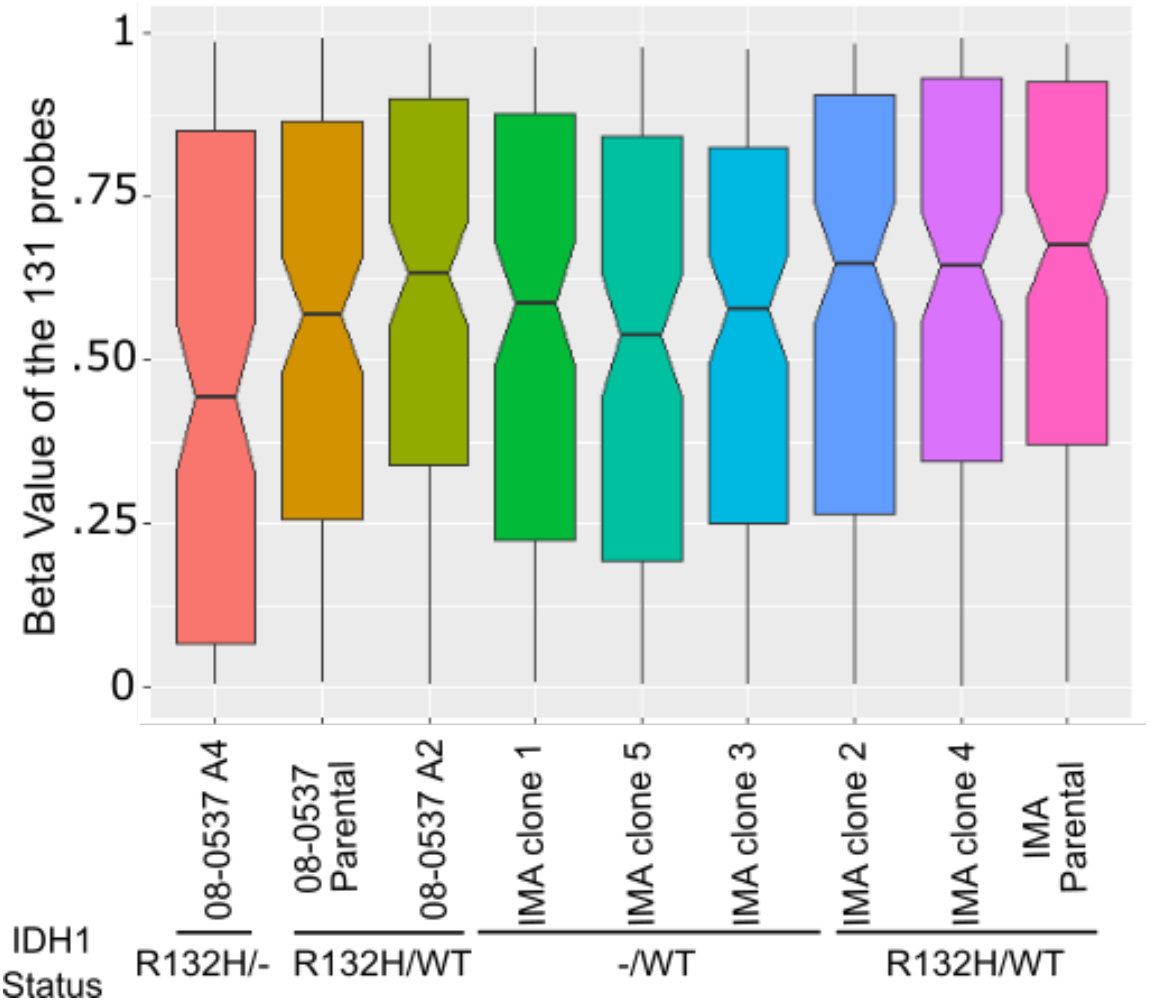

FIGURE 2.18: Notched boxplots showing median and confidence interval for methylation level of the 131 CpG probes. Clones with altered IDH1 show the largest decreases in median methylation level compared to their matched unedited controls.

Previous TCGA results characterizing the G-CIMP-low state also report a relative

enrichment for demethylation within CpG open sea regions, and a relative absence of CpG demethylation in CpG islands (Ceccarelli et al., 2016). While removing sites that showed methylation changes in unedited clones as a control, we explored the genomic context of all CpG sites showing conserved demethylation (delta Beta $\leqslant$-0.2) in all edited clones. In both IMA as well as 08-0537 there was a distinct over representation of demethylated CpG sites at intergenic open seas, 5'-UTR open seas, and CpG shore sites 1500 base pairs from transcription start sites (Figure 2.19A and Figure 2.19B).

We observed the relative absence of CpG demethylation in CpG islands, especially within the CpG regions 200bp from transcription start sites, as well as CpG sites located within gene bodies compared to the background frequency of these sites on the EPIC array. Previous reports, first describing a G-CIMP-low like state in astrocytoma, found similar patterns of demethylation when comparing global methylation patterns of identified G-CIMP-low cases with G-CIMP-high cases (Ceccarelli et al., 2016). Specifically, it was shown that G-CIMP-low cases showed enrichment for demethylation in CpG open sea regions, and under representation of demethylation in CpG islands when comparing differential probes of G-CIMP-low cases with all probes profiled (Ceccarelli et al., 2016). The genomic context of CpG probes undergoing demethylation in our model of IDH1 loss is therefore similar to the genomic context of CpG probes showing hypomethylation in the G-CIMP-low pattern in patient tumors.

2.3.4 Copy number analysis of isogenic clones

Others have previously shown that in IDH1$^{R132H/WT}$ gliomas, loss of heterozygosity at Chr2q, which contains the *IDH1* locus, leads to loss of methylation at a variety of sites outside of CpG islands (Mazor et al., 2017). We therefore, utilized copy number calls using the conumee R package to show that there were no copy number

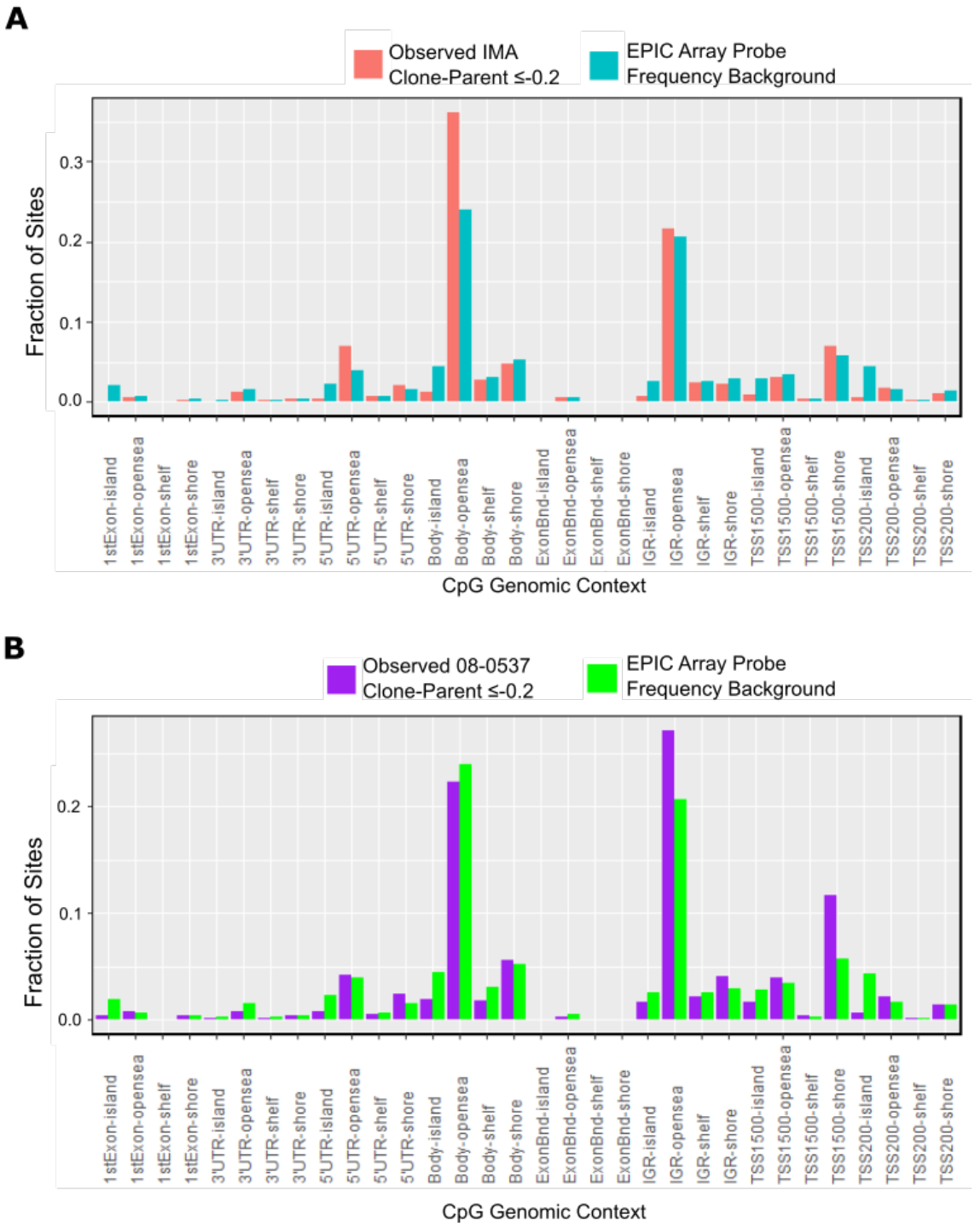
A
Observed IMA
Clone-Parent ≤-0.2
EPIC Array Probe
Frequency Background
Fraction of Sites
0.3
0.2
0.1
0.0
1stExon-island
1stExon-opensea
1stExon-shelf
1stExon-shore
3'UTR-island
3'UTR-opensea
3'UTR-shelf
3'UTR-shore
5'UTR-island
5'UTR-opensea
5'UTR-shelf
5'UTR-shore
Body-island
Body-opensea
Body-shelf
Body-shore
ExonBnd-island
ExonBnd-opensea
ExonBnd-shelf
ExonBnd-shore
IGR-island
IGR-opensea
IGR-shelf
IGR-shore
TSS1500-island
TSS1500-opensea
TSS1500-shelf
TSS1500-shore
TSS200-island
TSS200-opensea
TSS200-shelf
TSS200-shore
CpG Genomic Context
B
Observed 08-0537
Clone-Parent ≤-0.2
EPIC Array Probe
Frequency Background
Fraction of Sites
0.2
0.1
0.0
1stExon-island
1stExon-opensea
1stExon-shelf
1stExon-shore
3'UTR-island
3'UTR-opensea
3'UTR-shelf
3'UTR-shore
5'UTR-island
5'UTR-opensea
5'UTR-shelf
5'UTR-shore
Body-island
Body-opensea
Body-shelf
Body-shore
ExonBnd-island
ExonBnd-opensea
ExonBnd-shelf
ExonBnd-shore
IGR-island
IGR-opensea
IGR-shelf
IGR-shore
TSS1500-island
TSS1500-opensea
TSS1500-shelf
TSS1500-shore
TSS200-island
TSS200-opensea
TSS200-shelf
TSS200-shore
CpG Genomic Context

calls consistently changed among isogenic knockout clones in the IMA cell line (Figure 2.20).

2.4 Discussion

Utilizing patient-derived grade III and grade IV glioma cell lines from IDH1 mutant tumors, we have generated isogenic glioma cell lines that differ in the mutation status of IDH1. We show that knockout of either wildtype or R132H encoding *IDH1* allele was sufficient to eliminate elevated D-2HG production. We further characterize the DNA methylome of these isogenic pairs of cells to reveal that although some of the G-CIMP loci retain hypermethylation on loss of D-2HG, there is a genome-wide pattern of measurable demethylation especially in open sea regions and CpG island shores. While the G-CIMP-low phenotype does not strictly require loss of an *IDH1* allele in patient tumors, there are identified subsets of tumors with copy number alterations at the *IDH1* locus that display a G-CIMP-low phenotype (Mazor et al., 2017). Therefore, our results support the possibility that loss of an IDH1 allele and D-2HG production may be a driving factor of methylation changes in this subset of recurrent tumors (Mazor et al., 2017). In our IDH1-mutant glioma cell lines, we found that knockout of either $IDH1^{WT}$ (in 08-0537) or $IDH1^{R132H}$ (IMA) was suffi-

---

FIGURE 2.19 *(preceding page)*: Genomic context of differentially methylated probes shows enrichment for open sea regions of the genome and CpG Island shores near transcription start sites. A, Fraction of CpG sites identified as differentially methylated with change in Beta value ⩽-0.2 concurrent in all three $IDH1^{-/WT}$ clones of IMA and no corresponding change in Beta value ⩽-0.2 in either unedited clone. Plotted in blue is the frequency of CpG sites within each genomic context on the EPIC array. Chi-squared goodness of fit p-value for difference from expected background frequency < 2.2x10^-16 B, Similar enrichment plot for 08-0537 using change in Beta value ⩽-0.2 in the clone with loss of heterozygous $IDH1^{R132H/WT}$ status and removing probes showing a delta Beta value ⩽-0.2 change in matched unedited control clone. Chi-squared goodness of fit p-value for difference from expected background frequency < 2.2x10^-16.

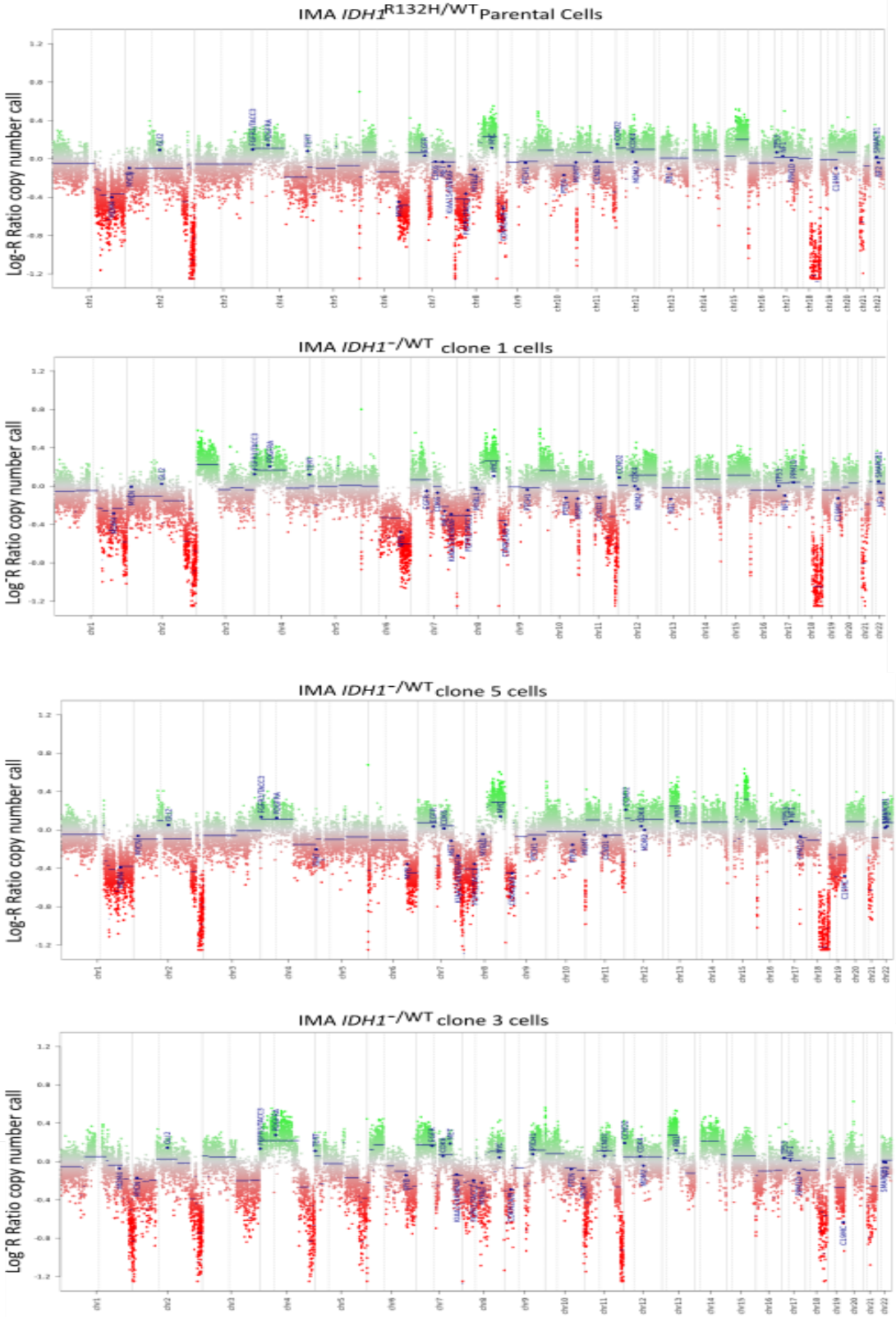
IMA IDH1R132H/WT Parental Cells
Log-R Ratio copy number call
IMA IDH1−/WT clone 1 cells
Log-R Ratio copy number call
IMA IDH1−/WT clone 5 cells
Log-R Ratio copy number call
IMA IDH1−/WT clone 3 cells
Log-R Ratio copy number call

cient to induce a trend of demethylation. This is consistent with loss of D-2HG mediated inhibition of alpha-ketoglutarate-dependent epigenetic enzymes, such as the ten-eleven translocation genes (TETs). Additionally, our results are complementary to previously published models used in investigations that characterized methylation changes after inhibitor treatment or spontaneous loss of *IDH1* alleles (Mazor et al., 2017). While the natural losses of single *IDH1* alleles tends to co-occur with multiple gene deletions on Chr2q, our cell models have no conserved significant differences in Chr2q copy number between clones at the locus surrounding *IDH1*, which allows us to parse effects of $IDH1^{R132H}$ loss from passenger effects of co-deleted genes (Mazor et al., 2017).

Likewise, small molecule inhibitors may have their own off-target effects, and might be difficult to apply consistently over the long periods of in vitro culture that have been required to see D-2HG suppression-mediated demethylation effects (Rohle et al., 2013; Tateishi et al., 2015; Turcan et al., 2018). For these reasons the use of genetically-engineered patient-derived IDH1 mutant cell lines provide a novel and complementary approach for studying the roles of IDH1 in maintenance of IDH1 mutation linked epigenetic changes over long time courses. While we cannot rule out the possibility that the genome wide patterns of demethylation observed were pre-existing alterations in a subset of the parental cell population, our results do suggest that loss of D-2HG production is causally related to genome wide changes in methylation. These methylation changes are largely limited to decreased hypermethylation in sub-sets of the G-CIMP-low loci in open sea CpG contexts, and we did not observe significant reversions of DNA hypermethylation in most contexts

---

FIGURE 2.20 *(preceding page)*: Conumee generated copy-number calls for IMA parental cells (top) or IMA IDH1-/WT clones (bottom) across the genome. Also highlighted in blue are individual commonly copy-altered cancer genes for each chromosome to aid orientation.

within gene promoters. Nonetheless 19/1308 CpG loci used previously (Ceccarelli et al., 2016) to cluster IDH1 mutant gliomas from IDH1 wildtype gliomas did show changes in methylation (absolute change in Beta > 0.2) in the IMA edited clones as detected by ChAMP calling of differentially methylated probes. This is in comparison to 6/1308 CpG probes being detected as DMPs in the unedited IMA clones. The retained hypermethylation in promoters may be a combination of methylation and 5-hydroxymethylation due to the inability of the detection modality to discriminate between the two marks; however, the observed complete removal of methylation in the G-CIMP-low loci is not affected by this limitation.

Recent studies have suggested that low levels of demethylation in IDH1-mutant G-CIMP positive gliomas may occur via passive demethylation (Nomura et al., 2019). This interpretation is based on the observation that demethylated loci in G-CIMP-low gliomas correlate closely with late replicating genomic regions of neural stem cells, and these late replicating regions may have insufficient methylation maintenance activity by DNMT1, occurring due to increasing genome replication rate (Nomura et al., 2019). Importantly, our results show that suppression of D-2HG production is likely a modifier of DNA methylation in IDH1 mutant tumors; however, further experiments will be required to understand whether the demethylation we observed in the IDH1 edited clones is due to changes in the fidelity of DNA maintenance methylation and consequently passive demethylation or alternatively to changes in active demethylation.

In future work it will be important to determine if these losses of DNA methylation in G-CIMP-low loci affect the activity of enhancer elements located in intergenic open sea regions, and what effects these activity changes have on the tumorigenicity of IDH1 mutant glioma cells. Although previous pre-clinical reports suggest that these methylation reversions are not required to see therapeutic effect of small molecule IDH1 inhibitor treatment (Rohle et al., 2013), there could be heterogeneity

in the dependence of different IDH1 mutant gliomas to the various epigenetic changes induced by the IDH1 mutation. We speculate that this heterogeneity in dependence and stability of the promoter associated DNA methylation could contribute to the failure to achieve therapeutic benefits following inhibition of mutant IDH1 in some orthotopic xenograft models (Kopinja et al., 2017; Tateishi et al., 2015). In conclusion, this study provides new ways of modeling IDH1 mutant glioma in a genetically relevant background that complements existing methods. We show that these models exhibit hypermethylation at the most conserved G-CIMP loci which persists after loss of IDH1 mutation linked D-2HG production. Furthermore, we also show loss of neomorphic IDH1 mutation results in broad genome-wide changes in CpG methylation in the G-CIMP-low like genomic context of open seas, similar to patient tumors and astrocyte overexpression systems (Mazor et al., 2017; Turcan et al., 2018; Zhang et al., 2014). Future work that utilizes these genetically relevant models will help to elucidate how IDH1 mutations continue to contribute to the malignant phenotype of IDH1 mutant glioma.

3

Chapter 3: CRISPR-Screen for Synthetic Sick/Lethal Interactions to the IDH1 Mutation

3.1 Introduction

D-2HG can affect the activity of alpha-ketoglutarate (α-KG) dependent enzymes due to structural similarity and as a result causes pro-tumorigenic changes in gene expression (Flavahan et al., 2016; Koivunen et al., 2012). However, this generally pro-tumoral gene expression reprogramming comes with potential metabolic costs. These costs include conversion of NADPH and α-KG into NADP+ and D-2HG respectively, and the inhibition of α-KG dependent enzymes such as transaminases (Dang et al., 2009; Lai et al., 2011). Consequently, both the imposed metabolic flux and D-2HG itself can alter conventional cell physiology and shape selective pressures in IDH mutant glioma cells (Carbonneau et al., 2016; Chen et al., 2014; Grassian et al., 2014; McBrayer et al., 2018). Understanding how IDH1 mutant cells adapt to the presence of the mutant enzyme and its imposed pressures will catalyze the development of new precision therapies for IDH1 mutant glioma. We utilized isogenic human glioma cell lines reported in previous chapters to explore the signaling

milieu that provides a fitness advantage to IDH1 mutant cells by applying a focused sub-genomic CRISPR-Cas9 library in a proof of principle systematic screen. The pathways uncovered include proteasome function, DNA repair, and specific regulators of the mTOR signaling pathway. Thus, this study reveals potential genetic elements that promote the fitness *in vitro* of IDH1 mutant glioma cells, and provides a valuable framework for further studies in understanding and exploiting IDH1 mutations in gliomas.

3.2 Methods

3.2.1 Lentiviral CRISPR-Cas9 Screening Library: Plasmid Construction

The lentiCRISPRv2 screening library was a kind gift from the Kris Wood Lab at Duke University. Briefly, a manually curated list of sgRNA sequences, 5 per gene for 2400 genes, was extracted in silico from the Activity-Optimized Human CRISPR Pooled Library (Wang et al., 2014). Individual guides were synthesized using oligonucleotide array synthesis and cloned into lentiCRISPRv2 using previously established Gibson cloning based protocols (Shalem et al., 2014). Distribution of individual sgRNA counts in the plasmid library were assessed before virus creation using NGS services provided by Hudson Alpha to ensure adequate representation of individual guides for pooled screening and appropriate GINI coefficients of .1.

3.2.2 Lentiviral CRISPR-Cas9 Screening Library: Virus Preparation

Six, 10 cm dishes of passage 10 HEK293FT cells were plated at 70% confluence 16 hours before transfection for virus creation in 10 mL of DMEM media supplemented with .1X of NEAA and 10% FBS. For transfection, 3 μg of pCMV-dR8.92_dvpr was co-transfected with 5 μg of lentiCRISPRv2 library and 2 μg of pCMV-VSV-g using Lipofectamine 2000 in a 1:3 ratio of plasmid to lipid reagent in Opti-MEM media. At 16 hours post-transfection, media was changed to virus production media containing

DMEM +1%BSA +20%FBS + 138 mg/mL sodium butyrate. Virus was harvested at 36 hours post media change and again at 60 hours post media change by removing conditioned medium, passing medium through .45 μM cellulose acetate filter and then concentrating overnight with PEG6000 as previously described (Kutner et al., 2009). Concentrated lentivirus was suspended in PBS and snap-frozen in dry-ice/ ethanol and stored long term at -80°C. A functional titer for each virus aliquot was determined using IMA cells subjected to puromycin selection after polybrene (8 μg/mL) enhanced transduction and varying concentrations of virus. All selection was performed using 1 μg/mL puromycin. Viral Titration for validation sgRNAs was performed by the Functional Genomics Shared Resource at Duke University.

3.2.3 Lentiviral CRISPR-Cas9 Screening Library: Infection and Sample Processing

A total of 72 million cells were plated at a density of 3 million cells per 15 cm dish in full media containing 8 μg/mL polybrene and transduced at MOI of .2 such that there was a 1000-fold library representation. This was followed by 5 days of puromycin selection starting at 48 hours post-transduction. Cells were then split into new 15 cm dishes with 1/2 of remaining cells spun down and frozen for DNA extraction of the Day 0 time point. Cells were cultured for an additional 10 population doublings at which point final cell samples were obtained and frozen down. DNA was extracted using a modified Qiagen Blood and Cell Culture DNA midi kit protocol that included a vacuum step instead of gravity filtration. PCR was carried out using the previously described nested PCR reaction and a total of 83.2 μg of sample DNA to amplify lentiCRISPRv2 inserts and add Illumina adaptors using a 2X KAPPA HiFi Hotstart Readymix as detailed below; Reaction 1: V2_adaptor primer set 1.6 μg of sample DNA per reaction for 52, 50 μL reactions Cycling conditions: 95C, 3min; 18 cycles of 98C,20s: 66C,15s: 72C,15s: 72C,60s Reaction 2: Indexed Illumina primers 5 μL of pooled product from reaction 1 for 3, 50 μL-reactions Cycling conditions: 95C,

3min; 24 cycles of 98C,20s: 70C,15s: 72C,15s: 72C,60s and as previously described (Wang et al., 2014). Multiple sample time points were individually barcoded, concentration normalized using densitometry of band on a 4-12% TBE polyacrylamide gel (ThermoFisher) stained with SYBR green diluted 1:30000 in TBE buffer, and pooled at an equal ratio for final column-based cleanup. Finally, pooled samples were isolated at a 380bp band on a 1% TAE agarose gel and extracted using the Qiaquick gel extraction kit. Resulting DNA was concentrated to 20 ng/μL using a Zymo DNA clean and concentrator kit and submitted to Hudson Alpha for Next-Seq based sequencing using a 75bp single-end high-output run.

3.2.4 Bioinformatics Analysis

FASTQ files provided by Hudson Alpha were converted to fastqsanger using fastq_groomer and concatenated using the text_processing tool, all through the usegalaxy.org server. Sequencing artifacts were removed using the cshl_fastx_artifacts_filter tool (1% of all reads), and then barcodes were de-multiplexed using cshl_fastx_barcode_splitter (Supplementary table 3). Assessment of sgRNA abundance was performed by taking de-multiplexed FASTQ files and performing count and mle analysis commands in the MAGeCK-VISPR (MAGeCK version.5.7) package on a linux virtual machine running Ubuntu as previously described with optional parameters –norm-method "control", –remove-outliers, and –permutation-round set to 10 (Li et al., 2014). Pan deleterious control genes for quality control plots were designated based on essentiality scores previously described using a CS of -2 as a cutoff (Wang et al., 2015). Graphics were made using base R, R package ggplot2, CRISPR-Analyzer, or R package MAGeCK-Flute version 1.10 (Li et al., 2015b; Winter et al., 2017).

3.2.5 Statistical Analysis

Comparisons between two groups were evaluated using two-tailed Student's T-test when only two groups were present. For multiple group comparisons of TCGA data Tukey's Honest Significant Difference (HSD) test was utilized for pairwise comparisons. CRISPR screens results were derived using an Expectation-Maximization algorithm (MAGeCK-mle) implemented in the MAGeCK-VISPR analysis package. For assessing significant depletion in the CRISPR screen an FDR corrected ward's p-value for beta values statistically significantly different from 0 was used with cutoff alpha=.05 after bootstrap permutation testing in MAGeCK-mle. Results are depicted as arithmetic mean +/- SD unless otherwise indicated in the figure legend. Experimenters were not systematically blinded to group assignment or outcome assessment.

3.3 Results

3.3.1 An unbiased CRISPR screen identifies genes which promote the fitness of $IDH1^{R132H}$ cell lines

We next sought to discover genes essential for the growth of *IDH1* mutation-bearing cells. We used the isogenic pairs to perform an unbiased sub-genomic screen utilizing a mid-sized manually curated CRISPR library containing sgRNAs against 2400 genes. The targets of the library included oncogenes, tumor suppressors, as well as pathways for which small molecule inhibitors are available. The screen was performed as previously described at 1000 fold representation, and we utilized the MAGeCK-mle algorithm to assess screen hits and relative effect size of depletion in parental $IDH1^{R132H/WT}$ cells or isogenic clone 1 ($IDH1^{-/WT}$) (Figure 3.1) (Li et al., 2014; Soderquist et al., 2018). Overall, the screen exhibited similar depletion values and high correlations among replicate samples in both cell lines tested, indicating highly reproducible output of the screen (Figure 3.2A, Figure 3.2B, Figure 3.3).

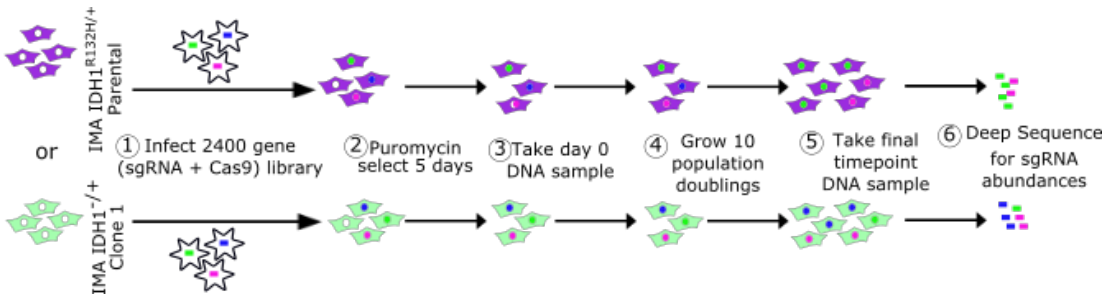

FIGURE 3.1: Visual guide to the CRISPR screening process in which each member of the isogenic pair is transduced with lentivirus at MOI¡.3 such that each cell line pool contains the entire sgRNA library but each cell on average contains only a single sgRNA. Cell lines are selected by puromycin to remove non-transduced cells and kept growing under sparse growth conditions for 10 population doublings. Abundance of individual sgRNAs are assessed at time 0 and after 10 population doublings by NGS on an Illumina Next-Seq machine.

Furthermore, loss of IDH1^{R132H} was not associated with any consistent changes in copy number as detected in the EPIC array analysis for copy number changes, which eliminates one major source of confounding variables in the CRISPR screen (Meyers et al., 2017) (2.20).

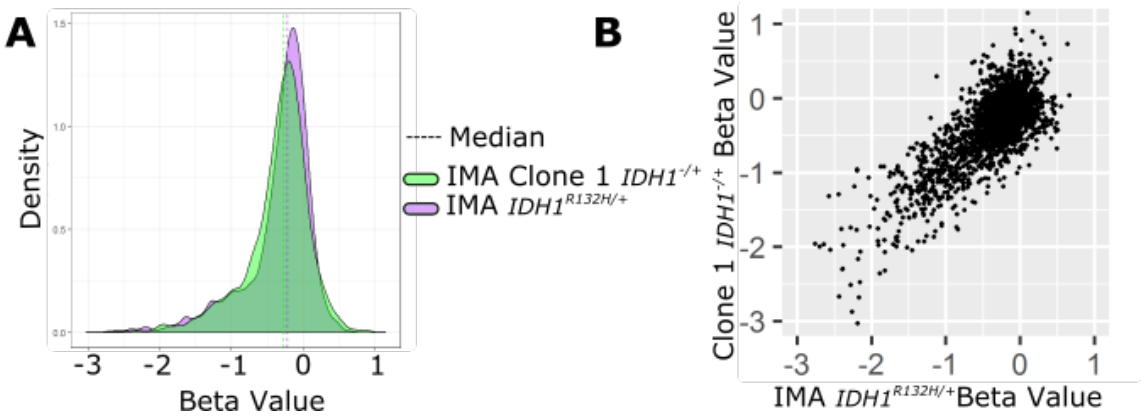

FIGURE 3.2: A, sgRNA frequency counts are used to obtain β scores by an Expectation-Maximization algorithm provided by MAGeCK-mle software, and IMA$^{R132H/+}$ and IMA$^{-/+}$ show similar distribution of β scores suggesting further correction for cell cycle differences between clones is unnecessary. B, Both members of the IMA$^{R132H/+}$ and IMAtextsuperscript-/+ isogenic pair behave similarly in the CRISPR screen when compared at the level of individual genes.

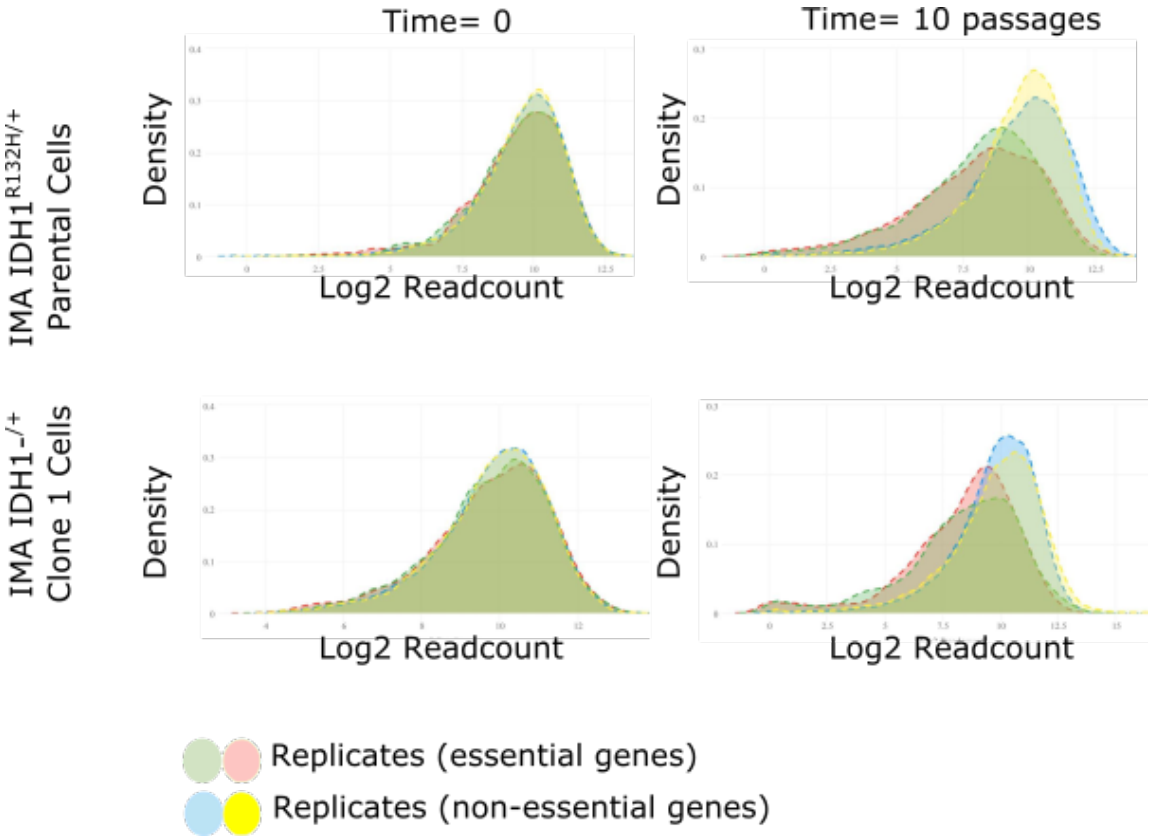

FIGURE 3.3: Density Plots of IMA cell log2 readcounts summed at the gene level for essential genes (red and green) or non-essential genes (blue and yellow). Colors denote each experiment was replicated in full twice and that each replicate shows similar change in Log2 readcount density for essential genes over time. Furthermore, As per recommendations by the authors of the MAGeCK-RRA and MLE algorithms and in keeping with the quality of most published screens we ensured reads for each demultiplexed sample could be mapped at high frequency 60% to the sgRNA library, that missing sgRNAs (zerocounts) were <5% of total sgRNAs in the library, and that the GiniIndex of sgRNA equality was ∼.1 for initial samples and <.2 for final timepoint samples.

To identify targeted pathways that were enriched in the screen (either in $IDH1^{R132H/WT}$ or $IDH1^{-/WT}$ cells) we calculated difference in beta value from MAGeCK-mle at the gene level and performed a gene-set enrichment analysis using the MAGeCKFlute R package. First, we analyzed gene sets for sgRNA targets under purifying-selection in the $IDH1^{R132H/WT}$ cells and saw the proteasome, nucleotide excision repair, hippo signaling, and mRNA surveillance pathways with FDR q-values <.2 (Figure 3.4). As

for the differences in positively selected pathways in the IDH1$^{R132H/WT}$ cells, we did not detect any statistically significantly enriched pathways different between parental or knockout clone cells using gene-set enrichment.

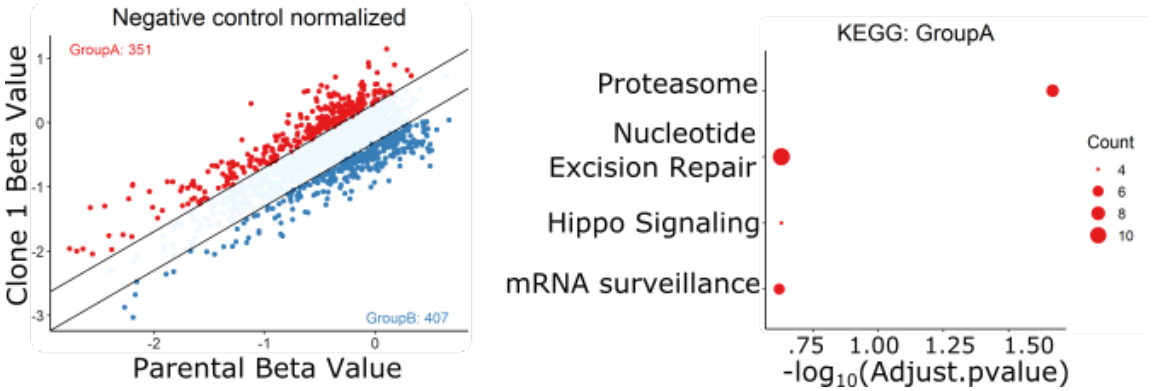

FIGURE 3.4: Dividing the screen results into thirds by +/− one standard deviation provides a list of groups for comparison between cell lines. GroupA genes are those genes showing more severe purifying selection, i.e. a lower β score, in the parental IDH1$^{R132H/+}$ cells than in the IDH1$^{-/WT}$ clone and Group B genes show more severe purifying selection in the IDH1$^{-/WT}$ cells than IDH1$^{R132H/+}$ cells. GSEA analysis using the KEGG pathway annotation dataset in MAGeCK-Flute suggests GroupA genes are enriched for components of the proteasome, nucleotide excision repair, Hippo signaling pathway, and mRNA surveillance pathways.

Among individual genes showing differential selection in the output we were surprised to observe TSC1 and TSC2 knockout under more severe purifying selection within the parental IDH1$^{R132H/WT}$ cells (Figure 3.5 and Appendix A.3). *TSC1* and *TSC2* genes encode hamartin and tuberin proteins whose deletion underlies tuberous sclerosis complex, a usually benign tumor syndrome of the brain, kidneys, liver, and other organs. Both genes function as part of the TSC complex along with TBC1D7 which was not included in the screen. We also observed a significant positive selection for sgRNAs targeting the *ARID2* gene in IDH1 mutant cells but not in the knockout clones, which has similarity to IDH1 mutant glioblastomas where *ARID2* deletions and truncating mutations are enriched in the IDH1 mutant cohort compared to the IDH1 wildtype cohort (Figure 3F and Supplementary Figure 6A). Indeed it has been

reported that *ARID2* deletions and truncating mutations are one of the common alterations gained in progressing IDH1 mutant gliomas (Bai et al., 2015). We then sought to further test and validate that *TSC1* and *TSC2*, which typically function as tumor suppressors, were not behaving in a tumor suppressor fashion in vitro, and thus we tested the hits using new sgRNAs not included in the original screen.

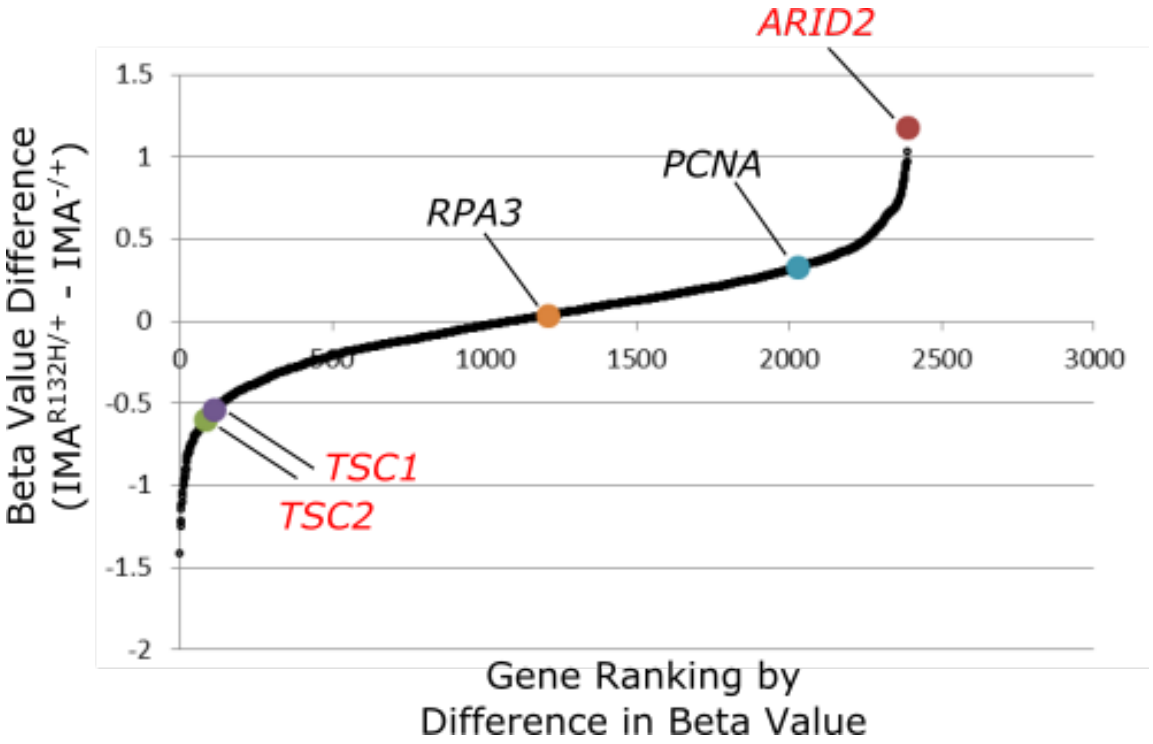

FIGURE 3.5: Genes ranked by beta value difference (Parental IMA-derived isogenic IDH1$^{-/WT}$ clone) with genes of interest highlighted. RPA3 and PCNA were previously identified as pan-deleterious targets in genome-wide CRISPR screens using haploid cell lines.

3.3.2 Preliminary validation and independent corroboration of IDH1 mutation linked hits

First we selected two new sgRNAs that were not included in the original screen to validate a subset of hits. We selected two new sgRNAs from the previously published Brunello library targeting *TSC1* and *TSC2* or two scrambled sgRNAs as non-targeting controls (Figure 3.6A and Figure 3.6B) (Doench et al., 2016).

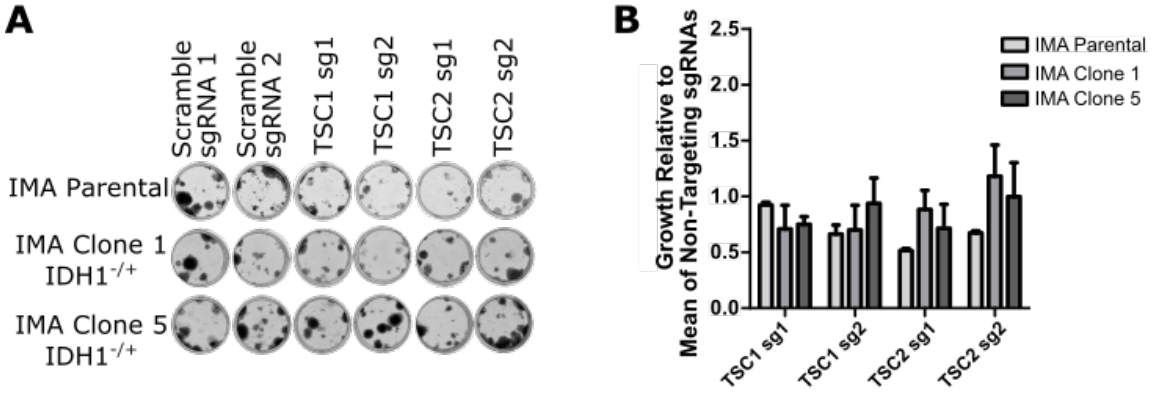

FIGURE 3.6: AIndividual sgRNAs against a set of control scramble sequences, *TSC1*, or *TSC2* genes were transduced at MOI of .5 into $IMA^{R132H/+}$ cells or either of two isogenic $IMA^{-/WT}$ single cell clones and resulting transduced cells were allowed to grow for 23 days before fixing in methanol and staining in .2% crystal violet. B, Relative cell density for each condition as measured by absorbance at 580 nm after liberation of crystal violet dye into solution by addition of 100% methanol.

Although there was no difference between parental cells and isogenic controls in growth relative to non-transduced controls on transduction of sgRNAs targeting TSC1, there was a marked difference between parental and derived clones on knock-out of TSC2 (Figure 3.6A, Figure 3.6B). In longer term cultures and under higher MOI the difference in TSC1 between parental and derived clones was also more striking perhaps suggesting the validation sgRNAs that we chose for TSC1 were relatively inefficient (Figure 3.7).

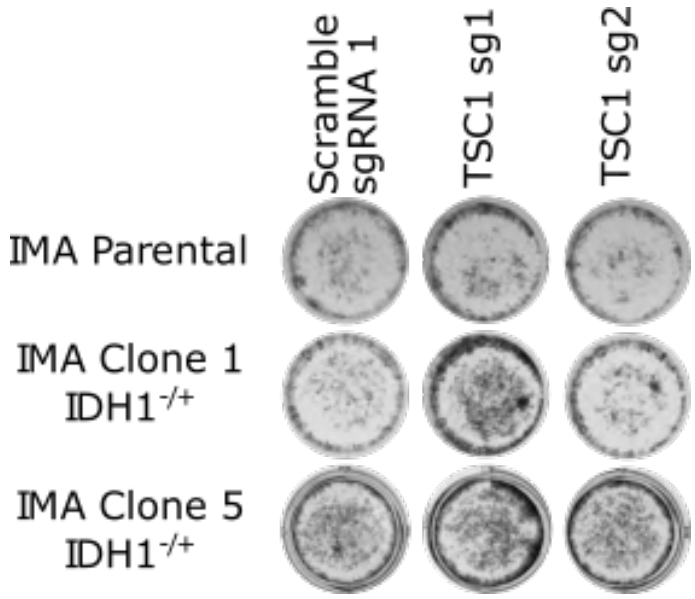

FIGURE 3.7: Alternative format of above assay with cells carried with splitting to highlight differences between $IMA^{-/WT}$ and $IMA^{R132H/WT}$ cells.

Furthermore we sought external validation of TSC hits by querying the recently published Cancer Dependency Map. Within the cancer dependency map the two IDH1 mutant lines available for analysis also showed purifying selection when transduced with sgRNAs targeting TSC1 or TSC2 , and these cell lines were among the most sensitivity to TSC1/TSC2 loss out of the approximately 400 cell lines tested in the CRISPR Avana dataset.(Figure 3.8) (Meyers et al., 2017).

To determine whether TSC complex activity might show additional evidence of importance in IDH mutant glioma we next looked at RNA sequencing data from the TCGA project for either low grade glioma (LGG) or glioblastoma (GBM) tumors while partitioning expression by IDH1 mutation status (Bowman et al., 2017). There was a clear pattern of increased expression at the mRNA level of TSC complex genes in IDH1 mutant tumors compared to IDH1 WT controls in both the low grade glioma cases and glioblastoma cases (Figure 3.9A and Figure 3.9B). Although circumstantial this pattern could be consistent with a selection for maintenance of TSC complex activity in IDH1 mutant glioma cells in patient tumors in vivo.

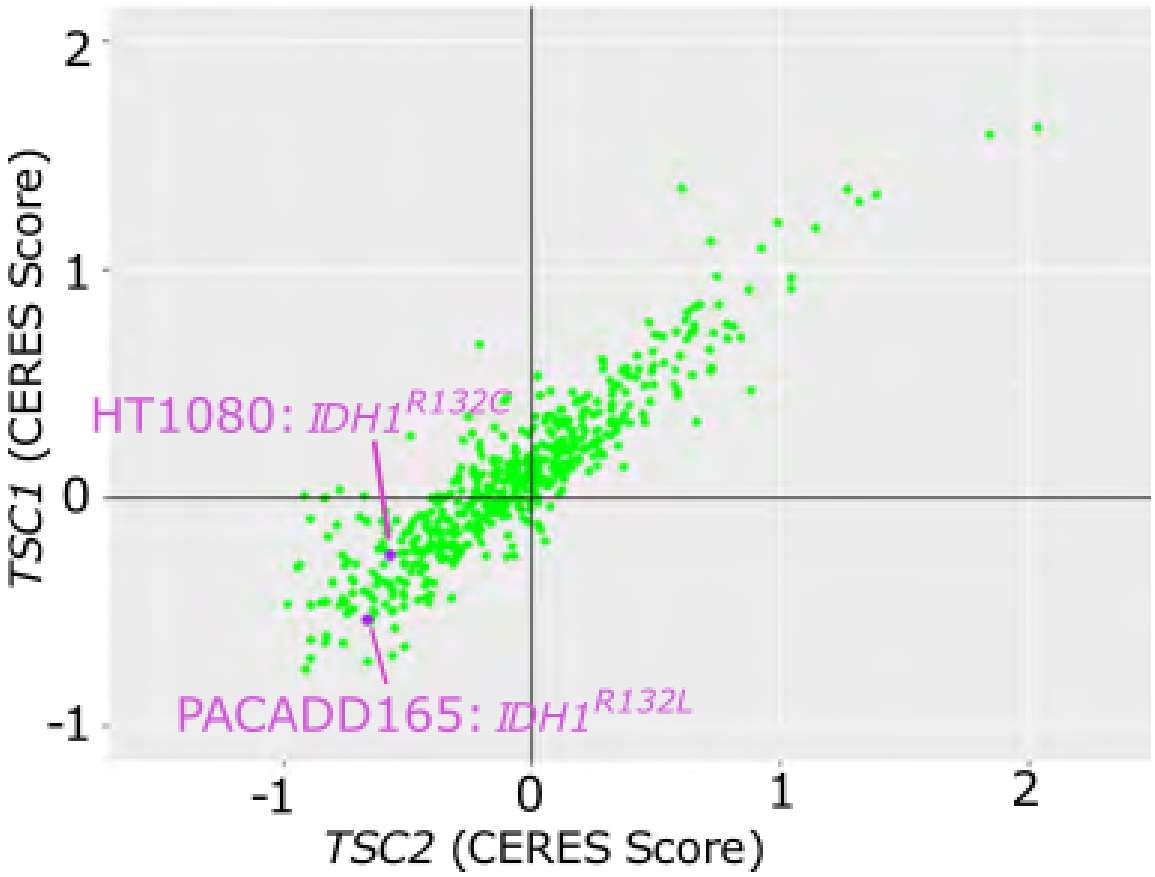

FIGURE 3.8: HT1080 cells which have an endogenous IDH1^{R132C} and PACADD165 with an endogenous IDH1textsuperscriptR132L heterozygous mutation show evidence of purifying selection when losing *TSC1* or *TSC2* gene function by CRISPR-Cas9. Also note high correlations between *TSC2* and *TSC1* selection scores across all cell lines tested in the Cancer Dependency Map as might be supposed for two components of the same molecular complex.

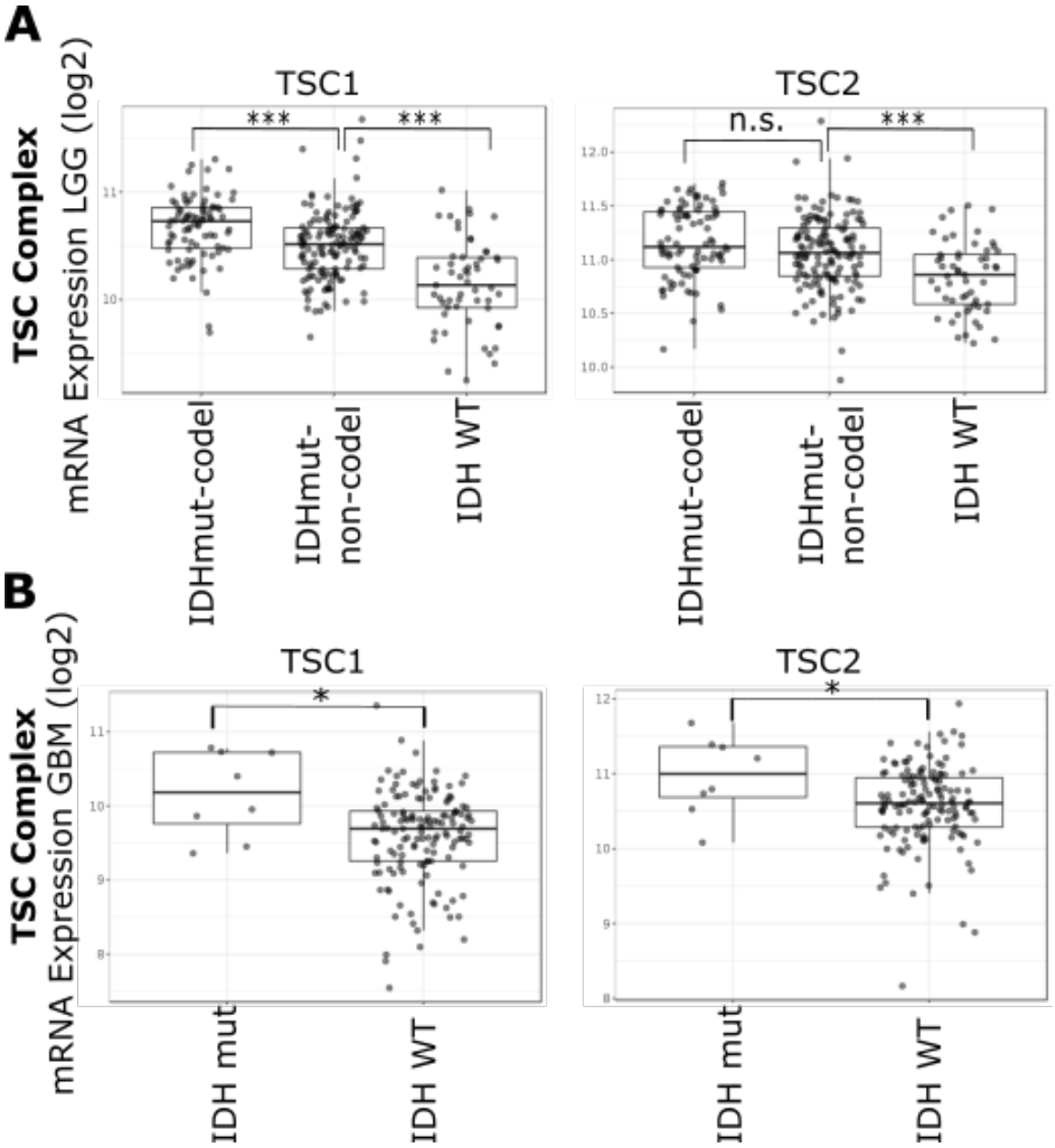

FIGURE 3.9: Overexpression of components of the TSC complex in both astrocytomas and oligodendrogliomas with endogenous IDH1 mutations. A, Log2 counts of mRNA of *TSC1* and *TSC2* , in IDH1 mutant astrocytoma (IDH1mut non-codel), IDH1 mutant oligodendroglioma (IDHmut-codel), and IDH WT tumors from the TCGA low grade glioma project. B, Log2 counts of mRNA of TSC1 and TSC2 in the TCGA glioblastoma project for IDH1 mutant and IDH1 wildtype GBM cases. Tukey's Honest Significant Difference derived p-values <.001 denoted by $\star\star\star$, p-values<.01 denoted by $\star\star$, p-values<.05 denoted by $\star$, and not significant denoted by n.s.

3.4 Discussion

Since losing IDH1 was not sufficient to inhibit cell growth we employed CRISPR screening to identify other genes/pathways on which IDH1 mutant cells depend. The isogenic cell lines also have the benefit of being experimentally tractable systems for systematic screens, as demonstrated by our proof of concept sub-genome CRISPR screen.

Intriguingly, in the results of the CRISPR screen we find that IDH1 mutant cells show evidence of selection against the loss of genes involved in both proteome function and in metabolism, notably *TSC1* and *TSC2* (Figure 3F). The TSC complex regulates the mTOR pathway and its components are classic tumor suppressor proteins responsible for tuberous sclerosis disease. However, despite their roles as tumor suppressors, previous studies have also shown that loss of TSC complex can have deleterious effects on cell growth when metabolic demand and sufficiency signals are not being integrated effectively (Choo et al., 2010). For example, when biosynthetic demand for glucose is not met TSC1$^{-/-}$ or TSC2$^{-/-}$ cell lines can show increased dependence on glutamate dehydrogenase-dependent glutamine metabolism for TCA cycle anaplerotic reactions, and failure to meet this demand impairs cell survival (Choo et al., 2010). In another closely related example, loss of TSC1/TSC2 can lead to increased ER stress due to upregulation of protein translation rates, and this proteotoxic stress can be lethal to cells if they lack compensatory mechanisms (Li et al., 2015a). However, due to mTOR's central role in integrating growth factor and metabolic inputs, it is challenging to assess experimentally the relative weighting of mTOR effector pathway function to the fitness defect we observed in our isogenic models although it is tempting to speculate based on previous literature that IDH1's effects on metabolism would be exacerbated with TSC complex dysfunction.

Previous work has shown that IDH1 mutant tumors can have increased require-

ment for glutamine/glutamate derived carbon to fuel TCA cycle anaplerotic reactions to compensate for alpha-ketoglutarate flux lost to D-2HG by the mutant IDH1 enzyme (Chen et al., 2014; Waitkus et al., 2018). Likewise, in the case of a *TSC1 / TSC2* deletion, cells also require glutamine derived carbon to maintain proper ATP levels and oxidative phosphorylation activity (Choo et al., 2010). This is due to $TSC1^{-/-}/TSC2^{-/-}$ cells failing to properly downregulate their ATP consumption when glutamine/glutamate is limiting (Choo et al., 2010). Therefore, we speculate that loss of TSC1/TSC2 may prevent downregulation of ATP consumption, and put additional stress on the already glutamine/glutamate stressed IDH1 mutant cells. Consistent with this speculation, previous studies have shown that introduction of IDH1 mutations into cells could lead to activation of AMPK, a component upstream to TSC complex, due to D-2HG's inhibitory effect on mitochondrial respiratory chain complex activity and resulting energy stress (Carbonneau et al., 2016; Karpel-Massler et al., 2017) . Further exploration of this hypothesis might be facilitated by fuller elucidation of the glutamine dependent mTORC1 activation/deactivation mechanisms present in cells (Bernfeld et al., 2018). As noted above, this hypothesis is not mutually exclusive with other mechanisms by which TSC1/TSC2 loss could stress the IDH1 mutant cells.

Another hypothesis is that loss of TSC1/TSC2 could contribute to increased ER stress in IDH1 mutant cells through upregulation of protein translation rates. Misfolding of collagen due to D-2HG's inhibitory effect on prolyl-hydroxylases has previously been implicated in the death of knock-in $IDH1^{R132H/WT}$ murine models (Sasaki et al., 2012). Also there has been a recent identification of increased endoplasmic reticulum autophagy in response to collagen misfolding in IDH1 mutant cells as a compensatory mechanism (Viswanath et al., 2018). In this scenario increasing protein translation rates may increase the rate of production of misfolded collagen and put further stress on the ER potentially beyond what the-autophagy

response can mitigate. ER-stress increases, if not mitigated, lead to apoptosis, and these apoptotic decisions may also be affected indirectly by effects of TSC1/TSC2 loss on mTORC2/Akt. TSC1/2 complex increases mTORC2 activity, which in turn regulates AKT activity and downstream Akt-dependent survival pathways (Li et al., 2015a). Potentially, these pathways would be necessary in IDH1 mutant cells under conditions where the IDH1 mutation impairs ATP production and causes metabolic stress. In corroboration with this speculation is the relatively high expression of mTORC2 component RICTOR at the mRNA level in IDH1 mutant gliomas (Network, 2015). Our findings thus provide another example highlighting the essential roles of regulation of mTOR signaling in cancer cell fitness; however, further functional and mechanistic study will be required to expand on our exploratory findings reported here.

In conclusion this study provides the research community with new ways of modeling IDH1 mutant glioma in a genetically relevant background that complements existing methods. The fact that loss of IDH1 mediated D-2HG production did not affect cell fitness then prompted us to explore alternative ways of therapeutically targeting IDH1 mutant cells. To this end we demonstrate that these isogenic models are capable of being utilized for CRISPR-Cas9 screening, which we hope will benefit the IDH1 mutation's research community in identifying IDH1 mutant linked synthetic sick/lethal interactions.

4

Chapter 4: Conclusions

4.1 Summary and conclusions

The studies presented in this dissertation provide evidence that the loss of D-2HG production, either through loss of the mutant or wildtype allele of *IDH1*, in human glioma cells results in a genome-wide pattern of DNA demethylation that is enriched for CpG sites in open sea regions of the genome. Combined with the evidence that *in vivo* IDH1 mutant tumors, with losses of either allele of *IDH1*, also show methylation patterns with similar genomic context enrichments, strongly argues for an active role of IDH1 in contributing to the epigenetic state of glioma cells, at least at the level of specific regional DNA methylation, of advanced glioma. This result is potentially important for groups attempting to utilize DNA methylation signatures for prognostic purposes as not all G-CIMP-low astrocytoma cells need necessarily have losses of IDH1 mutation linked D-2HG production. In this case; therefore, there is the potential that the G-CIMP-low classifying tumors could be further subgrouped by IDH1 loss status, though the prognostic implications are unclear due to the lack of many matched patient tumor samples from which to draw conclusions about the relative

morbidity and mortality of these potential G-CIMP-low subgroups. Furthermore, the tools developed during this dissertation have the potential to provide the field of researchers studying IDH1 mutations in glioma with a powerful new genetic model of progressive IDH1 mutant astrocytoma. These models can be utilized to dissect out the role of different genetic elements in supporting the growth of IDH1 mutant cells under various possible experimental and *in situ* constraints on tumor growth. Such a screen done in proof-of-principle is reported in Chapter 3, but could likely be extended as discussed below. Thus this dissertation research makes contributions to both the knowledge of how IDH1 mutant tumors behave on progression, and loss of IDH1-mutation linked D-2HG production, as well as research methods that are employed by the field.

4.2 Future Directions

4.2.1 Studies of epigenetic states requiring an active IDH1 mutation

Although the results of chapter 2 provide causal evidence that an active IDH1 mutation is required for the maintenance of hypermethylation at CpG sites within open sea regions of the genome, the mechanism by which this demethylation is occurring is still obscure. One potential avenue of research is to utilize oxidative-bisulphite conversion of DNA to detect 5-hydroxy-methyl-cytosine (5hmC), and to determine with either array based or sequencing based methods whether there is an increase in active demethylation precursors in these areas of the genome in the IDH1 knock-out cells compared to parental cells. A gain of 5hmC at these areas of the genome with lack of relative enrichment in other hypermethylated CpG island contexts could provide an initial test of the idea that active demethylation processes are at work and mediating at least part of the change in open sea region methylation. Another valuable tool would be the generation of inducible loss models of IDH1 mutations in IDH1 mutant glioma cell lines by first stably transducing cells with a doxycycline

inducible donor IDH1 mutant cDNA before cloning out CRISPR-edited clones with indels disrupting the endogenous *IDH1* mutant allele. Such a system could be utilized to study the temporal effects of loss of the IDH1 mutation on DNA methylation or other epigenetic state determinants such as histone methylation. Such a system would have much tighter temporal control and could potentially differentiate early chromatin modifications induced by IDH1 loss from longer term changes that can be difficult to differentiate from selection events occurring on particular sub-clonal epi-alleles within the parental cell population. Analysis of more immediate-early linked changes would also benefit from the use of cell-permeable D-2HG, which is experimentally more tractable in shorter term cultures than the long term growth assays described in this dissertation. Furthermore, small molecule inhibitors of mutant IDH1 could be employed to provide additional evidence as maintaining D-2HG suppression over short periods of time is experimentally practical.

There is also a rich literature suggesting that IDH1 mutations can function to inhibit stem cell/progenitor cell differentiation through the inhibition of demethylation of specific histone marks. The area of histone based chromatin structure is a rich area for future exploration of IDH1 linked epigenetic effects, and may even be more important for pro-tumorigenic abilities conferred by the IDH1 mutation than DNA methylation (Koivunen et al., 2012; Schvartzman et al., 2019). The 08-0537 cell line is particularly well suited to this potential avenue of research as it is cultured in a neural-stem cell proliferation culture medium, forms neurospheres, and may be capable of undergoing differentiation-like-cell state transitions based on preliminary data generated by Rui Yang within the Yan laboratory. Such a differentiation could be induced by a pro-differentiation cytokine such as BMP2 or a more poorly defined differentiation millieu could be utilized such as fetal bovine serum.

4.2.2 Utilizing systematic screens for cancer dependencies in IDH1 mutant glioma

The results of chapter 3 show that systematically screening for genetic dependencies is possible even using the slow growing IDH1 mutant patient-derived glioma lines. Although there were several potentially interesting hits within the genetic screen performed, for therapy development a larger effect size than any hit we observed would most likely provide an advantage to further development.

In terms of follow-up experiments to initial interesting screen hits the first and most important work is in validating cancer dependency map data in HT1080 and PACADD165 using hold-out sgRNAs and similar screening conditions as those employed by the depmap consortium. It is unknown why TSC would create a decrease in fitness in IDH1 mutant cells specifically, and we are reduced to speculating about the possible ways TSC complex activity could contribute to the fitness of IDH1 mutant cells. Liabilities in cell growth on TSC loss have been a major area of study for the development of synthetic sick/lethal based therapies for tuberous sclerosis syndrome which is a rare benign growth syndrome (Li et al., 2015a). It is possible but speculative that IDH1 mutant gliomas might have synthetic sick interactions with total TSC complex loss due to unregulated mTORC1 activity, which in the context of insufficient glutaminase activity could create some form of proteotoxic or ER stress as had been previously reported for murine embryonic fibroblast cells (Li et al., 2015a). However, it must be noted that as IDH1 mutant gliomas typically gain activating mutations in PIK3CA it is the case that IDH1 mutant tumors select for high PI3K/mTORC1 pathway activity *in vivo*. The other interesting hit from the screen was a gain in fitness in IDH1 mutant cells on ARID2 deletion.

ARID2 is known to function in the PBAF complex a member of the SWI/SNF family of complexes that is known to regulate chromatin remodeling (Raab et al., 2015). It has been commonly found to be deleted in progressing IDH1 mutant gliomas

although it is rarer for the deletion to be found in IDH1 wildtype glioblastomas (Bai et al., 2015). Expanding ARID2 validation to other IDH1 mutant cell lines and validating that ARID2 is still functional in IMA knockout clones through Western Blotting and functional assays should be a priority in follow-up of this initial finding. Exploration of this avenue may answer basic cancer biology questions about why ARID2 homozygous deletions are seen in IDH1 mutant progressing tumors, although in terms of therapy development it is difficult to speculate how the knowledge gained from these studies could inform treatment.

Because we only targeted approximately 1/10th of the protein coding genome in this initial screen, resources could be devoted to trying a larger genome-wide library to target the remaining 9/10ths of protein coding genes in an effort to find better targets for studies aiming at therapeutic interventions. Furthermore, screens utilizing neural sphere forming conditions have recently been reported, which could provide a rationale for attempting a similar style screen using the 08-0537 isogenic pair developed in this dissertation. Having both the IMA and 08-0537 cell lines would allow for stronger inference to be made, that any genetic dependence linked to mutant IDH1 would really be due to large creation flux or large metabolite pool presence of D-2HG, as the 08-0537 isogenic pair continues to produce full length mutant IDH1 protein. As an additional consideration the 08-0537 cell line is tumorigenic in nude murine orthotopic glioma models, and potential hits could be followed-up with in vivo tests for genetic dependency in this line. Whether the knockout clone in this model is also similarly tumorigenic remains to be conclusively determined.

4.3 Final Notes

Studies of the role of IDH mutations in tumor initiation and progression represent an interesting grounds for understanding how various aspects of metabolism, cell signaling, gene expression, and intercellular communication can shape the process of

tumorigenesis. Few examples of gain-of-function mutations in a metabolic enzyme gained somatically are known in human genetics, and even fewer in human cancer. The models and methods developed in this dissertation, should provide useful tools to the field of researchers studying the roles of IDH1 in oncogenesis.

Appendix A

Appendicies

A.1 Permissions

Figures from (Yan et al., 2009) are reproduced with permission according to NEJM policies governing inclusion of figures in theses and dissertations, and are Copyright Massachusetts Medical Society. Chapter 2 contains excepts and figures from an accepted manuscript at *Molecular Cancer Research*, which requires no special permissions from first authors for reuse in dissertations. TCGA data is provided under the following provisions: TCGA requests that authors who use data from TCGA acknowledge the TCGA Research Network in the acknowledgements section of their work.

A.2 Exome Sequencing Data

Table A.1: Results of IMA Exome Sequencing

Gene Symbol	Mutation Position Nucleotide (genomic)	Nucleotide (transcript)	Amino Acid (protein)	Mutation Type
ADAMTS13	chr9:135310320G>T	3342G>T	1114Q>H	Missense
ATRX	chrX:76825063G>A	2341C>T	781R>X	Nonsense
BMP8A	chr1:39764013C>A	1165C>A	389R>S	Missense
BRD1	chr22:48602885A>G	1085T>C	362M>T	Missense
C18orf19	chr18:13656606T>C	692A>G	231Y>C	Missense
C2orf65	chr2:74656138G>T	1009C>A	337Q>K	Missense
CADPS2	chr7:122048993delG	1118delC	NA	Frameshift
CR1L	chr1:205934330G>A	473G>A	158C>Y	Missense
CUBN	chr10:17166370T>C	2207A>G	736Y>C	Missense
DFNB31	chr9:116208516C>T	2176G>A	726V>I	Missense
DMRT3	chr9:980952T>C	1366T>C	456Y>H	Missense
EML2	chr19:50816615C>T	962G>A	321W>X	Nonsense
EXOC6B	chr2:72545883C>T	1894G>A	632G>R	Missense
EYS	chr6:66101636C>T	1724G>A	575C>Y	Missense
FBXO40	chr3:122823757C>A	791C>A	264P>H	Missense
GMCL1	chr2:69950437A>G	1301A>G	434N>S	Missense
GRK6	chr5:176791866C>G	288C>G	96D>E	Missense
HSF2	chr6:122786486C>G	1132C>G	378L>V	Missense
IDH1	chr2:208821357C>T	395G>A	132R>H	Missense
ITIH2	chr10:7811953G>T	1312G>T	438V>F	Missense
KCNK2	chr1:213412146G>T	820G>T	274A>S	Missense
KIAA1632	chr18:41782522G>C	1516C>G	506P>A	Missense
KLC4	chr6:43146565G>A	1193G>A	398R>Q	Missense
KRBA2	chr17:8214153T>C	503A>G	168Q>R	Missense
KRT5	chr12:51199962C>T	386G>A	129G>D	Missense
LFNG	chr7:2531635G>A	643G>A	215A>T	Missense
LY75	chr2:160419122C>A	2590G>T	864A>S	Missense
MCOLN2	chr1:85179217A>G	893T>C	298I>T	Missense

MGEA5	chr10:103547686C>A	2025G>T	675L>F	Missense
MURC	chr9:102388207C>A	748C>A	250Q>K	Missense
NOTCH1	chr9:138532073C>T	1393G>A	465A>T	Missense
NR4A3	chr9:101634893G>C	1086G>C	362K>N	Missense
OR1S1	chr11:57739208T>G	416T>G	139I>S	Missense
PDS5B	chr13:32242376C>T	3742C>T	1248R>X	Nonsense
PEX5L	chr3:181010154insAA	IVS11-4insTT	NA	Splice site
PIH1D1	chr19:54644636G>C	245C>G	82T>S	Missense
PLEKHH1	chr14:67112458G>T	2335G>T	779G>C	Missense
PLK2	chr5:57787255C>A	1493G>T	498S>I	Missense
PLXNC1	chr12:93165996C>A	2575C>A	859L>M	Missense
RGS12	chr4:3289089C>T	1394C>T	465A>V	Missense
RPL23	chr17:34262815C>A	83G>T	28C>F	Missense
SAMD9	chr7:92572449A>C	898T>G	300S>A	Missense
SEC31A	chr4:84010531T>G	853A>C	285I>L	Missense
SEZ6L2	chr16:29798707C>A	1552G>T	518D>Y	Missense
SMARCD3	chr7:150568265C>T	1039G>A	347V>M	Missense
TECTA	chr11:120513687G>C	3289G>C	1097D>H	Missense
TECTA	chr11:120533856-8delGAG	4402-4delGAG	NA	In-frame deletion
THSD7B	chr2:138150641T>C	4826T>C	1609M>T	Missense
TMEM198	chr2:220117834G>T	141G>T	47L>F	Missense
TP53	chr17:7518272C>A	734G>T	245G>V	Missense
TRIM3	chr11:6435632C>A	385G>T	129A>S	Missense
TRIM42	chr3:141880027A>G	266A>G	89Y>C	Missense
TSPAN31	chr12:56425819G>A	88G>A	30V>M	Missense
UTP20	chr12:100274887G>A	5587G>A	1863D>N	Missense
VAMP2	chr17:8006496C>T	5'UTR-2G>A	NA	UTR
WDFY4	chr10:49664735C>A	3622C>A	1208P>T	Missense
WNK1	chr12:864372G>T	4141G>T	1381E>X	Nonsense
ZCCHC2	chr18:58368620G>C	1260G>C	420Q>H	Missense

Table A.2: Selection of a subset of mutations detected in 08-0537

Gene Symbol	Mutation PositionNucleotide (genomic)	Amino Acid (protein)	Mutation Type	Consequence
ATRX	chrX_76939375-76939375_G_T	458S>X	Substitution	Nonsense
IDH1	chr2_209108185-209108185_G_A	222R>C	Substitution	Nonsynonymous coding
IDH1	chr2_209113112-209113112_C_T	132R>H	Substitution	Nonsynonymous coding
TP53	chr17_7576658-7576658_C_T	NA	Substitution	Splice site acceptor
TP53	chr17_7577120-7577120_C_T	273R>H	Substitution	Nonsynonymous coding

A.3 Subset of MAGeCK-mle-CRISPR-screen results

Table A.3: Top 5 percent of differentially required genes for CRISPR screen

Gene	IMA-/+|beta	IMA-/+|wald-p-value	IMA-/+|wald-fdr	IMA PAR|beta	IMA PAR|wald-p-value	IMA PAR|wald-fdr	Difference in Beta Value
SGOL1	0.29557	0.56051	0.68216	-1.1202	0.035006	0.10283	-1.41577
ACTL6A	-1.322	1.71E-05	0.00014568	-2.5729	2.28E-14	3.06E-12	-1.2509
NIPBL	-0.9609	0.00067422	0.0031118	-2.1899	2.42E-14	3.06E-12	-1.229
CENPM	-0.98006	0.00028351	0.0014987	-2.1932	6.21E-16	1.24E-13	-1.21314
POLD2	-1.2976	1.33E-09	4.80E-08	-2.4428	5.47E-29	1.31E-25	-1.1452
ATRIP	0.47627	0.39293	0.5265	-0.64142	0.25936	0.44813	-1.11769
CDKL1	0.49182	0.18412	0.30412	-0.61022	0.099803	0.23098	-1.10204
BMP2K	0.70954	0.18526	0.30516	-0.36014	0.50543	0.68538	-1.06968
NLK	0.58171	0.24462	0.37489	-0.48784	0.32979	0.52711	-1.06955
PCGF1	1.1468	0.16124	0.277	0.10563	0.89734	0.94627	-1.04117
SMC1A	-1.1865	0.00017115	0.00097802	-2.2265	3.84E-11	2.01E-09	-1.04
PLAT	0.93635	0.1108	0.20955	-0.059685	0.91943	0.95758	-0.996035
PCK1	0.4881	0.13834	0.24777	-0.50747	0.1249	0.27003	-0.99557
SH3TC2	0.55234	0.14708	0.26071	-0.43572	0.2604	0.44928	-0.98806
EIF3G	-1.0733	0.0027123	0.010046	-2.0383	2.37E-08	5.53E-07	-0.965
TOPBP1	-0.92094	0.017252	0.04779	-1.8762	3.31E-06	3.65E-05	-0.95526
RHOA	-0.26654	0.29416	0.42684	-1.2032	3.67E-06	3.97E-05	-0.93666
MOB1B	0.86878	0.12005	0.22353	-0.058347	0.91686	0.95756	-0.927127
PI4KA	0.37513	0.17877	0.29753	-0.53217	0.061897	0.16165	-0.9073
CLSPN	-0.92364	9.89E-05	0.00060396	-1.8288	1.24E-13	1.30E-11	-0.90516
MEN1	0.11925	0.58714	0.70475	-0.78094	0.00039555	0.0024341	-0.90019
HLTF	0.33383	0.35291	0.48901	-0.52743	0.15996	0.32387	-0.86126
KDR	0.43692	0.091897	0.18179	-0.4188	0.10737	0.24295	-0.85572
ERN1	0.45783	0.080948	0.16492	-0.37359	0.16322	0.3289	-0.83142
CETN2	0.45416	0.26983	0.40024	-0.36599	0.37911	0.57008	-0.82015
PMS2	0.4046	0.19033	0.31138	-0.4104	0.18829	0.36424	-0.815
PSMA3	-1.9604	1.39E-11	1.19E-09	-2.7614	5.15E-21	6.18E-18	-0.801
RUVBL1	-0.67353	0.025157	0.064105	-1.4742	1.69E-06	2.05E-05	-0.80067
SETDB1	0.0044727	0.98882	0.99545	-0.79325	0.017705	0.060272	-0.7977227
NAGK	0.12307	0.57019	0.6901	-0.67441	0.0019627	0.0095861	-0.79748
POLD4	0.41275	0.39304	0.5265	-0.38342	0.42757	0.61733	-0.79617
SF3B1	-0.61102	0.027857	0.069935	-1.3881	6.86E-07	9.74E-06	-0.77708
SETDB2	-0.010683	0.96745	0.98131	-0.78562	0.0034661	0.015462	-0.774937
RAD17	-0.66962	0.0065246	0.021047	-1.437	1.10E-08	2.87E-07	-0.76738
RDH8	0.42664	0.34504	0.48118	-0.33646	0.45679	0.6445	-0.7631
NF2	0.77601	0.00045271	0.0022183	0.018928	0.93187	0.96359	-0.757082
PTEN	0.23823	0.11719	0.21939	-0.51274	0.00077002	0.0042097	-0.75097
ALOX5	0.63093	0.20147	0.32473	-0.11775	0.81219	0.8995	-0.74868
SRCAP	-0.76208	0.00041531	0.0020897	-1.5088	5.16E-12	3.17E-10	-0.74672
RXRB	0.072817	0.70553	0.8006	-0.66932	0.00063339	0.0035853	-0.742137
POLE3	-0.68396	0.003417	0.012131	-1.425	2.34E-09	7.21E-08	-0.74104
CLP1	-1.0034	0.0031705	0.011494	-1.7416	3.98E-07	6.20E-06	-0.7382
STK4	0.17208	0.61458	0.72767	-0.5656	0.10378	0.23789	-0.73768
PLK1	-0.91409	0.0047538	0.016024	-1.6446	6.05E-07	8.96E-06	-0.73051
STAG2	0.8981	0.078588	0.16121	0.17661	0.72971	0.84916	-0.72149
IPPK	0.58661	0.16272	0.27855	-0.13077	0.75616	0.86418	-0.71738
EIF3I	-0.93944	0.002456	0.0093414	-1.6419	1.26E-07	2.34E-06	-0.70246
GTF3C4	-1.0616	0.00048913	0.0023763	-1.7585	1.05E-08	2.77E-07	-0.6969
LATS2	0.24581	0.41245	0.54539	-0.44951	0.13921	0.29104	-0.69532
FANCG	-0.96676	0.00020778	0.0011474	-1.6607	2.03E-10	8.84E-09	-0.69394
ETF1	-2.0012	8.06E-11	4.83E-09	-2.6939	4.86E-18	2.33E-15	-0.6927
TAF1	-0.20982	0.33348	0.46969	-0.90206	4.41E-05	0.00034397	-0.69224
POLR2E	-1.3187	1.11E-06	1.43E-05	-2.0106	1.10E-13	1.20E-11	-0.6919
MYO3A	0.29854	0.34624	0.48201	-0.39236	0.21869	0.40036	-0.6909

TSSK3	0.20141	0.36158	0.49787	-0.48911	0.026849	0.082869	-0.69052
COPS4	-0.63781	0.025506	0.064778	-1.3265	4.93E-06	5.12E-05	-0.68869
TET1	0.071846	0.84476	0.89709	-0.61558	0.098118	0.229	-0.687426
DPF2	-0.60996	0.012641	0.037043	-1.2895	1.40E-07	2.50E-06	-0.67954
KMT5B	0.36819	0.090957	0.18116	-0.30587	0.16219	0.3271	-0.67406
PRKAR1A	-1.0183	2.34E-05	0.00018758	-1.6923	3.89E-12	2.45E-10	-0.674
TNFSF11	0.5739	0.1539	0.26844	-0.10006	0.80409	0.89606	-0.67396
PSMB3	-1.9667	2.01E-11	1.51E-09	-2.6383	4.65E-17	1.39E-14	-0.6716
NF1	-0.20915	0.24916	0.37943	-0.87338	2.03E-06	2.39E-05	-0.66423
HAUS7	-0.41595	0.021724	0.056548	-1.079	3.32E-09	9.84E-08	-0.66305
WRN	0.37495	0.33867	0.4756	-0.28627	0.47365	0.66112	-0.66122
TOP1	-0.49353	0.056735	0.12539	-1.1531	1.38E-05	0.00012862	-0.65957
TARBP1	0.21229	0.37025	0.50654	-0.44577	0.060379	0.15893	-0.65806
PBK	0.53765	0.13586	0.24457	-0.11815	0.74424	0.85915	-0.6558
HTR4	0.22799	0.18076	0.30044	-0.42727	0.01234	0.045353	-0.65526
TAF2	-0.63426	0.018629	0.050349	-1.2887	3.12E-06	3.48E-05	-0.65444
MAPK15	-0.17903	0.45936	0.59036	-0.83312	0.00066326	0.0037279	-0.65409
PHF20	-0.06272	0.83378	0.887	-0.70964	0.023462	0.075252	-0.64692
MAP3K7	0.4042	0.22646	0.35384	-0.23958	0.47414	0.6612	-0.64378
RFC3	-1.7605	2.67E-10	1.31E-08	-2.4042	1.04E-17	4.16E-15	-0.6437
EPHB2	0.26225	0.18209	0.30195	-0.37983	0.05361	0.14604	-0.64208
NEDD8	-0.99194	9.45E-06	8.65E-05	-1.6329	5.38E-13	4.16E-11	-0.64096
CDK3	-0.037678	0.9281	0.95231	-0.66484	0.11879	0.2599	-0.627162
KDM4C	0.26408	0.19405	0.31574	-0.35893	0.078561	0.19579	-0.62301
SUFU	0.29027	0.28435	0.41572	-0.32982	0.23733	0.42475	-0.62009
ACTA2	0.51556	0.28641	0.41786	-0.1016	0.8337	0.90991	-0.61716
DDX18	-0.38002	0.2026	0.32598	-0.99644	0.00091109	0.0048861	-0.61642
TAF7	-0.27932	0.1601	0.27611	-0.89302	1.14E-05	0.0001083	-0.6137
YWHAZ	0.2445	0.35461	0.49109	-0.36732	0.16596	0.33275	-0.61182
CCT3	-0.67671	0.0013101	0.0054859	-1.2829	1.29E-09	4.41E-08	-0.60619
TSC2	-0.36505	0.023432	0.060339	-0.96853	2.33E-09	7.21E-08	-0.60348
GRIN3A	0.45291	0.21866	0.34435	-0.14093	0.70216	0.83304	-0.59384
DHX32	0.59451	0.24397	0.37438	0.00077099	0.9988	0.99885	-0.59373901
RIOK2	-0.65199	0.0033201	0.011911	-1.2443	2.35E-08	5.53E-07	-0.59231
SNU13	-0.72152	0.0015624	0.006334	-1.3119	2.13E-08	5.26E-07	-0.59038
ATE1	0.071609	0.68801	0.78968	-0.51813	0.0038711	0.017078	-0.589739
KEAP1	0.18701	0.26684	0.39728	-0.40072	0.017546	0.059901	-0.58773
MAPK11	0.59956	0.032557	0.078689	0.016137	0.95419	0.97539	-0.583423
GABRG1	0.34608	0.58104	0.699	-0.2354	0.71616	0.8409	-0.58148
ALKBH1	-0.41378	0.16542	0.2818	-0.99442	0.0016203	0.0081869	-0.58064
TDRD6	0.10039	0.73186	0.81924	-0.47984	0.10191	0.23489	-0.58023
ZEB1	-0.53667	0.078711	0.16132	-1.1149	0.00044794	0.0027286	-0.57823
CDC42	-0.79793	0.0023038	0.0088894	-1.3752	2.31E-07	3.93E-06	-0.57727
ASH2L	-1.0097	9.70E-05	0.00060072	-1.5829	1.16E-09	4.08E-08	-0.5732
EPHA6	0.25155	0.50122	0.62849	-0.31126	0.43165	0.62075	-0.56281
THUMPD2	-0.037177	0.83142	0.88488	-0.59699	0.00067019	0.0037493	-0.559813
TXNRD1	-1.0306	2.91E-06	3.19E-05	-1.5891	8.62E-13	6.46E-11	-0.5585
MCL1	-0.2745	0.48722	0.61564	-0.83109	0.038266	0.11092	-0.55659
BCHE	0.28863	0.20566	0.32971	-0.26784	0.24275	0.43124	-0.55647
CEBPG	0.43961	0.08949	0.17883	-0.116	0.65571	0.79964	-0.55561
G6PD	-1.3679	1.60E-09	5.57E-08	-1.9222	2.05E-16	5.46E-14	-0.5543
NQO2	0.067451	0.67368	0.77934	-0.48263	0.0026729	0.012529	-0.550081
NPM1	-0.58478	0.0079993	0.025162	-1.131	3.03E-07	4.92E-06	-0.54622
INSR	0.22095	0.27963	0.41173	-0.32352	0.11529	0.25437	-0.54447
GTF2H4	-0.25643	0.33276	0.46922	-0.79814	0.0026054	0.012331	-0.54171
CDCP2	0.30336	0.097518	0.18982	-0.23763	0.19606	0.37405	-0.54099
ZAP70	0.16438	0.34348	0.4803	-0.37349	0.031504	0.094043	-0.53787
MAOB	0.24862	0.086834	0.17425	-0.28905	0.047853	0.13352	-0.53767
TSC1	-0.16267	0.37443	0.50972	-0.6993	0.00014716	0.00098105	-0.53663
PSMC1	-0.77145	0.0014753	0.0060214	-1.3064	1.19E-07	2.24E-06	-0.53495

IFNA21	0.26701	0.18181	0.30195	-0.26762	0.18409	0.3595	-0.53463
SLC2A5	0.095181	0.61306	0.72731	-0.43849	0.022476	0.072994	-0.533671
HJURP	-1.7448	8.54E-09	2.28E-07	-2.2775	2.67E-13	2.37E-11	-0.5327
MCRS1	-0.4557	0.018829	0.050775	-0.98791	3.68E-07	5.81E-06	-0.53221
SETD7	-0.075359	0.82013	0.87734	-0.60598	0.070194	0.17827	-0.530621

Bibliography

Aryee, M. J., Jaffe, A. E., Corrada-Bravo, H., Ladd-Acosta, C., Feinberg, A. P., Hansen, K. D., and Irizarry, R. A. (2014), "Minfi: a flexible and comprehensive Bioconductor package for the analysis of Infinium DNA methylation microarrays," *Bioinformatics*, 30, 1363–9.

Bai, H., Harmanci, A. S., Erson-Omay, E. Z., Li, J., Coskun, S., Simon, M., Krischek, B., Ozduman, K., Omay, S. B., Sorensen, E. A., Turcan, S., Bakirciglu, M., Carrion-Grant, G., Murray, P. B., Clark, V. E., Ercan-Sencicek, A. G., Knight, J., Sencar, L., Altinok, S., Kaulen, L. D., Gulez, B., Timmer, M., Schramm, J., Mishra-Gorur, K., Henegariu, O., Moliterno, J., Louvi, A., Chan, T. A., Tannheimer, S. L., Pamir, M. N., Vortmeyer, A. O., Bilguvar, K., Yasuno, K., and Gunel, M. (2015), "Integrated genomic characterization of IDH1-mutant glioma malignant progression," *Nat Genet*, advance online publication.

Bernfeld, E., Menon, D., Vaghela, V., Zerin, I., Faruque, P., Frias, M. A., and Foster, D. A. (2018), "Phospholipase D–dependent mTOR complex 1 (mTORC1) activation by glutamine," *Journal of Biological Chemistry*, 293, 16390–16401.

Bleeker, F. E., Atai, N. A., Lamba, S., Jonker, A., Rijkeboer, D., Bosch, K. S., Tigchelaar, W., Troost, D., Vandertop, W. P., Bardelli, A., and Noorden, C. J. F. V. (2010), "The prognostic IDH1 R132 mutation is associated with reduced NADP-dependent IDH activity in glioblastoma," *Acta Neuropathologica*, 119, 487–494.

Bowman, R. L., Wang, Q., Carro, A., Verhaak, R. G. W., and Squatrito, M. (2017), "GlioVis data portal for visualization and analysis of brain tumor expression datasets," *Neuro-Oncology*, 19, 139–141.

Brat, D. J., Verhaak, R. G., Aldape, K. D., Yung, W. K., Salama, S. R., Cooper, L. A., Rheinbay, E., Miller, C. R., Vitucci, M., Morozova, O., Robertson, A. G., Noushmehr, H., Laird, P. W., Cherniack, A. D., Akbani, R., Huse, J. T., Ciriello, G., Poisson, L. M., Barnholtz-Sloan, J. S., Berger, M. S., Brennan, C., Colen, R. R., Colman, H., Flanders, A. E., Giannini, C., Grifford, M., Iavarone, A., Jain, R., Joseph, I., Kim, J., Kasaian, K., Mikkelsen, T., Murray, B. A., O'Neill, B. P., Pachter, L., Parsons, D. W., Sougnez, C., Sulman, E. P., Vandenberg, S. R.,

Van Meir, E. G., von Deimling A, Zhang, H., Crain, D., Lau, K., Mallery, D., Morris, S., Paulauskis, J., Penny, R., Shelton, T., Sherman, M., Yena, P., Black, A., Bowen, J., Dicostanzo, K., Gastier-Foster, J., Leraas, K. M., Lichtenberg, T. M., Pierson, C. R., Ramirez, N. C., Taylor, C., Weaver, S., Wise, L., Zmuda, E., Davidsen, T., Demchok, J. A., Eley, G., Ferguson, M. L., Hutter, C. M., Mills Shaw, K. R., Ozenberger, B. A., Sheth, M., Sofia, H. J., Tarnuzzer, R., Wang, Z., Yang, L., Zenklusen, J. C., Ayala, B., Baboud, J., Chudamani, S., Jensen, M. A., Liu, J., Pihl, T., Raman, R., Wan, Y., Wu, Y., Ally, A., Auman, J. T., Balasundaram, M., Balu, S., Baylin, S. B., Beroukhim, R., Bootwalla, M. S., Bowlby, R., Bristow, C. A., Brooks, D., Butterfield, Y., Carlsen, R., Carter, S., Chin, L., Chu, A., Chuah, E., Cibulskis, K., Clarke, A., Coetzee, S. G., Dhalla, N., Fennell, T., Fisher, S., Gabriel, S., Getz, G., Gibbs, R., Guin, R., Hadjipanayis, A., Hayes, D. N., Hinoue, T., Hoadley, K., Holt, R. A., Hoyle, A. P., Jefferys, S. R., Jones, S., Jones, C. D., Kucherlapati, R., Lai, P. H., Lander, E., Lee, S., Lichtenstein, L., Ma, Y., Maglinte, D. T., Mahadeshwar, H. S., Marra, M. A., Mayo, M., Meng, S., Meyerson, M. L., Mieczkowski, P. A., Moore, R. A., Mose, L. E., Mungall, A. J., Pantazi, A., Parfenov, M., Park, P. J., Parker, J. S., Perou, C. M., Protopopov, A., Ren, X., Roach, J., Sabedot, T. S., Schein, J., Schumacher, S. E., Seidman, J. G., Seth, S., Shen, H., Simons, J. V., Sipahimalani, P., Soloway, M. G., Song, X., Sun, H., Tabak, B., Tam, A., Tan, D., Tang, J., Thiessen, N., Jr, T. T., Van Den Berg, D. J., Veluvolu, U., Waring, S., Weisenberger, D. J., Wilkerson, M. D., Wong, T., Wu, J., Xi, L., Xu, A. W., Yang, L., Zack, T. I., Zhang, J., Aksoy, B. A., Arachchi, H., Benz, C., Bernard, B., Carlin, D., Cho, J., DiCara, D., Frazer, S., Fuller, G. N., Gao, J., Gehlenborg, N., Haussler, D., Heiman, D. I., Iype, L., Jacobsen, A., Ju, Z., Katzman, S., Kim, H., Knijnenburg, T., Kreisberg, R. B., Lawrence, M. S., Lee, W., Leinonen, K., Lin, P., Ling, S., Liu, W., Liu, Y., Liu, Y., Lu, Y., Mills, G., Ng, S., Noble, M. S., Paull, E., Rao, A., Reynolds, S., Saksena, G., Sanborn, Z., Sander, C., Schultz, N., Senbabaoglu, Y., Shen, R., Shmulevich, I., Sinha, R., Stuart, J., Sumer, S. O., Sun, Y., Tasman, N., Taylor, B. S., Voet, D., Weinhold, N., Weinstein, J. N., Yang, D., Yoshihara, K., Zheng, S., Zhang, W., Zou, L., Abel, T., Sadeghi, S., Cohen, M. L., Eschbacher, J., Hattab, E. M., Raghunathan, A., Schniederjan, M. J., Aziz, D., Barnett, G., Barrett, W., Bigner, D. D., Boice, L., Brewer, C., Calatozzolo, C., Campos, B., Jr, C. C. G., Chan, T. A., Cuppini, L., Curley, E., Cuzzubbo, S., Devine, K., DiMeco, F., Duell, R., Elder, J. B., Fehrenbach, A., Finocchiaro, G., Friedman, W., Fulop, J., Gardner, J., Hermes, B., Herold-Mende, C., Jungk, C., Kendler, A., Lehman, N. L., Lipp, E., Liu, O., Mandt, R., McGraw, M., Mclendon, R., McPherson, C., Neder, L., Nguyen, P., Noss, A., Nunziata, R., Ostrom, Q. T., Palmer, C., Perin, A., Pollo, B., Potapov, A., Potapova, O., Rathmell, W. K., Rotin, D., Scarpace, L., Schilero, C., Senecal, K., Shimmel, K., Shurkhay, V., Sifri, S., Singh, R., Sloan, A. E., Smolenski, K., Staugaitis, S. M., Steele, R., Thorne, L., Tirapelli, D. P., Unterberg, A., Vallurupalli, M., Wang, Y., Warnick, R., Williams, F., Wolinsky, Y., Bell, S., Rosenberg, M., Stewart, C., Huang, F., Grimsby, J. L., Radenbaugh,

A. J., and Zhang, J. (2015), "Comprehensive, Integrative Genomic Analysis of Diffuse Lower-Grade Gliomas," *New England Journal of Medicine*, 372, 2481–2498.

Capper, D., Jones, D. T. W., Sill, M., Hovestadt, V., Schrimpf, D., Sturm, D., Koelsche, C., Sahm, F., Chavez, L., Reuss, D. E., Kratz, A., Wefers, A. K., Huang, K., Pajtler, K. W., Schweizer, L., Stichel, D., Olar, A., Engel, N. W., Lindenberg, K., Harter, P. N., Braczynski, A. K., Plate, K. H., Dohmen, H., Garvalov, B. K., Coras, R., Hölsken, A., Hewer, E., Bewerunge-Hudler, M., Schick, M., Fischer, R., Beschorner, R., Schittenhelm, J., Staszewski, O., Wani, K., Varlet, P., Pages, M., Temming, P., Lohmann, D., Selt, F., Witt, H., Milde, T., Witt, O., Aronica, E., Giangaspero, F., Rushing, E., Scheurlen, W., Geisenberger, C., Rodriguez, F. J., Becker, A., Preusser, M., Haberler, C., Bjerkvig, R., Cryan, J., Farrell, M., Deckert, M., Hench, J., Frank, S., Serrano, J., Kannan, K., Tsirigos, A., Brück, W., Hofer, S., Brehmer, S., Seiz-Rosenhagen, M., Hänggi, D., Hans, V., Rozsnoki, S., Hansford, J. R., Kohlhof, P., Kristensen, B. W., Lechner, M., Lopes, B., Mawrin, C., Ketter, R., Kulozik, A., Khatib, Z., Heppner, F., Koch, A., Jouvet, A., Keohane, C., Mühleisen, H., Mueller, W., Pohl, U., Prinz, M., Benner, A., Zapatka, M., Gottardo, N. G., Driever, P. H., Kramm, C. M., Müller, H. L., Rutkowski, S., von Hoff, K., Frühwald, M. C., Gnekow, A., Fleischhack, G., Tippelt, S., Calaminus, G., Monoranu, C.-M., Perry, A., Jones, C., et al. (2018), "DNA methylation-based classification of central nervous system tumours," *Nature*, 555, 469.

Carbonneau, M., M. Gagné, L., Lalonde, M.-E., Germain, M.-A., Motorina, A., Guiot, M.-C., Secco, B., Vincent, E. E., Tumber, A., Hulea, L., Bergeman, J., Oppermann, U., Jones, R. G., Laplante, M., Topisirovic, I., Petrecca, K., Huot, M.-t., and Mallette, F. A. (2016), "The oncometabolite 2-hydroxyglutarate activates the mTOR signalling pathway," *Nature Communications*, 7, 12700.

Ceccarelli, M., Barthel, F., Malta, T., Sabedot, T., Salama, S., Murray, B., Morozova, O., Newton, Y., Radenbaugh, A., Pagnotta, S., Anjum, S., Wang, J., Manyam, G., Zoppoli, P., Ling, S., Rao, A., Grifford, M., Cherniack, A., Zhang, H., Poisson, L., Carlotti Jr, C., Tirapelli, D., Rao, A., Mikkelsen, T., Lau, C., Yung, W. K. A., Rabadan, R., Huse, J., Brat, D., Lehman, N., Barnholtz-Sloan, J., Zheng, S., Hess, K., Rao, G., Meyerson, M., Beroukhim, R., Cooper, L., Akbani, R., Wrensch, M., Haussler, D., Aldape, K., Laird, P., Gutmann, D., Anjum, S., Arachchi, H., Auman, J. T., Balasundaram, M., Balu, S., Barnett, G., Baylin, S., Bell, S., Benz, C., Bir, N., Black, K., Bodenheimer, T., Boice, L., Bootwalla, M., Bowen, J., Bristow, C., Butterfield, Y. N., Chen, Q.-R., Chin, L., Cho, J., Chuah, E., Chudamani, S., Coetzee, S., Cohen, M., Colman, H., Couce, M., D'Angelo, F., Davidsen, T., Davis, A., Demchok, J., Devine, K., Ding, L., Duell, R., Elder, J. B., Eschbacher, J., Fehrenbach, A., Ferguson, M., Frazer, S., Fuller, G., Fulop, J., Gabriel, S., Garofano, L., Gastier-Foster, J., Gehlenborg, N., Gerken, M., Getz, G., Giannini, C., Gibson, W., Hadjipanayis, A., Hayes, D. N., Heiman, D., Hermes, B., Hilty, J., Hoadley, K., Hoyle, A., Huang, M., Jefferys, S., et al.

(2016), "Molecular Profiling Reveals Biologically Discrete Subsets and Pathways of Progression in Diffuse Glioma," *Cell*, 164, 550–563.

Chen, R., Nishimura, M. C., Kharbanda, S., Peale, F., Deng, Y., Daemen, A., Forrest, W. F., Kwong, M., Hedehus, M., Hatzivassiliou, G., Friedman, L. S., and Phillips, H. S. (2014), "Hominoid-specific enzyme GLUD2 promotes growth of IDH1R132H glioma," *Proc Natl Acad Sci U S A*, 111, 14217–22.

Choo, A. Y., Kim, S. G., Vander Heiden, M. G., Mahoney, S. J., Vu, H., Yoon, S. O., Cantley, L. C., and Blenis, J. (2010), "Glucose addiction of TSC null cells is caused by failed mTORC1-dependent balancing of metabolic demand with supply," *Mol Cell*, 38, 487–99.

Cong, L., Ran, F. A., Cox, D., Lin, S., Barretto, R., Habib, N., Hsu, P. D., Wu, X., Jiang, W., Marraffini, L. A., and Zhang, F. (2013), "Multiplex Genome Engineering Using CRISPR/Cas Systems," *Science*, 339, 819–823.

Dang, L., White, D. W., Gross, S., Bennett, B. D., Bittinger, M. A., Driggers, E. M., Fantin, V. R., Jang, H. G., Jin, S., Keenan, M. C., Marks, K. M., Prins, R. M., Ward, P. S., Yen, K. E., Liau, L. M., Rabinowitz, J. D., Cantley, L. C., Thompson, C. B., Vander Heiden, M. G., and Su, S. M. (2009), "Cancer-associated IDH1 mutations produce 2-hydroxyglutarate," *Nature*, 462, 739–44.

Dang, L., White, D. W., Gross, S., Bennett, B. D., Bittinger, M. A., Driggers, E. M., Fantin, V. R., Jang, H. G., Jin, S., Keenan, M. C., Marks, K. M., Prins, R. M., Ward, P. S., Yen, K. E., Liau, L. M., Rabinowitz, J. D., Cantley, L. C., Thompson, C. B., Heiden, M. G. V., and Su, S. M. (2010), "Cancer-associated IDH1 mutations produce 2-hydroxyglutarate," *Nature*, 465, 966–966.

de Souza, C. F., Sabedot, T. S., Malta, T. M., Stetson, L., Morozova, O., Sokolov, A., Laird, P. W., Wiznerowicz, M., Iavarone, A., Snyder, J., deCarvalho, A., Sanborn, Z., McDonald, K. L., Friedman, W. A., Tirapelli, D., Poisson, L., Mikkelsen, T., Carlotti, C. G., J., Kalkanis, S., Zenklusen, J., Salama, S. R., Barnholtz-Sloan, J. S., and Noushmehr, H. (2018), "A Distinct DNA Methylation Shift in a Subset of Glioma CpG Island Methylator Phenotypes during Tumor Recurrence," *Cell Rep*, 23, 637–651.

Diplas, B. H., Liu, H., Yang, R., Hansen, L. J., Zachem, A. L., Zhao, F., Bigner, D. D., McLendon, R. E., Jiao, Y., He, Y., Waitkus, M. S., and Yan, H. (2018), "Sensitive and rapid detection of TERT promoter and IDH mutations in diffuse gliomas," *Neuro Oncol*.

Doench, J. G., Fusi, N., Sullender, M., Hegde, M., Vaimberg, E. W., Donovan, K. F., Smith, I., Tothova, Z., Wilen, C., Orchard, R., Virgin, H. W., Listgarten, J., and Root, D. E. (2016), "Optimized sgRNA design to maximize activity and minimize off-target effects of CRISPR-Cas9," *Nat Biotech*, 34, 184–191.

Duncan, C. G., Barwick, B. G., Jin, G., Rago, C., Kapoor-Vazirani, P., Powell, D. R., Chi, J.-T., Bigner, D. D., Vertino, P. M., and Yan, H. (2012), "A heterozygous IDH1R132H/WT mutation induces genome-wide alterations in DNA methylation," *Genome Research*, 22, 2339–2355.

Fack, F., Tardito, S., Hochart, G., Oudin, A., Zheng, L., Fritah, S., Golebiewska, A., Nazarov, P. V., Bernard, A., Hau, A.-C., Keunen, O., Leenders, W., Lund-Johansen, M., Stauber, J., Gottlieb, E., Bjerkvig, R., and Niclou, S. P. (2017), "Altered metabolic landscape in IDH-mutant gliomas affects phospholipid, energy, and oxidative stress pathways," *EMBO Molecular Medicine*, 9, 1681–1695.

Favero, F., McGranahan, N., Salm, M., Birkbak, N. J., Sanborn, J. Z., Benz, S. C., Becq, J., Peden, J. F., Kingsbury, Z., Grocok, R. J., Humphray, S., Bentley, D., Spencer-Dene, B., Gutteridge, A., Brada, M., Roger, S., Dietrich, P.-Y., Forshew, T., Gerlinger, M., Rowan, A., Stamp, G., Eklund, A. C., Szallasi, Z., and Swanton, C. (2015), "Glioblastoma adaptation traced through decline of an IDH1 clonal driver and macro-evolution of a double-minute chromosome," *Annals of Oncology*, 26, 880–887.

Flavahan, W. A., Drier, Y., Liau, B. B., Gillespie, S. M., Venteicher, A. S., Stemmer-Rachamimov, A. O., Suvà, M. L., and Bernstein, B. E. (2016), "Insulator dysfunction and oncogene activation in IDH mutant gliomas," *Nature*, 529, 110–114.

Grassian, A. R., Parker, S. J., Davidson, S. M., Divakaruni, A. S., Green, C. R., Zhang, X., Slocum, K. L., Pu, M., Lin, F., Vickers, C., Joud-Caldwell, C., Chung, F., Yin, H., Handly, E. D., Straub, C., Growney, J. D., Vander Heiden, M. G., Murphy, A. N., Pagliarini, R., and Metallo, C. M. (2014), "IDH1 mutations alter citric acid cycle metabolism and increase dependence on oxidative mitochondrial metabolism," *Cancer Res*, 74, 3317–31.

Houillier, C., Wang, X., Kaloshi, G., Mokhtari, K., Guillevin, R., Laffaire, J., Paris, S., Boisselier, B., Idbaih, A., Laigle-Donadey, F., Hoang-Xuan, K., Sanson, M., and Delattre, J.-Y. (2010), "IDH1 or IDH2 mutations predict longer survival and response to temozolomide in low-grade gliomas," *Neurology*, 75, 1560–1566.

Jiao, Y., Killela, P. J., Reitman, Z. J., Rasheed, B., Heaphy, C. M., de Wilde, R. F., Rodriguez, F. J., Rosemberg, S., Obashinjo, S. M., Marie, S. K. N., Bettegowda, C., Agrawal, N., Lipp, E., Pirozzi, C., Lopez, G., He, Y., Friedman, H., Friedman, A. H., Riggins, G. J., Holdhoff, M., Burger, P., McLendon, R., Bigner, D. D., Vogelstein, B., Meeker, A. K., Kinzler, K. W., Papadopoulos, N., Diaz, L. A., and Yan, H. (2012), "Frequent ATRX, CIC, FUBP1 and IDH1 mutations refine the classification of malignant gliomas," *Oncotarget*, 3.

Jin, G., Reitman, Z. J., Duncan, C. G., Spasojevic, I., Gooden, D. M., Rasheed, B. A., Yang, R., Lopez, G. Y., He, Y., McLendon, R. E., Bigner, D. D., and

Yan, H. (2013), "Disruption of wild-type IDH1 suppresses D-2-hydroxyglutarate production in IDH1-mutated gliomas," *Cancer Res*, 73, 496–501.

Johannessen, T.-C. A., Mukherjee, J., Viswanath, P., Ohba, S., Ronen, S. M., Bjerkvig, R., and Pieper, R. O. (2016), "Rapid Conversion of Mutant IDH1 from Driver to Passenger in a Model of Human Gliomagenesis," *Molecular Cancer Research*.

Juratli, T. A., Kirsch, M., Robel, K., Soucek, S., Geiger, K., von Kummer, R., Schackert, G., and Krex, D. (2012), "IDH mutations as an early and consistent marker in low-grade astrocytomas WHO grade II and their consecutive secondary high-grade gliomas," *Journal of Neuro-Oncology*, 108, 403–410.

Karpel-Massler, G., Ishida, C. T., Bianchetti, E., Zhang, Y., Shu, C., Tsujiuchi, T., Banu, M. A., Garcia, F., Roth, K. A., Bruce, J. N., Canoll, P., and Siegelin, M. D. (2017), "Induction of synthetic lethality in IDH1-mutated gliomas through inhibition of Bcl-xL," *Nature Communications*, 8, 1067.

Kim, Y.-H., Nobusawa, S., Mittelbronn, M., Paulus, W., Brokinkel, B., Keyvani, K., Sure, U., Wrede, K., Nakazato, Y., Tanaka, Y., Vital, A., Mariani, L., Stawski, R., Watanabe, T., Girolami, U. D., Kleihues, P., and Ohgaki, H. (2010), "Molecular Classification of Low-Grade Diffuse Gliomas," *The American Journal of Pathology*, 177, 2708–2714.

Koivunen, P., Lee, S., Duncan, C. G., Lopez, G., Lu, G., Ramkissoon, S., Losman, J. A., Joensuu, P., Bergmann, U., Gross, S., Travins, J., Weiss, S., Looper, R., Ligon, K. L., Verhaak, R. G. W., Yan, H., and Kaelin, W. G. (2012), "Transformation by the R Enantiomer of 2-Hydroxyglutarate Linked to EglN Activation," *Nature*, 483, 484–488.

Kopinja, J., Sevilla, R. S., Levitan, D., Dai, D., Vanko, A., Spooner, E., Ware, C., Forget, R., Hu, K., Kral, A., Spacciapoli, P., Kennan, R., Jayaraman, L., Pucci, V., Perera, S., Zhang, W., Fischer, C., and Lam, M. H. (2017), "A Brain Penetrant Mutant IDH1 Inhibitor Provides In Vivo Survival Benefit," *Scientific Reports*, 7, 13853.

Kutner, R. H., Zhang, X.-Y., and Reiser, J. (2009), "Production, concentration and titration of pseudotyped HIV-1-based lentiviral vectors," *Nat. Protocols*, 4, 495–505.

Lai, A., Kharbanda, S., Pope, W. B., Tran, A., Solis, O. E., Peale, F., Forrest, W. F., Pujara, K., Carrillo, J. A., Pandita, A., Ellingson, B. M., Bowers, C. W., Soriano, R. H., Schmidt, N. O., Mohan, S., Yong, W. H., Seshagiri, S., Modrusan, Z., Jiang, Z., Aldape, K. D., Mischel, P. S., Liau, L. M., Escovedo, C. J., Chen, W., Nghiemphu, P. L., James, C. D., Prados, M. D., Westphal, M., Lamszus,

K., Cloughesy, T., and Phillips, H. S. (2011), "Evidence for sequenced molecular evolution of IDH1 mutant glioblastoma from a distinct cell of origin," *J Clin Oncol*, 29, 4482–90.

Li, J., Csibi, A., Yang, S., Hoffman, G. R., Li, C. G., Zhang, E., Yu, J. J., and Blenis, J. (2015a), "Synthetic lethality of combined glutaminase and Hsp90 inhibition in mTORC1-driven tumor cells," *Proceedings of the National Academy of Sciences of the United States of America*, 112, E21–E29.

Li, W., Xu, H., Xiao, T., Cong, L., Love, M. I., Zhang, F., Irizarry, R. A., Liu, J. S., Brown, M., and Liu, X. S. (2014), "MAGeCK enables robust identification of essential genes from genome-scale CRISPR/Cas9 knockout screens," *Genome Biol*, 15, 554.

Li, W., Köster, J., Xu, H., Chen, C.-H., Xiao, T., Liu, J. S., Brown, M., and Liu, X. S. (2015b), "Quality control, modeling, and visualization of CRISPR screens with MAGeCK-VISPR," *Genome Biology*, 16, 281.

Losman, J.-A., Looper, R. E., Koivunen, P., Lee, S., Schneider, R. K., McMahon, C., Cowley, G. S., Root, D. E., Ebert, B. L., and Kaelin, W. G. (2013), "(R)-2-Hydroxyglutarate Is Sufficient to Promote Leukemogenesis and Its Effects Are Reversible," *Science*, 339, 1621–1625.

Louis, D. N., Perry, A., Reifenberger, G., von Deimling, A., Figarella-Branger, D., Cavenee, W. K., Ohgaki, H., Wiestler, O. D., Kleihues, P., and Ellison, D. W. (2016), "The 2016 World Health Organization Classification of Tumors of the Central Nervous System: a summary," *Acta Neuropathologica*, 131, 803–820.

Luchman, H. A., Chesnelong, C., Cairncross, J. G., and Weiss, S. (2013), "Spontaneous loss of heterozygosity leading to homozygous R132H in a patient-derived IDH1 mutant cell line," *Neuro-Oncology*, 15, 979–980.

Mazor, T., Chesnelong, C., Pankov, A., Jalbert, L. E., Hong, C., Hayes, J., Smirnov, I. V., Marshall, R., Souza, C. F., Shen, Y., Viswanath, P., Noushmehr, H., Ronen, S. M., Jones, S. J. M., Marra, M. A., Cairncross, J. G., Perry, A., Nelson, S. J., Chang, S. M., Bollen, A. W., Molinaro, A. M., Bengtsson, H., Olshen, A. B., Weiss, S., Phillips, J. J., Luchman, H. A., and Costello, J. F. (2017), "Clonal expansion and epigenetic reprogramming following deletion or amplification of mutant IDH1," *Proceedings of the National Academy of Sciences*, 114, 10743–10748.

McBrayer, S. K., Mayers, J. R., DiNatale, G. J., Shi, D. D., Khanal, J., Chakraborty, A. A., Sarosiek, K. A., Briggs, K. J., Robbins, A. K., Sewastianik, T., Shareef, S. J., Olenchock, B. A., Parker, S. J., Tateishi, K., Spinelli, J. B., Islam, M., Haigis, M. C., Looper, R. E., Ligon, K. L., Bernstein, B. E., Carrasco, R. D., Cahill, D. P.,

Asara, J. M., Metallo, C. M., Yennawar, N. H., Vander Heiden, M. G., and Kaelin, W. G. (2018), "Transaminase Inhibition by 2-Hydroxyglutarate Impairs Glutamate Biosynthesis and Redox Homeostasis in Glioma," *Cell*, 175, 101–116.e25.

Meyers, R. M., Bryan, J. G., McFarland, J. M., Weir, B. A., Sizemore, A. E., Xu, H., Dharia, N. V., Montgomery, P. G., Cowley, G. S., Pantel, S., Goodale, A., Lee, Y., Ali, L. D., Jiang, G., Lubonja, R., Harrington, W. F., Strickland, M., Wu, T., Hawes, D. C., Zhivich, V. A., Wyatt, M. R., Kalani, Z., Chang, J. J., Okamoto, M., Stegmaier, K., Golub, T. R., Boehm, J. S., Vazquez, F., Root, D. E., Hahn, W. C., and Tsherniak, A. (2017), "Computational correction of copy number effect improves specificity of CRISPR-Cas9 essentiality screens in cancer cells," *Nat Genet*, 49, 1779–1784.

Morris, T. J., Butcher, L. M., Feber, A., Teschendorff, A. E., Chakravarthy, A. R., Wojdacz, T. K., and Beck, S. (2014), "ChAMP: 450k Chip Analysis Methylation Pipeline," *Bioinformatics*, 30, 428–30.

Network, T. C. G. A. R. (2015), "Comprehensive, Integrative Genomic Analysis of Diffuse Lower-Grade Gliomas," *New England Journal of Medicine*, 372, 2481–2498.

Nomura, M., Saito, K., Aihara, K., Nagae, G., Yamamoto, S., Tatsuno, K., Ueda, H., Fukuda, S., Umeda, T., Tanaka, S., Takayanagi, S., Otani, R., Nejo, T., Hana, T., Takahashi, S., Kitagawa, Y., Omata, M., Higuchi, F., Nakamura, T., Muragaki, Y., Narita, Y., Nagane, M., Nishikawa, R., Ueki, K., Saito, N., Aburatani, H., and Mukasa, A. (2019), "DNA demethylation is associated with malignant progression of lower-grade gliomas," *Scientific reports*, 9, 1903–1903.

Noushmehr, H., Weisenberger, D. J., Diefes, K., Phillips, H. S., Pujara, K., Berman, B. P., Pan, F., Pelloski, C. E., Sulman, E. P., Bhat, K. P., Verhaak, R. G. W., Hoadley, K. A., Hayes, D. N., Perou, C. M., Schmidt, H. K., Ding, L., Wilson, R. K., Van Den Berg, D., Shen, H., Bengtsson, H., Neuvial, P., Cope, L. M., Buckley, J., Herman, J. G., Baylin, S. B., Laird, P. W., and Aldape, K. (2010), "Identification of a CpG Island Methylator Phenotype that Defines a Distinct Subgroup of Glioma," *Cancer Cell*, 17, 510–522.

Ohgaki, H. and Kleihues, P. (2007), "Genetic Pathways to Primary and Secondary Glioblastoma," *The American Journal of Pathology*, 170, 1445–1453.

Ostrom, Q. T., Gittleman, H., Liao, P., Rouse, C., Chen, Y., Dowling, J., Wolinsky, Y., Kruchko, C., and Barnholtz-Sloan, J. (2014), "CBTRUS Statistical Report: Primary Brain and Central Nervous System Tumors Diagnosed in the United States in 2007-2011," *Neuro-Oncology*, 16, iv1–iv63.

Ostrom, Q. T., Gittleman, H., Truitt, G., Boscia, A., Kruchko, C., and Barnholtz-Sloan, J. S. (2018), "CBTRUS Statistical Report: Primary Brain and Other Cen-

tral Nervous System Tumors Diagnosed in the United States in 2011–2015," *Neuro-Oncology*, 20, iv1–iv86.

Parsons, D. W., Jones, S., Zhang, X., Lin, J. C.-H., Leary, R. J., Angenendt, P., Mankoo, P., Carter, H., Siu, I.-M., Gallia, G. L., Olivi, A., McLendon, R., Rasheed, B. A., Keir, S., Nikolskaya, T., Nikolsky, Y., Busam, D. A., Tekleab, H., Diaz, L. A., Hartigan, J., Smith, D. R., Strausberg, R. L., Marie, S. K. N., Shinjo, S. M. O., Yan, H., Riggins, G. J., Bigner, D. D., Karchin, R., Papadopoulos, N., Parmigiani, G., Vogelstein, B., Velculescu, V. E., and Kinzler, K. W. (2008), "An Integrated Genomic Analysis of Human Glioblastoma Multiforme," *Science*, 321, 1807–1812.

Pelletier, J. and Sonenberg, N. (1988), "Internal initiation of translation of eukaryotic mRNA directed by a sequence derived from poliovirus RNA," *Nature*, 334, 320–325.

Peters, T. J., Buckley, M. J., Statham, A. L., Pidsley, R., Samaras, K., R, V. L., Clark, S. J., and Molloy, P. L. (2015), "De novo identification of differentially methylated regions in the human genome," *Epigenetics Chromatin*, 8, 6.

Pusch, S., Schweizer, L., Beck, A.-C., Lehmler, J.-M., Weissert, S., Balss, J., Miller, A. K., and von Deimling, A. (2014), "D-2-Hydroxyglutarate producing neo-enzymatic activity inversely correlates with frequency of the type of isocitrate dehydrogenase 1 mutations found in glioma," *Acta Neuropathologica Communications*, 2.

Raab, J. R., Resnick, S., and Magnuson, T. (2015), "Genome-Wide Transcriptional Regulation Mediated by Biochemically Distinct SWI/SNF Complexes," *PLOS Genetics*, 11, e1005748.

Ran, F. A., Hsu, P. D., Wright, J., Agarwala, V., Scott, D. A., and Zhang, F. (2013), "Genome engineering using the CRISPR-Cas9 system," *Nat Protoc*, 8, 2281–308.

Rohle, D., Popovici-Muller, J., Palaskas, N., Turcan, S., Grommes, C., Campos, C., Tsoi, J., Clark, O., Oldrini, B., Komisopoulou, E., Kunii, K., Pedraza, A., Schalm, S., Silverman, L., Miller, A., Wang, F., Yang, H., Chen, Y., Kernytsky, A., Rosenblum, M. K., Liu, W., Biller, S. A., Su, S. M., Brennan, C. W., Chan, T. A., Graeber, T. G., Yen, K. E., and Mellinghoff, I. K. (2013), "An inhibitor of mutant IDH1 delays growth and promotes differentiation of glioma cells," *Science*, 340, 626–30.

Rose, N. R. and Klose, R. J. (2014), "Understanding the relationship between DNA methylation and histone lysine methylation," *Biochimica et Biophysica Acta (BBA) - Gene Regulatory Mechanisms*, 1839, 1362–1372.

Sandoval, J., Heyn, H., Moran, S., Serra-Musach, J., Pujana, M. A., Bibikova, M., and Esteller, M. (2011), "Validation of a DNA methylation microarray for 450,000 CpG sites in the human genome," *Epigenetics*, 6, 692–702.

Sasaki, M., Knobbe, C. B., Itsumi, M., Elia, A. J., Harris, I. S., Chio, I. I. C., Cairns, R. A., McCracken, S., Wakeham, A., Haight, J., Ten, A. Y., Snow, B., Ueda, T., Inoue, S., Yamamoto, K., Ko, M., Rao, A., Yen, K. E., Su, S. M., and Mak, T. W. (2012), "D-2-hydroxyglutarate produced by mutant IDH1 perturbs collagen maturation and basement membrane function," *Genes & Development*, 26, 2038–2049.

Schvartzman, J.-M., Reuter, V. P., Koche, R. P., and Thompson, C. B. (2019), "2-hydroxyglutarate inhibits MyoD-mediated differentiation by preventing H3K9 demethylation," *Proceedings of the National Academy of Sciences*, 116, 12851–12856.

Shalem, O., Sanjana, N. E., Hartenian, E., Shi, X., Scott, D. A., Mikkelsen, T. S., Heckl, D., Ebert, B. L., Root, D. E., Doench, J. G., and Zhang, F. (2014), "Genome-Scale CRISPR-Cas9 Knockout Screening in Human Cells," *Science*, 343, 84–87.

Smyth, G. K. (2004), "Linear models and empirical bayes methods for assessing differential expression in microarray experiments," *Stat Appl Genet Mol Biol*, 3, Article3.

Soderquist, R. S., Crawford, L., Liu, E., Lu, M., Agarwal, A., Anderson, G. R., Lin, K. H., Winter, P. S., Cakir, M., and Wood, K. C. (2018), "Systematic mapping of BCL-2 gene dependencies in cancer reveals molecular determinants of BH3 mimetic sensitivity," *Nat Commun*, 9, 3513.

Su, R., Dong, L., Li, C., Nachtergaele, S., Wunderlich, M., Qing, Y., Deng, X., Wang, Y., Weng, X., Hu, C., Yu, M., Skibbe, J., Dai, Q., Zou, D., Wu, T., Yu, K., Weng, H., Huang, H., Ferchen, K., Qin, X., Zhang, B., Qi, J., Sasaki, A. T., Plas, D. R., Bradner, J. E., Wei, M., Marcucci, G., Jiang, X., Mulloy, J. C., Jin, J., He, C., and Chen, J. (2018), "R-2HG Exhibits Anti-tumor Activity by Targeting FTO/m6A/MYC/CEBPA Signaling," *Cell*, 172, 90–105.e23.

Tateishi, K., Wakimoto, H., Iafrate, A. J., Tanaka, S., Loebel, F., Lelic, N., Wiederschain, D., Bedel, O., Deng, G., Zhang, B., He, T., Shi, X., Gerszten, R., Zhang, Y., Yeh, J.-R., Curry, W., Zhao, D., Sundaram, S., Nigim, F., Koerner, M. A., Ho, Q., Fisher, D., Roider, E., Kemeny, L., Samuels, Y., Flaherty, K., Batchelor, T., Chi, A., and Cahill, D. (2015), "Extreme Vulnerability of IDH1 Mutant Cancers to NAD+ Depletion," *Cancer Cell*, 28, 773–784.

Teschendorff, A. E., Marabita, F., Lechner, M., Bartlett, T., Tegner, J., Gomez-Cabrero, D., and Beck, S. (2013), "A beta-mixture quantile normalization method

for correcting probe design bias in Illumina Infinium 450 k DNA methylation data," *Bioinformatics*, 29, 189–96.

Turcan, S., Rohle, D., Goenka, A., Walsh, L. A., Fang, F., Yilmaz, E., Campos, C., Fabius, A. W. M., Lu, C., Ward, P. S., Thompson, C. B., Kaufman, A., Guryanova, O., Levine, R., Heguy, A., Viale, A., Morris, L. G. T., Huse, J. T., Mellinghoff, I. K., and Chan, T. A. (2012), "IDH1 mutation is sufficient to establish the glioma hypermethylator phenotype," *Nature*, 483, 479–483.

Turcan, S., Makarov, V., Taranda, J., Wang, Y., Fabius, A. W. M., Wu, W., Zheng, Y., El-Amine, N., Haddock, S., Nanjangud, G., LeKaye, H. C., Brennan, C., Cross, J., Huse, J. T., Kelleher, N. L., Osten, P., Thompson, C. B., and Chan, T. A. (2018), "Mutant-IDH1-dependent chromatin state reprogramming, reversibility, and persistence," *Nature Genetics*, 50, 62–72.

Viswanath, P., Radoul, M., Izquierdo-Garcia, J. L., Ong, W. Q., Luchman, H. A., Cairncross, J. G., Huang, B., Pieper, R. O., Phillips, J. J., and Ronen, S. M. (2018), "2-Hydroxyglutarate-Mediated Autophagy of the Endoplasmic Reticulum Leads to an Unusual Downregulation of Phospholipid Biosynthesis in Mutant IDH1 Gliomas," *Cancer Res*, 78, 2290–2304.

Volker Hovestadt, M. Z. (2017), "conumee," .

Waitkus, M. S., Diplas, B. H., and Yan, H. (2016), "Isocitrate dehydrogenase mutations in gliomas," *Neuro Oncol*, 18, 16–26.

Waitkus, M. S., Pirozzi, C. J., Moure, C. J., Diplas, B. H., Hansen, L. J., Carpenter, A. B., Yang, R., Wang, Z., Ingram, B. O., Karoly, E. D., Mohney, R. P., Spasojevic, I., McLendon, R. E., Friedman, H. S., He, Y., Bigner, D. D., and Yan, H. (2018), "Adaptive Evolution of the GDH2 Allosteric Domain Promotes Gliomagenesis by Resolving IDH1(R132H)-Induced Metabolic Liabilities," *Cancer Res*, 78, 36–50.

Wang, T., Wei, J. J., Sabatini, D. M., and Lander, E. S. (2014), "Genetic screens in human cells using the CRISPR-Cas9 system," *Science*, 343.

Wang, T., Birsoy, K., Hughes, N. W., Krupczak, K. M., Post, Y., Wei, J. J., Lander, E. S., and Sabatini, D. M. (2015), "Identification and characterization of essential genes in the human genome," *Science*, 350, 1096.

Ward, P. S., Patel, J., Wise, D. R., Abdel-Wahab, O., Bennett, B. D., Coller, H. A., Cross, J. R., Fantin, V. R., Hedvat, C. V., Perl, A. E., Rabinowitz, J. D., Carroll, M., Su, S. M., Sharp, K. A., Levine, R. L., and Thompson, C. B. (2010), "The Common Feature of Leukemia-Associated IDH1 and IDH2 Mutations Is a Neomorphic Enzyme Activity Converting α-Ketoglutarate to 2-Hydroxyglutarate," *Cancer Cell*, 17, 225–234.

Wettenhall, J. M. and Smyth, G. K. (2004), "limmaGUI: a graphical user interface for linear modeling of microarray data," *Bioinformatics*, 20, 3705–6.

Winter, J., Schwering, M., Pelz, O., Rauscher, B., Zhan, T., Heigwer, F., and Boutros, M. (2017), "CRISPRAnalyzeR: Interactive analysis, annotation and documentation of pooled CRISPR screens," *bioRxiv*.

Xu, W., Yang, H., Liu, Y., Yang, Y., Wang, P., Kim, S.-H., Ito, S., Yang, C., Wang, P., Xiao, M.-T., xia Liu, L., qing Jiang, W., Liu, J., ye Zhang, J., Wang, B., Frye, S., Zhang, Y., hui Xu, Y., ying Lei, Q., Guan, K.-L., min Zhao, S., and Xiong, Y. (2011), "Oncometabolite 2-Hydroxyglutarate Is a Competitive Inhibitor of α-Ketoglutarate-Dependent Dioxygenases," *Cancer Cell*, 19, 17–30.

Yan, H., Parsons, D. W., Jin, G., McLendon, R., Rasheed, B. A., Yuan, W., Kos, I., Batinic-Haberle, I., Jones, S., Riggins, G. J., Friedman, H., Friedman, A., Reardon, D., Herndon, J., Kinzler, K. W., Velculescu, V. E., Vogelstein, B., and Bigner, D. D. (2009), "IDH1 and IDH2 mutations in gliomas," *N Engl J Med*, 360, 765–73.

Zhang, L., Chen, L. H., Wan, H., Yang, R., Wang, Z., Feng, J., Yang, S., Jones, S., Wang, S., Zhou, W., Zhu, H., Killela, P. J., Zhang, J., Wu, Z., Li, G., Hao, S., Wang, Y., Webb, J. B., Friedman, H. S., Friedman, A. H., McLendon, R. E., He, Y., Reitman, Z. J., Bigner, D. D., and Yan, H. (2014), "Exome sequencing identifies somatic gain-of-function PPM1D mutations in brainstem gliomas," *Nat Genet*, 46, 726–30.

Zhou, W., Laird, P. W., and Shen, H. (2017), "Comprehensive characterization, annotation and innovative use of Infinium DNA methylation BeadChip probes," *Nucleic Acids Res*, 45, e22.

Biography

Casey Joseph Moure received his bachelors of science (B.S.) degree in Biomedical Engineering *summa cum laude* in 2011 while at Rutgers University in Piscataway N.J. While working at Rutgers he had the opportunity to perform two years of research in the biomedical engineering laboratory of Dr. Martin Yarmush working on optimizing tissue explant culture conditions. After this formative research experience in an engineering department he sought to broaden his research experience and exposure to different fields of science by taking master's classes in developmental and cell biology also at Rutgers, while also interning at Celgene corporation. Having found an interest in more basic biology he sought out PhD training programs in basic science departments, and after much deliberation decided to accept an offer of admission to Duke University and a Dean's graduate fellowship under the gateway PhD T32 program of Developmental and Stem Cell Biology. This program allowed him to rotate through various laboratories at Duke until he found his fit in the Yan lab in 2013. While in the Yan lab, Casey was awarded a National Institutes of Health Ruth L. Kirstein Research Service Award for his research work.

He is graduating with a Ph.D. from the Department of Pathology at Duke in August 2019.

The following is a list of his publications while at Duke.

Published Manuscripts

Diplas, B. H., Liu, H., Yang, R., Hansen, L. J., Zachem, A. L., Zhao, F., Bigner, D. D., McLendon, R. E., Jiao, Y., He, Y., Waitkus, M. S., and Yan, H. (2018), "Sensitive and rapid detection of TERT promoter and IDH mutations in diffuse gliomas," *Neuro Oncol*.

Lei, K., Sun, R., Chen, L. H., Diplas, B. H., Moure, C. J., Wang, W., Hansen, L. J., Tao, Y., Chen, X., Chen, C.-P. J., Greer, P. K., Zhao, F., Yan, H., Bigner, D. D., Huang, J., and He, Y. (2018), "Mutant allele quantification reveals a genetic basis for TP53 mutation-driven castration resistance in prostate cancer cells," *Scientific Reports*, 8.

Moure, C. J., Diplas, B. H., Chen, L. H., Yang, R., Pirozzi, C. J., Wang, Z., Spasojevic, I., Waitkus, M. S., He, Y., and Yan, H. (2019), "CRISPR editing of mutant IDH1 R132H induces a CpG methylation-low state in patient-derived glioma models of G-CIMP," *Molecular Cancer Research*, p. molcanres.0309.2019.

Waitkus, M. S., Pirozzi, C. J., Moure, C. J., Diplas, B. H., Hansen, L. J., Carpenter, A. B., Yang, R., Wang, Z., Ingram, B. O., Karoly, E. D., Mohney, R. P., Spasojevic, I., McLendon, R. E., Friedman, H. S., He, Y., Bigner, D. D., and Yan, H. (2018), "Adaptive Evolution of the GDH2 Allosteric Domain Promotes Gliomagenesis by Resolving IDH1(R132H)-Induced Metabolic Liabilities," *Cancer Res*, 78, 36–50.

Yang, R., Chen, L. H., Hansen, L. J., Carpenter, A. B., Moure, C. J., Liu, H., Pirozzi, C. J., Diplas, B. H., Waitkus, M. S., Greer, P. K., Zhu, H., McLendon, R. E., Bigner, D. D., He, Y., and Yan, H. (2017), "CicLoss Promotes Gliomagenesis via Aberrant Neural Stem Cell Proliferation and Differentiation," *Cancer Research*, 77, 6097–6108.